

LARGE SCALE RETINAL MODELING FOR THE DESIGN

OF

NEW GENERATION RETINAL PROSTHESES

by

Tran Trung Kien, BSc.

Thesis submitted to the University of Nottingham Malaysia Campus

for the degree of Doctor of Philosophy

DECEMBER 2014

Copyright 2014

Tran Trung Kien

All Rights Reserved

I would like to dedicate this thesis to my loving parents...

LARGE SCALE RETINAL MODELING FOR THE DESIGN
OF
NEW GENERATION RETINAL PROSTHESES

by

TRAN TRUNG KIEN, BSC.

DISSERTATION

Presented to the

School of Computer Science

Faculty of Science

for the Degree of

DOCTOR OF PHILOSOPHY IN

COMPUTER SCIENCE

THE UNIVERSITY OF NOTTINGHAM MALAYSIA CAMPUS

December 2014

ACKNOWLEDGMENTS

First of all, I would like to acknowledge Dr. Tomas Maul for his help and time to guide and assist me to overcome many obstacles on the road of being a researcher. I also want to give many thanks to Prof. Andrej Bargiela as well as Mr. Ho Sooi Hock for their useful and meaningful comments in my publications and this thesis.

Secondly, I want to give a big dedication to my parents, Tran Ngoc Dan and Nguyen Thi Thu for their unstoppable hard works to support me in living and studying. Furthermore, I also want to thank my brother for encouraging and supporting me whenever I needed.

Thirdly, I would give my big love to my beloved wife Nguyen Bach Anh Thu who sacrificed a lot for my studying and working, and also my little cute princess Tran Ngoc Man Tien for her smiles that give me more energy to work.

Last but not least, I want to thank all my friends, both at the Nottingham Malaysia Campus and in Vietnam, for supporting me during work on this thesis.

December 2014

LARGE SCALE RETINAL MODELING FOR THE DESIGN
OF
NEW GENERATION RETINAL PROSTHESES

Tran Trung Kien, BSc

The University of Nottingham Malaysia Campus, 2014

First Supervisor : Dr. Tomas Maul

Second Supervisor : Prof. Andrzej Bargiela

ABSTRACT

With the help of modern technology, blindness caused by retinal diseases such as age-related macular degeneration or retinitis pigmentosa is now considered reversible. Scientists from various fields such as Neuroscience, Electrical Engineering, Computer Science, and Bioscience have been collaborating to design and develop retinal prostheses, with the aim of replacing malfunctioning parts of the retina and restoring vision in the blind. Human trials conducted to test retinal prostheses have yielded encouraging results, showing the potential of this approach in vision recovery. However, a retinal prosthesis has several limitations with regard to its hardware and biological functions, and several attempts have been made to overcome these limitations.

This thesis focuses on the biological aspects of retinal prostheses: the biological processes occurring inside the retina and the limitations of retinal prostheses corresponding to those processes have been analysed. Based on these analyses, three major findings regarding information processing inside the retina have been presented and these findings have been used to conceptualise retinal prostheses that have the characteristics of asymmetrical and separate pathway stimulations. In the future, when nanotechnology gains more popularity and is completely integrated inside the prosthesis, this concept can be utilized to restore useful visual information such as colour, depth, and contrast to achieve high-quality vision in the blind.

TABLE OF CONTENTS

CHAPTER 1	INTRODUCTION	1
1.1	Motivation.....	1
1.2	Currents challenges of retinal prostheses.....	3
1.3	Thesis aim and objective.....	6
1.4	The need of a retinal model	7
1.5	Major contributions.....	8
1.5.1	Proposed model to explain the Hermann grid illusion	10
1.5.2	A model to enhance contrast under mesopic lighting conditions.....	10
1.5.3	A model to enhance colour vision.....	11
1.5.4	Conceptual design of retinal prosthesis.....	12
1.6	Thesis overview	13
CHAPTER 2	BACKGROUND STUDIES.....	1
2.1	The retina	1
2.1.1	Structure of the retina.....	1
2.1.2	Retinal connectivity.....	7
2.2	Functions of the retina	8
2.2.1	Visual photo-transduction	9
2.2.2	Data compression	11
2.2.3	Light/dark adaptation	12
2.2.4	Spatial filtering.....	13
2.3	Retinal diseases.....	15
2.4	Retinal prosthesis	16
2.4.1	The device	16
2.4.2	Device output	17
2.5	Summary.....	20
CHAPTER 3	RETINAL PROSTHESIS REVIEW	21

3.1	Extraocular prostheses	22
3.1.1	Surface cortical prosthesis.....	22
3.1.2	Optic nerve prostheses	24
3.2	Intraocular	26
3.2.1	Epiretinal prostheses	26
3.2.1.1	Advantages and disadvantages of epiretinal prostheses..	37
3.2.2	Subretinal prostheses.....	38
3.2.2.1	Advantages and disadvantages of subretinal prostheses .	50
3.3	Summary	51
CHAPTER 4	RETINAL MODELING REVIEW.....	52
4.1	Conductance-based models.....	53
4.1.1	Hodgkin–Huxley model	53
4.1.2	Morris–Lecar model.....	55
4.1.3	Advantages and disadvantages.....	58
4.2	Threshold-fire models.....	59
4.2.1	Integrate-and-fire.....	59
4.2.2	Spike Response Model	62
4.2.3	Izhikevich model.....	64
4.2.4	Advantages and disadvantages.....	66
4.3	Compartment model.....	67
4.3.1	Advantages and disadvantages.....	70
4.4	Linear-Non-linear-Poisson model.....	70
4.4.1	Advantages and disadvantages.....	73
4.5	Discussion	74
4.6	Summary	76
CHAPTER 5	SYSTEM MODELING	77
5.1	The retinal model	77
5.2	Linear–non-linear system.....	77
5.3	Model receptive field	79
5.4	ON and OFF pathways.....	84
5.5	Cone and rod pathway	85

5.5.1	Cone pathway	86
5.5.2	Rod pathway.....	88
5.6	Implementation in the proposed model.....	89
5.7	Spiking neurons	96
5.8	Model simulation	97
5.9	Summary	99
CHAPTER 6 OUTER PLEXIFORM LAYER RECEPTIVE FIELDS AS UNDERLYING FACTORS OF THE HERMANN GRID ILLUSION.....		101
6.1	Introduction.....	101
6.2	The Hermann grid illusion	103
6.3	A unified model based on Hermann grid illusion.....	107
6.4	Proposed model.....	108
6.5	Experiments and results	111
6.5.1	Line width ratio	111
6.5.2	Orientation.....	113
6.5.3	Luminance.....	115
6.5.4	Distortion.....	116
6.6	Discussion	117
6.7	Summary	122
CHAPTER 7 A RETINAL MODEL OF CONTRAST ADJUSTMENT IN MESOPIC CONDITIONS.....		124
7.1	Introduction.....	124
7.2	Contrast processing in the retina.....	125
7.3	The rod pathway in the retina	128
7.4	Rod pathway modelling	131
7.5	Experimental setups	134
7.6	Results.....	136
7.7	Discussion	146
7.8	Summary	151
CHAPTER 8 A RETINAL MODEL OF COLOUR ADJUSTMENT.....		153
8.1	Introduction.....	153
8.2	Colour pathway and colour correction in the retina.....	155

8.3	Colour correction hypothesis	157
8.4	The model of colour processing in the retina.....	158
8.5	Experimental setups	162
8.6	Results.....	164
8.7	Discussion	172
8.8	Summary	176
CHAPTER 9	CONCLUSIONS AND FUTURE WORK	177
9.1	Discussion	177
9.1.1	Device concept	178
9.1.2	Intraocular part	180
9.1.3	Extra-ocular part.....	186
9.1.4	Informational configuration components	187
9.2	Conclusions.....	188
9.3	Future work.....	190
9.4	Summary	191
CHAPTER 10	REFERENCES	193

LIST OF FIGURES

Figure 2.1: Location and structure of the retina.....	2
Figure 3.1: Different approaches of retinal prostheses and their placements.	22
Figure 3.2: The optic nerve prosthesis.....	25
Figure 3.3: The schematic of the prosthesis.....	27
Figure 3.4: The detail of the intraocular implant.	28
Figure 3.5: EPIRET-3 retinal prosthesis.....	36
Figure 3.6: The Artificial Silicon Retina (ASR).	41
Figure 3.7: The first generation of the retinal prosthesis.....	46
Figure 3.8: The hermetic implant in the second generation of the prosthesis.	46
Figure 3.9: Alpha-IMS retinal prosthesis.....	48
Figure 4.1: A neuron as an RC circuit.	59
Figure 4.2: A neuron cell as compartment circuitry.	67
Figure 4.3: Linear-Non-linear-Poisson model.	71
Figure 5.1: The response of receptive field of ganglion cells.....	80
Figure 5.2: Edge detection as a result from receptive field	81
Figure 5.3: Different types of receptive fields.....	84
Figure 5.4: Cone pathway in retina.....	86
Figure 5.5: Rod pathway in retina.....	88
Figure 5.6: Proposed retina model.....	90
Figure 5.7: Rod pathway circuitry in the model.	91

Figure 5.8: The cone pathway in the model.....	92
Figure 6.1: The original Hermann grid (A) and its inverted colour version (B). ..	102
Figure 6.2: Baumgartner’s explanation for the Hermann grid illusion.....	103
Figure 6.3: The original Hermann grid (A) and grid rotated by 45° (B).	104
Figure 6.4: Colour variant (A) and distorted (B) versions of the Hermann grid. ..	105
Figure 6.5: Simplified illustration of receptive field integration	109
Figure 6.6: The Hermann grid output from the model.....	112
Figure 6.7: The Hermann grid output from the model.....	113
Figure 6.8: Output from the model for grids rotated at 15°, 30°, 45°, and 60° ...	114
Figure 6.9: The output with the same orientations as in Figure 6.8.....	114
Figure 6.10: The output of model with colour grids.....	115
Figure 6.11: Distorted Hermann grid as input to and output from the model.	116
Figure 6.12: Binary maps of connectivity in bipolar receptive field.	119
Figure 7.1: The rod pathway in the retina.....	129
Figure 7.2: The root mean square error pertaining to ON ganglion cells.....	138
Figure 7.3: The root mean square error pertaining to OFF ganglion cells	138
Figure 7.4: Without ON/OFF integration	139
Figure 7.5: With ON/OFF integration.	140
Figure 7.6: ON and OFF ganglion cell processing.....	144
Figure 7.7: Responses from ON ganglion cells	145
Figure 7.8: Responses from OFF ganglion cells.....	145
Figure 8.1: The retinal colour pathway.....	156
Figure 8.2: Results for simulated deuteranopia.	165

Figure 8.3: Colour correction output from the model.....	166
Figure 8.4: Comparison of the proposed model outcomes	167
Figure 8.5: The root mean square error (RMSE).....	168
Figure 8.6: Comparison of RMSE across eight different algorithms	169
Figure 8.7: Connective topology of ganglion cell receptive fields.....	170
Figure 8.8: Temporal responses of blue ganglion cells	173
Figure 8.9: Spike synchronization analysis of ganglion cells.....	174
Figure 9.1: The conceptual prosthesis.	183
Figure 9.2: The electrode array in operation.....	183

LIST OF TABLES

Table 3.1: Result from testing an Artificial Silicon Retina.	39
Table 4.1: FLOPS comparison of different retinal models.	75
Table 5.1: Processing block and its definition in proposed model.	93
Table 6.1: Ratio test cases.....	111
Table 6.2: Colour test cases	115
Table 6.3: MSE between the output from a rotated Hermann grid.....	118
Table 7.1: Without ON/OFF integration.....	142
Table 7.2: With ON/OFF integration.....	143

LIST OF ABBREVIATIONS

Abbreviation	Meaning
AMD	Age-Related Macular Degeneration
RP	Retinitis Pigmentosa
ASR	Artificial Silicon Retina
L, M, S	Long, Medium and Short
Na, K, Ca, Cl	Sodium, Potassium, Calcium and Chloride ions
RPE	Retinal Pigment Epithelium
FPGA	Field-Programmable Gate Array
IRP	Intraocular Retinal Prosthesis
RE, RS	Retinal Encoder, Retinal Stimulator
SIROF	Sputtered Iridium Oxide Film
Alpha-IMS	Retina Implant
MPDA	Micro-photodiode Array
RC	Resistor-Capacitor
LNP	Linear-Nonlinear-Poisson
FLOPS	Floating Point Operations per Second
MEMS/NEMS	Micro-mechanical System/Nano-mechanical System
CNTs	Carbon Nano Tubes
CPU/GPU	Central Processing Unit/ Graphics Processing Unit
SF, TF	Spatial Filter, Temporal Filter
RF	Receptive Field

CHAPTER 1

INTRODUCTION

1.1 Motivation

Of all the human senses, the sense of sight is considered to be the most important one. Vision enables human beings to interact with their surrounding environment. Vision is a result of sequential activity, which begins with the reflection of light from an object to the lens of the eyes. The lens refracts the light onto a light-sensitive layer of tissue that lines the back of the eye called the retina. The retina encodes the light beam into spiking signal; thereafter, the brain ‘understands’ the information sent to it by the retina through the optic nerve. The retina thus acts as a ‘recorder and encoder’ in the visual perception.

Retinal diseases such as age-related macular degeneration or retinitis pigmentosa damage the retina, rendering patients partially or completely blind. To restore vision in these cases, various approaches have been proposed and tested, both in vitro and in vivo (Maynard, 2001; Kien, Maul and Bargiela, 2012; Luo and da Cruz, 2014). Among these approaches, a retinal prosthesis can potentially restore basic vision in partially or completely blind patients. Moreover, it also assists patients with some basic activities such as navigation, reading large letters, or using utensils.

A retinal prosthesis is a device comprising various components that are responsible for supplying power, acquiring images, processing signals, and stimulating retinal cells. Through these functions, the prosthesis can replicate damaged parts or the whole retina. To this end, various studies have proposed different designs to improve prostheses in terms of visual resolution, biocompatibility, and quality of the implantation (Banarji et al., 2009; Karagoz and Ozden, 2011). At present, a retinal prosthesis can restore partial and simple vision, which is still far from ideal. There are two main reasons for this problem: hardware limitations and limited understanding of the retina. In the prosthesis currently available, the hardware does not allow the device to stimulate the retinal cells precisely, independently, and simultaneously. In particular, with current technologies, the size of the electrodes is not sufficiently small to stimulate one isolated retinal cell and this leads to the cross-talk between the stimulated retinal cell and its adjacent cells. This problem affects the quality of visual perception of the blind. Furthermore, incomplete knowledge regarding retinal processing and cell distribution limits the accuracy of placement of the stimulator unit. Therefore, it consumes more energy and causes heating of the retina.

The next generation of retinal prostheses should be able to tackle the aforementioned issues, which will also require a much better understanding of retinal processing within the retina. To understand this pathway, it is important to determine how retinal cells are connected and how connectivity affects output

signals with different configurations. For this, the processing information and cell connectivity inside the retina must be examined to determine the optimal way to replicate it when using retinal prostheses. Therefore, a model to simulate the processing information and connectivity of the retinal cells is required. Using this retinal model, a different configuration of the retinal connectivity could be simulated, and the corresponding output could be evaluated to determine the relationship between connectivity and processing information in the retina. The design for the next-generation retinal prostheses could be developed by using the knowledge gained from simulating and evaluating various configurations of retinal cell connectivity in order to determine the constitution of the device, potential for implementation, and operation of the device.

1.2 Currents challenges of retinal prostheses

From the review of retina prosthesis (Kien, Maul and Bargiela, 2012), it is clear that both epiretinal and subretinal prostheses use the same approach for stimulating retinal cells, that is, they use electrodes controlled by a stimulation chip. Animal and human trials have shown that many prostheses using this approach operate satisfactorily, and they are able to restore acceptable vision in the blind after training. Although some prostheses have been approved for commercial purposes, many challenges need to be overcome in order to improve the next generation of prostheses. These challenges are categorized into hardware and software

challenges, which are discussed in this section. The most important hardware challenge is related to stimulation, where one electrode can stimulate many cells adjacent to the target cell (Asher *et al.*, 2007; Fromherz, 2008). However, minimizing the number of electrodes also leads to another problem: many small electrodes located close together can lead to cross-talk, which decreases the accuracy of the stimulation signal; moreover, the electrodes themselves cause interference (Lorach *et al.*, 2013). On the other hand, more electrodes require more energy, and the heat required to stimulate the electrodes will damage the retinal cells or make the user uncomfortable. Regarding implantation, more accurate stimulation of the retinal cells requires closer contact of the electrodes to the cells, making it more difficult to implant the device into the retina (Chuang, Margo and Greenberg, 2014; Luo and da Cruz, 2014). However, the deeper the electrodes are in the retina, the more complicated the surgery is. In addition, the training process is different for various devices; moreover, training is a time-consuming process, since the users need to adapt to the device in addition to allowing the retina to rest during training (Maidenbaum, Abboud and Amedi, 2013). In particular, the users need to adapt to the poor resolution of the restored vision due to the small array of electrodes; they have to learn and familiarize themselves with this using poor signal to map their environment. Moreover, the lack of detailed information regarding colour and depth in restored vision prevents blind users from coping in a complicated environment.

Since stimulation is an important aspect of retinal prostheses, this thesis focuses on stimulation. However, it focuses on the software aspect, instead of the hardware, because future advances in nanotechnology will make it possible to develop nano-scale electrodes, which would be much smaller than the micro-scale electrodes used in current devices. When the size of the electrodes is reduced, the problem of crosstalk will be solved because the nano-electrodes will be able to stimulate only one or two individual cells, without affecting the neighbouring cells. With nanotechnology, the hardware of the retinal prosthesis devices will be significantly upgraded, and these devices will serve patients better because of their longer lifespan and light weight. Consequently, an upgrade in hardware would require a corresponding update in software in order to allow the device to operate properly and efficiently. The methods used for stimulation in the current generation of retinal prostheses have been developed whilst keeping in mind that many cells are stimulated at the same time, and that this situation will not change in upgraded devices in the near future. Besides, the upgraded device will not work efficiently if the stimulations are not placed at the correct position in the retina, even if the electrode size is reduced to a nano scale. From these facts, a research on improving the stimulating precision of the retinal prostheses was conducted in order to explore the current limitation of retinal prostheses and provide a possible solution for the next generation retinal prostheses.

1.3 Thesis aim and objective

From previous discussion, a research is conducted in order to propose a method to improve the stimulating precision of retinal prostheses in the future. In detail, this thesis is expected to propose a stimulating method for the next generation retinal prostheses thus the users of future device will be able to perceive more visual information than in current devices. In order to find out the capable stimulating method for future device, a computer model was implemented and utilized to simulate and analyse different connectivity inside the retina. Hence, the aim of this thesis is focusing on simulating different processing pathways inside the retina through the retinal model.

To achieve the aim of this thesis, a retinal model would be implemented and in order to do that several studies about the retina, retinal processing pathways, retinal prostheses and retinal modelling will be completed. Firstly, a review of retinal prostheses will be conducted to summarize the current state-of-art of stimulating technologies and methods applied in the visual prosthesis devices. Secondly, different methods to model the retinal will be reviewed to select the best approach for simulating the retinal processing pathways. The next step will be to implement the model using methods and techniques decided from the retinal modelling review. After that, different experiments will be conducted to adequately test and verify the model and evaluate different stimulating method proposals.

Based on the experiments and the evaluations of the model, a stimulating pattern and a retinal prosthesis device concept would be proposed and discussed in term of possibility and validation for future usage.

1.4 The need of a retinal model

As discussed above, software used for retinal prostheses needs to be updated in order to match potentially upgraded hardware in the future. In this regard, it is difficult to determine an optimal method to stimulate the retinal cells, especially the ganglion cells, in epiretinal prostheses. By successfully stimulating specific ganglion cells for specific information, it may be possible to restore vision at a minimal cost. This leads to the question of the arrangement of the ganglion cells in the retina and their behaviours during firing while responding to different type of stimuli in the normal retina and in the stimulation of retinal prostheses. Besides, the processing pathway inside the retina also needs to be addressed. This thesis focuses on the ON and OFF pathways and their relationships with colour and contrast processing inside the retina. Although many other models have addressed these issues, they did not discuss the retinal prosthesis aspect or a complete model with all retinal cell layers. It is necessary to determine how different information such as motion, contrast, colour, or depth processed in the retina, especially at the ganglion level, will bring the prosthesis device one-step closer to restoring meaningful visual signals in the blind. To achieve this, a retinal model must be developed to simulate

retinal processing of the different information and the response of ganglion cells to that information. The responses from this model are both in the spatial and temporal domain for visual performance and the model also has the capability to generate a spiking train to analyse the behaviour of ganglion cells. This model is described in detail in the next chapter.

1.5 Major contributions

As mentioned above, next-generation retinal prostheses should be able to simulate the retinal cells precisely and independently, with the goal of improving the quality of restored vision, while reducing power consumption and heat-induced retinal cell damage. Considering these aspects, a model of retinal processing is proposed to study the information processing pathways inside the retina, through experiments based on different theories, especially with regard to receptive asymmetric processing, contrast, and colour processing. These criteria have been selected due to the limitations of restored visual information in current retinal prostheses. In detail, in current prostheses, the restored vision is perceived as a black and white dot matrix with low resolution, without any perception of colour, depth, or contrast. Although this vision is sufficient for blind users to be able to navigate after long-term training, it prevents them from performing certain advanced activities, such as differentiating a real door from a sketch of a door, dodging obstacles on a pathway, or seeing a red ‘danger’ label on a dangerous item. Therefore, this thesis focuses on

exploring retinal processing and connectivity according to these criteria in order to determine the relationship between visual responses and connectivity configurations. For the first criterion, retinal cell distribution formation has been examined using different configurations. Then, the visual outputs have been evaluated using the Hermann grid illusion. The Hermann grid was employed to facilitate an easy comparison between the results from the model and perception of the naked eye. For the second criterion, a circuit used to process contrast information in the retina was simulated and evaluated for both visual and neuronal responses. The same method was applied to the final criterion, except that the colour processing pathway was taken into account. The results from simulation and validation of the different criteria showed that asymmetrical and parallel simulations play an important role inside the retina, especially in restoring contrast and colour information. This suggests a wrap-up design for next-generation retinal prostheses. With the proposed design, the next generation of visual prostheses will be able to overcome the current issues of precise simulation. It would not only provide information such as contrast and colour but also improve the quality of restored vision. This development in retinal prostheses will help the blind perceive more meaningful information and perform more operations comfortably for a longer period and with fewer problems.

1.5.1 Proposed model to explain the Hermann grid illusion

With regard to visual perception illusions such as motion, luminance, contrast, and colour, the Hermann grid illusion is an optical illusion that has received significant attention from psychologists and physiologists. The grid is an array of black squares that is formed by horizontal and vertical white bars on a black background. The illusion is described as the appearance of black or grey dots at the intersection of the white bars. Although many theories have been proposed to explain this illusion, questions regarding the underlying neural and computational causes of the illusion remain unanswered. Therefore, a retinal model focused on the receptive field structure at the outer-plexiform layer is presented, and this model is used to explain the illusion. The results of this thesis show that the illusion may be explained on the basis of the connection of the outer-plexiform layer in the retina, especially by changing the shape of the receptive field. According to these results, the shape of the receptive field in the retina is non-circular or asymmetrical. This suggests that the stimulation must be performed asymmetrically instead of symmetrical, circular stimulation as implemented in current retinal prostheses.

1.5.2 A model to enhance contrast under mesopic lighting conditions

Visual perception under mesopic lighting condition is the perception of the eyes in low-light conditions such as that during sunset, dusk, or twilight. Two possible pathways inside the retina, namely, cone gap junction and rod-AII amacrine cells,

have been proposed as the underlying process in mesopic lighting conditions. This thesis focuses on the second pathway and proposes a possible circuitry at the amacrine cell level to explain the mechanism of contrast enhancement. The findings show the capability of the model to process information in mesopic lighting conditions; moreover, they are consistent with the results of other studies with regard to the temporal output of the retina. The findings of this study show that a different circuit to enhance the contrast under low-light conditions possibly exists in the retina. Furthermore, this switching mechanism is helpful in next-generation retinal prostheses, since users may be able to perceive contrast better in low-light scenarios.

1.5.3 A model to enhance colour vision

Besides contrast enhancement, colour correction has attracted the interest of many researchers to explore the underlying mechanisms in the retina, although various researchers believe that colour correction occurs in the V4 area. In the retinal approach, previous studies have proposed a correction mechanism at the horizontal and ganglion cell levels (Heywood, Gadotti and Cowey, 1992; Kamermans, Kraaij and Spekreijse, 1998; Vanleeuwen *et al.*, 2007). This thesis proposes a hypothesis that the non-linear circuit at the ganglion cell with midlevel amacrine cells plays a critical role in spatial and temporal response of the retina in colour correction. The results of this thesis clarify that the correction occurs at the ganglion–amacrine

level, and in the temporal domain, the ganglion cells respond in a ‘push–pull’ fashion. This result is consistent to observations in a recording of ganglion cells in the New Zealand White rabbit in another study conducted by Roska et al. (Roska, Molnar and Werblin, 2013). These simulations show that parallel stimulation, in general, and ON and OFF stimulations, in particular, are possible in the retina. This feature should be integrated in the retinal prostheses in the future. With this feature, the device will be able to provide more accurate signals. Therefore, it will reduce the energy used, and prevent the device from heating up the retina after prolonged use.

1.5.4 Conceptual design of retinal prosthesis

The above-mentioned studies of the retinal model have led to the suggestion that future retinal prosthesis should be able to assist with vision during night time, indoor vision, and recognition of coloured objects. Based on simulations of the different proposed theories, a next-generation design of retinal prostheses is presented with an improved design with regard to stimulation. In detail, the arrangement of the stimulating electrodes is proposed to be mobilized, forming an asymmetrical receptive field, as further explored during the Hermann grid experiments. Application of this proposal will enable the device to more precisely transfer signals to the retina, thus reducing the operational energy needed. Using this concept, future retinal prostheses may provide more useful visual information

to the blind, and help them to perform activities of daily living both easily and comfortably.

1.6 Thesis overview

The remainder of this thesis is organized into nine chapters. Chapter two presents background studies of the retina, retinal diseases, and retinal prosthesis. The chapter aims to provide information about the biological structure of the retina and introduces the concept of the retinal prosthesis for restoring vision loss caused by popular retinal diseases.

The third and fourth chapters review several related studies of the state-of-the-art retinal prostheses and retinal modelling, respectively. In these chapters, a complete review of various types of retinal prosthesis devices and their current statuses are presented. These chapters also describe the state-of-the-art of different approaches in retinal modelling.

Chapter five presents the retinal model that was developed in this thesis, and describes the biological and electronic aspects of this model. Analysis of the model structure and methodologies to create the model are also discussed in this chapter.

Chapter six describes the application of the proposed model based on Hermann's grid illusion, and discusses the results obtained from different configurations. This chapter focuses on the receptive field in the retina, and on how

the model can successfully explain the Hermann grid illusion using its receptive field concept.

Chapter seven discusses another application modelling the contrast-processing mechanism under mesopic conditions. The results from the model show that the rod-AII amacrine cell pathway plays an important role in adjusting the contrast under specific conditions of the retina. This chapter also discusses the spatial responses of the model in contrast processing and assessment in order to compare the outputs of the model in different configurations.

Chapter eight presents the role of amacrine cells in processing contrast and colour, and in generating the ‘push–pull’ mechanism in firing of the ganglion cells in colour processing. This chapter also focuses on the temporal responses of the model, and analyses the spike train to highlight the role of amacrine cells in synchronizing the responses of the ON and OFF pathways.

Chapter nine presents a conceptual design of the next-generation retinal prosthesis based on discoveries using the proposed model. This chapter focuses on further development of the prosthesis device, and what should be included in the next-generation prosthesis to help the blind achieve better vision for daily activities.

Chapter ten concludes with the success of the proposed model in modelling different circuitries inside the retina and discusses related topics focusing on near-future developments.

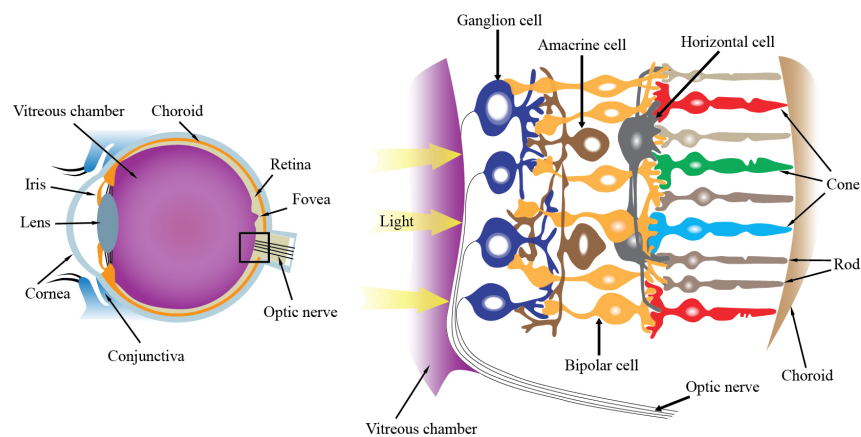
CHAPTER 2

BACKGROUND STUDIES

2.1 The retina

2.1.1 Structure of the retina

The world is perceived through the eyes, which processes the light that is reflected from the objects to form images in the brain. Light stimuli enter the eyes, which are then converted into the electrical stimuli by the retina. The electrical patterns generated by the retina represent an early, yet complex, level of information processing. This low-level information is passed on to the higher regions of the brain, eventually leading to a visual understanding of the environment. As shown in the anatomical depiction in Figure 2.1, the retina consists of several layers, each



with its own name and functionality.

Figure 2.1: Location and structure of the retina. On the left: Location of the retina in the eye. On the right: Retina and its cells.

There are six main layers in the retina: the photoreceptor, outer nuclear, outer plexiform, inner nuclear, inner-plexiform (IPL), and ganglion cell layers. The layers are differentiated primarily based on their constituent cells and connections. In terms of the cellular composition, there are five major cells in the retina:

- Rods and cones

These cells are present in the photoreceptor layer; they sense the light stimuli and convert it into electrical signals. Rod and cones have different morphologies and functions. Rods primarily assist with night (scotopic) vision and have only one type of cell in terms of wavelength sensitivity. Cones are of three types (red, green, and blue), and each type responds to different wavelengths (i.e. long [L], medium [M], and short [S] wavelengths), which primarily assist with day (photopic) vision.

- Horizontal cells

These retinal cells are present in the inner nuclear layer. They connect to rods, cones, and bipolar cells. Horizontal cells receive an input primarily from photoreceptors, and provide lateral inhibition to both bipolar cells and photoreceptors. In addition, there are three types of horizontal cells called H1, H2, and H3. Each of these cells connect to the specific cones in the photoreceptor layer. H1 connects to L and M cones, H2 connects to M and S

cones, and H3 connects only to blue cones. Moreover, each cell provides a feedback signal to the cones connected to them. H1 and H2 play a role in distinguishing colour pathways in colour vision. Because the role of H3 cells remains unclear, only H1 and H2 cells will be discussed further in CHAPTER 8.

- Bipolar cells

These cells are present in the inner nuclear layer, and they transfer signals from the rods, cones, and horizontal cells to the amacrine and ganglion cells. Due to the separation of photoreceptor pathways as L, M, S and rods, four different pathways are formed at the bipolar cell layer, namely L bipolar, M bipolar, S bipolar, and rod bipolar cells. These cells receive the corresponding signal from photoreceptors and transfer it to the IPL as an excitation or inhibition signal. If the signal received from the bipolar cell is an excitation signal, that bipolar cell is called the ON bipolar cell; in contrast, the OFF bipolar cell transmits an inhibition signal. This forms the ON and OFF pathway in the retina, and these pathways traverse the retina from the bipolar cells to the ganglion cells.

- Amacrine cells

Between the bipolar cells and the ganglion cells lie the amacrine cells, which consist of many sub-types. These cells make a network of lateral inhibition signals, and they alter signals primarily from the bipolar and ganglion cells. There are several types of amacrine cells, and most of them are not yet fully

understood. In this thesis, the AII and cone amacrine cells have been focused on. The connection between them in the retina is discussed in CHAPTER 7 and CHAPTER 8 later.

- Ganglion cells

Ganglion cells are the output cells of the retina. They mostly receive analogue input (i.e. graded potentials) from the bipolar and amacrine cells. They convert them into digital signals (i.e. action potentials or spikes) and send them to the higher regions of the brain via the optic nerve. Similar to the bipolar cells mentioned above, the ganglion cells are also classified into ON and OFF types, which spike differentially from each other. The pattern of ON and OFF firing of the ganglion cells and the differences between the ON and OFF signals will be discussed in CHAPTER 8.

Beyond the retina, the visual signal travels to the brain via the optic nerve where it arrives at the lateral geniculate nucleus (LGN). There are six layers in the human LGN. The inner two layers named are called the magnocellular layers, while the outer layers named are called the parvocellular layers, and this layering is variable between primate species. On the other hand, the LGN serves to connect the optic nerve and occipital lobe and locates as two parts in half left and right hemispheres. Thus, the left visual field from both eyes is sent to the right hemisphere while the right visual field in both eyes connects to left hemisphere, respectively. After the LGN, the information is sent to visual cortex area called V1 and higher cortical

areas such as V2, V3, V4 and V5. In terms of visual information processing, V3 and V4 are responsible for shape and colour, respectively, while V5 is responsible for motion processing.

As mentioned above, the ganglion cell is the primary generator of action potential signalling to the brain; however, several bipolar and amacrine cells have the ability to generate this signal. Saszik and Steven have found that ON bipolar cells in ground squirrels use not only graded potentials but also action potentials to encode light (Saszik and DeVries, 2012). Baden and colleagues also found that the bipolar cells in fish convert graded potentials to action potentials (Baden et al., 2011, 2013). Heflin and Cook reported that narrow and wide dendritic field amacrine cells fire action potentials in two different ways—single spiking and repetitive spiking, respectively (Heflin and Cook, 2007). In addition, Zhou and Fain found that starburst amacrine cells transform from spiking to non-spiking cells during retinal development (Zhou and Fain, 1996). Moreover, bipolar and amacrine cells use spike coding simultaneously with graded potentials. Thus, two different types of codes are used to compute signals in these cells. The action potential in bipolar and amacrine cells is still attracting the attention of many scientists to explain the origin and mechanism behind spike generation in these cells. In this thesis, only the ganglion cell has been considered to generate the action potential. The scope of this thesis is focused on the relationship between image processing and retinal processing mechanisms, rather than the biological phase in the retina.

These types of cells responsible for these processing mechanisms are not yet fully understood, especially with regard to the number of subclasses of amacrine cells that are able to fire action potentials. In addition, the starburst amacrine cell, an amacrine cell that is well known for generating action potentials, is mostly used for the purpose of direction selectivity in the retina. Thus, image-processing mechanisms such as depth and motion responses in the retina are beyond the scope of this thesis because this information can be inferred from the visual signal in the current prosthesis device. In terms of depth information, Stiles et al. used phosphine information to determine the distance from the user to objects in front of them. In particular, larger phosphine indicates closer objects while further objects are indicated by smaller phosphine (Stiles et al., 2014). In terms of motion perception, other reports show that training can help patients to use utensils or even shoot a basketball with the current generation of retinal prostheses (Luo and da Cruz, 2014) and this is done by training the user to become familiar with the phosphine vision. On the other hand, colour and contrast information have not been inferred from phosphine information because the vision constructed with phosphine is black and white vision. Hence, finding an optimized method to stimulate the brain with colour and contrast information will be the focus of this thesis.

2.1.2 Retinal connectivity

In the retina, all the cells are connected through two different connectivity types called electrical and chemical synapses. In electrical synapse, the synapse between two abutting cells allows ions to flow from one cell to another cell, called the presynaptic and postsynaptic cells, respectively (Kandel, Schwartz and Jessell, 2000). The electrical synapse is also called the gap junction between two cell membranes, and there are several gap junctions between cells in the nervous system and retina in particular. In each gap junction, there are several channels. Each channel has one hemi-channel on presynaptic and one hemi-channel on postsynaptic cells, which allows ions such as sodium and potassium to pass to maintain metabolic and electrical continuity (Hormuzdi *et al.*, 2004). Additionally, there are gap junctions between the same types of cells such as cones, rods, horizontal, amacrine cells, and ganglion cells and between different cells such as rods and cones (Gibson, Beierlein and Connors, 2005). The chemical synapse, on the other hand, is a small gap between two cell membranes, which allows neurotransmitters to flow from the transmitter terminal in a presynaptic cell to receptors in a postsynaptic cell. When the action potential arrives at the cell axon terminal, it creates an influx of calcium ions through calcium-selected gate channels. This flow triggers a cascade of biochemical processes, resulting in the release of neurotransmitters into the transmitter terminals. When these transmitters

arrive at the receptor terminal, they change the concentration of ions in postsynaptic cells. This leads to the generation of action potential in postsynaptic cells (Bennett and Zukin, 2004; Palacios-Prado *et al.*, 2013). In the retina, chemical synapses occur between different cell types, causing the transfer of chemical signals from one cell to another, such as from photoreceptor to horizontal and from horizontal to bipolar cells, and this mechanism is the same for transferring signals between bipolar, amacrine, and ganglion cells (Kandel, Schwartz and Jessell, 2000). In addition, in chemical synapse, chemical flow occurs only from a presynaptic cell to a postsynaptic cell; therefore, chemical synapse is considered unidirectional synapse. In contrast, in electrical synapses, ions freely move through ion gate channels; thus, this type of synapse is bidirectional. Moreover, the electrical synapse is faster than the chemical synapse, but neuronal connectivity is widely established by chemical synapses (Llinás, Steinberg and Walton, 1981; Lytton and William, 2002).

2.2 Functions of the retina

The retina performs several major functions such as photon transduction, data compression, light/dark adaptation, and spatial filtering for encoding the light stimulus into spiking signal. Although there are other functions, the aforementioned functions are necessary for the retina to encode visual information; thus, only these functions are discussed in this section.

2.2.1 Visual photo-transduction

The photoreceptor layer contains rods and cones, which have an outer segment that is composed of a membranous disk for absorbing light through the light-sensitive photo-pigments in cones and rhodopsin in rods. The inner segments, in contrast, contain a cell nucleus and connections to both the bipolar cells and horizontal cells. In the outer segment, the protein portion of a molecule called opsin has seven trans-membrane domains that traverse the membrane bilayer. Besides the opsin is bound to the retinal, which is a type of lipid made from vitamin A that exists in two forms, trans and cis, indicative of the relative orientation of functional groups within a molecule. In the dark, the retinal is in the cis-form, absorbing the photons and quickly changing to the trans-form. This process is called the bleaching process (Hubbard, Wald and J, 1952; Hubbard and Kropf, 1958). In contrast, the cis-form retinal changes to the trans-form when the retina perceives the change in light conditions from light to dark, and this explains the temporary blindness experienced when entering a dark room from bright light conditions. Before the transduction process, one must understand the roles of the different currents in the retina. Basically, sodium (Na^+) and potassium (K^+) ions are present both inside and outside the membrane, and corresponding to these ions are the cGMP-gated Na^+ and non-gated K^+ channels that allow only Na^+ to move into the membrane and only K^+ move out the membrane, respectively; moreover, the Na^+ channel remain open in

the dark. This movement creates an inward Na^+ current flux from the outside to the inside of the membrane and a contrasting outward K^+ current flux from the inside to the outside of the membrane. In addition, Calcium (Ca^+) and Chloride (Cl^-) currents are also formed based on the flow of Ca^+ and Cl^- ions. In addition, the photoreceptor membrane is hyperpolarized by a K^+ current at -70 mV and depolarized at -40 mV by a Na^+ current (Leskov *et al.*, 2000; Ebrey and Koutalos, 2001).

In the dark, due to the steady Na^+ current, the rod membrane is continuously depolarized, and this leads to the release of neurotransmitters into the synapse between photoreceptor and bipolar cells through an increase in Ca^+ in the membrane. This neurotransmitter is a glutamate that binds to a glutamate receptor in bipolar cell synapse and renders specific channels close in ON and open in OFF bipolar cells. Consequently, ions move through the channels in ON bipolar cells and stop moving in OFF bipolar cells, leading to hyperpolarization in the ON bipolar cells and depolarization in the OFF bipolar cells in the dark (Baylor, Lamb and Yau, 1979).

When light strikes the eye and photons approach the photoreceptors, rhodopsin changes from the cis form to the trans form, which initiates a cascade event that lowers the concentration of cGMP by converting it to GMP. As a result, the cGMP-gated Na^+ channel is closed; this leads to reduced current in the inward Na^+ influx and the membrane is hyperpolarized. The release of glutamate decreases due to the

decreased calcium level, and the glutamate cannot bind to the bipolar cell receptor, which in turn depolarizes the ON and hyperpolarizes the OFF bipolar cells. This process is the same for both cone and rod cells, and the difference between them is the wavelength of the light that affects the rhodopsin (Baylor, Lamb and Yau, 1979).

2.2.2 Data compression

In the retina, the hundred million photoreceptor cells outnumber the half a million ganglion cells. This gives rise to the problem of data transfer from several photoreceptors to a few ganglion cells, since the retina has to cover every detail in the scene being viewed. To overcome this issue, data compression takes place in the retina by creating a blurry vision in the periphery and a clearer vision in the point that the eyes focus on. This reduces redundant information in the surrounding vision but still maintains important information in the central vision for processing (Kelly, 1984). This compression originates from the visual eccentricity in the retina where the cone density is the highest at the central fovea. In particular, around 150000 cells per mm^2 are present for processing in the central fovea. This number is decreased to approximately 2000 cells per mm^2 in the peripheral vision. In addition, the cones in this field connect as ‘one-to-one’ to the bipolar cell and ganglion cell, which allow high visual acuity in central vision. This is because the signal from one cone to the ganglion cell is not combined with or affected by the

neighbouring cones (Tannazzo, Kurylo and Bukhari, 2014). With the data compression mechanism, redundant information is reduced and only useful information is processed; thus, the retina transfers and processes less information. This helps the retina cope with a large amount of information perceived from the environment by processing vital information and temporarily ignoring irrelevant data.

2.2.3 Light/dark adaptation

Another function of the retina is the ability to maintain vision when switching from dark to bright light areas and vice versa. When people move from a dark area to a bright area, they will perceive a change in vision, such as white light, and normal vision returns after few seconds. The photoreceptor layer, particularly the cones and rods, is responsible for this phenomenon (Bartlett and Graham, 1965). As discussed previously, cones are responsible for vision in day light and rods are responsible for vision in dark light areas; the switching of vision from cones to rods and vice versa is called light/dark adaptation in the retina. In light adaptation from dark to bright light, both rods and cones are saturated because the light level exceeds the maximum threshold of rods; therefore, white light is perceived initially. After saturation, the cones start to function while the rods are suspended, restoring normal vision in bright light, with the light intensity decreasing from bright light to normal, and this process can last for five to ten minutes. On the other hand, dark

adaptation is the process of switching from cones to rods when moving from bright light to a dark area (Bartlett and Graham, 1965). In the light area, rods are suspended and only cones are activated. When moving to a dark area, rhodopsin is regenerated in the rods, and this increases the sensitivity of rods in dark areas; thus, normal vision is restored (Aguilar and Stiles, 1954). In addition, during light and dark adaptation, the pupil reduces and enlarges in size, respectively, to allow the light to reach the photoreceptors where the cones and rods have the highest density in the fovea. Moreover, horizontal cells in the retina control the suspension of rods and cones while adapting to the scene through their inhibition feedback to photoreceptors.

2.2.4 Spatial filtering

As discussed in the previous section, peripheral vision is blurred to compress the data that needs to be processed in the retina, and this blurred vision is the result of a process called filtering (Morgan and Watt, 1997; Zeck, Xiao and Masland, 2005). Filtering, by definition, is a process that keeps only the wanted elements and removes the unwanted elements, and retinal filtering is performed to cope with the many details of perceived vision. During the compression process, peripheral vision is filtered out and only central vision is clearly maintained for processing. The mechanism underlying this function is the connection between the hundred million photoreceptors and the million ganglion cells, which forms a structure called

‘receptive field’ in the retina. Basically, the receptive field of a cell has been defined as a space that contains stimulated cells that connect and provide an output to that cell. In the retina, the receptive fields of the ganglion cells are divided into two regions—centre and surround—separated by the responses of connected photoreceptors to the light stimulus; thus, the receptive field is categorized into ON-centre/OFF-surround and OFF-centre/ON-surround (Lorach *et al.*, 2012). For the first type, the ganglion cells respond with more spikes when light falls on the centre region and less spikes in the case of the surround region. The second type is the reverse of the first type, which makes the ganglion cells respond with less spikes on centre stimulation and vice versa. The variations in the receptive field not only help the retina to compress processed information but also filter out the details. For example, when the centre–surround receptive field is involved, the retina filters out the details in the visual information and retains information regarding the boundaries of the object only (Holliday, Ruddock and Skinner, 1984). This helps the retina to distinguish the objects by their boundaries and eliminate other information that is not helpful in differentiating the object. By utilizing this function, the redundant information is reduced in some basic tasks and the retina can process more information at the same time.

In summary, the retina is a multilayer neural tissue that converts light signals into electrical signals that can be decoded by the brain. There are six layers in the retina, and each layer consists of specific types of cells and/or connections. Retinal

cells are connected to each other in complex ways, forming circuits that implement rich information-processing channels. As the retina is a complex information-processing system, different types of damage to its circuits lead to different types of vision problems, some of which are discussed in the next section.

2.3 Retinal diseases

Each year, millions of people succumb to blindness through eye diseases such as age-related macular degeneration (AMD) or retinitis pigmentosa (RP). Approximately 700,000 new AMD cases are diagnosed every year in the US, and approximately 10% of them are considered legally blind.

AMD is caused by the abnormal aging of the retinal pigment epithelium (RPE). The major symptoms of AMD are the formation of yellow drusen on the RPE and the proliferation of leaky vessels in the subretinal space. In terms of vision, early AMD symptoms consist of a distorted field of view in the centre, eventually leading to an almost complete loss of vision in the central 30 degrees. A number of treatments focus on slowing the progress of AMD but no complete cure exists for this disease.

Symptoms of early retinitis pigmentosa consist of poor night vision due to damaged rods (Berson, 1993; Sharma and Ehinger, 1999). Following this, the cones are gradually damaged leading to loss of vision in the mid-periphery. Complete peripheral vision is eventually lost. In few exceptional cases, RP patients still have

major vision in the foveal or parafoveal regions, whereas vision in the remaining parts of the retina is completely lost. The photoreceptors can be subject to over 100 defects, and thus far, no treatment has been established for RP (Heckenlively *et al.*, 1988).

Although retinal cells are destroyed due to AMD or RP, some parts of the retina are still intact. For instance, in RP, although only 4% of the photoreceptors remain, approximately 30% of the ganglion cells and 80% of the inner retinal cells remain intact (Kim *et al.*, 2002). In AMD, the percentage is higher, with 90% of the inner retinal cells remaining intact (Weiland, Liu and Humayun, 2005). Thus, AMD and RP do not cause complete degeneration of the retina, and vision may be restored by using the remaining cells.

2.4 Retinal prosthesis

2.4.1 The device

A retinal prosthesis is a device that can help the blind to restore the visual function of the damaged parts of the retina by stimulating the ganglion cells inside the retina through an electrode array implanted in the retina. In general, the device contains three major components: a video recorder, encoder, and electrode array, with other peripheral components such as battery, power, and data transmitter. The video recorder, encoder, and peripheral components are designed as a wearable device and placed outside the retina, whereas the electrode array is implanted inside the

retina. In particular, the video recorder is a commercial camera with a resolution of 640×480 (Lytton and William, 2002; Asher *et al.*, 2007), which is supplied by external power via a power cord. In many designs, the camera is mounted on a glass so that it can capture a scene in accordance with the head direction of the patient. Typically, the encoder is manufactured as an FPGA (Field-Programmable Gate Array) or SoC (System on Chip), with different configurations based on different approaches, which are also supplied via external power. On the other hand, the stimulation component is a $520\text{-}\mu\text{m}$ μm array of electrodes that are located in the retina, such that the array of electrodes will communicate with the retinal cells, such as the ganglion or bipolar cells, depending on the prosthesis approach. Each electrode can provide a certain amount of electrical stimulus to the cell it comes in contact with. The data from the encoder to the electrode array can be transferred using a wire or by wireless technology, depending on the design of the prosthesis.

2.4.2 Device output

The camera will record and transfer the received signal to the encoder for processing. After receiving the signal, the encoder processes the signal using various algorithms to convert the spatial and temporal signal into spiking signals. The spiking signals are then transferred to the stimulation component that is implanted inside the retina. At this stage, depending on the algorithms and configurations in the encoder, the electrode array provides a sequence of stimulus

signals that substitute for the damaged part of the retina and stimulate the ganglion cell that they come in contact with. Thus, the ganglion cells are stimulated by these stimuli and generate action potential, propagating along the optic nerve to the brain. The brain receives and translates this signal into visual perception such as edge detail, motion, and colour, based on the format of the spike train from the ganglion cells, and different spike patterns provide different information to the brain. How the brain translates the spike into visual perception and how the format of the action potential affects vision remains debatable.

Besides electrical stimulus, a retinal prosthesis based on chemical stimulation of the retinal cells has also been developed by a few groups of researchers. Instead of providing an electrical stimulus, this prosthesis uses microfluidics to inject the neurotransmitter glutamate into the retinal cell and modulate spike rates. In this type of prosthesis, the encoder and stimulation components are different from the electrical stimulus-based prosthesis with regard to the placement of the stimulating electrode and encoding for controlling the chemical flow through the chemical transmitters. For example, Noolandi et al. introduced a neurotransmitter retinal prosthesis using an inkjet print-head in 2003, whereas Finlayson and Iezzi used glutamate to stimulate the ganglion cells in cats (Noolandi, Peterman and Huie, 2003; Iezzi and Finlayson, 2009). Recently, Rountree et al. developed a neurotransmitter prosthesis, which was tested on ganglion cells and bipolar cells in rats in 2013 (Rountree *et al.*, 2013). Based on these attempts, chemical stimulation

has been found to have some advantages over electrical stimulation, such as no excitotoxic effects in the short term (Rountree *et al.*, 2013) and lower energy consumption than the electrical prosthesis (Noolandi, Peterman and Huie, 2003). On the down side, the spiking rate of ganglion cells is limited due to the chemical injection durations and difficulty in stimulating ON and OFF pathways simultaneously. Because the neurotransmitter prostheses have only been recently developed, this thesis focuses only on electrical prosthesis.

In both electrical and chemical prostheses, the two compulsory components are the encoder and stimulator, which convert visual information into neural signals and stimulate retinal cells, respectively. In an ideal retinal prosthesis, the encoder would be able to filter the important information in the visual scene and convert these visual inputs to a neural code such as a spiking signal. In this encoder, the accuracy of spiking outputs is affected by the algorithm to convert the visual signal into neuronal coding. If the algorithm is not properly optimized, the information of the visual signal is not fully converted to the neural code, resulting in inconsistent stimulation of the retinal cells. In contrast, the ideal stimulator would be placed in an optimized position to maximize the contact with the retinal cells through the electrode array. In an optimized position, the retinal cells are precisely stimulated; thus, the current used for stimulation is reduced. This improves the impact of the retinal prosthesis, because with reduced current, the power used is decreased, and consequently, the retinal cells receive less heat. Reducing the heat involved makes

the retinal cells less prone to damage, thus increasing the usage time of the device after implantation. In conclusion, use of proper algorithms for the encoder and placement of the stimulation component are important factors that should be considered when designing and developing an ideal retinal prosthesis.

2.5 Summary

The motivation and overview of this thesis are presented in the beginning of this chapter followed by introductions to the retina, retinal diseases, and retinal prosthesis. The retinal structure and retinal diseases are discussed to provide a better understanding of the concept of retinal prostheses and how they can be used for restoring vision. The details and variations in retinal prostheses will be further discussed in the next section.

CHAPTER 3

RETINAL PROSTHESIS REVIEW

In general, retinal prostheses are categorized into two major types, namely extraocular, when the device is placed outside the eye, and intraocular, when the device is placed inside the eye. Cortical prosthesis is an extraocular prosthesis, whereas optic nerve, epiretinal, and subretinal prostheses are intraocular prostheses. In detail, a cortical prosthesis replicates signals in the visual cortex directly, whereas an optic nerve prosthesis stimulates the optic nerve to mimic the visual signals to the brain. A subretinal prosthesis stimulates bipolar cells, whereas the epiretinal prostheses stimulate the ganglion cells in the retina. A general view of these prostheses is provided in Figure 3.1. This chapter will discuss each type of prosthesis and analyse the strength and drawbacks of the different approaches.

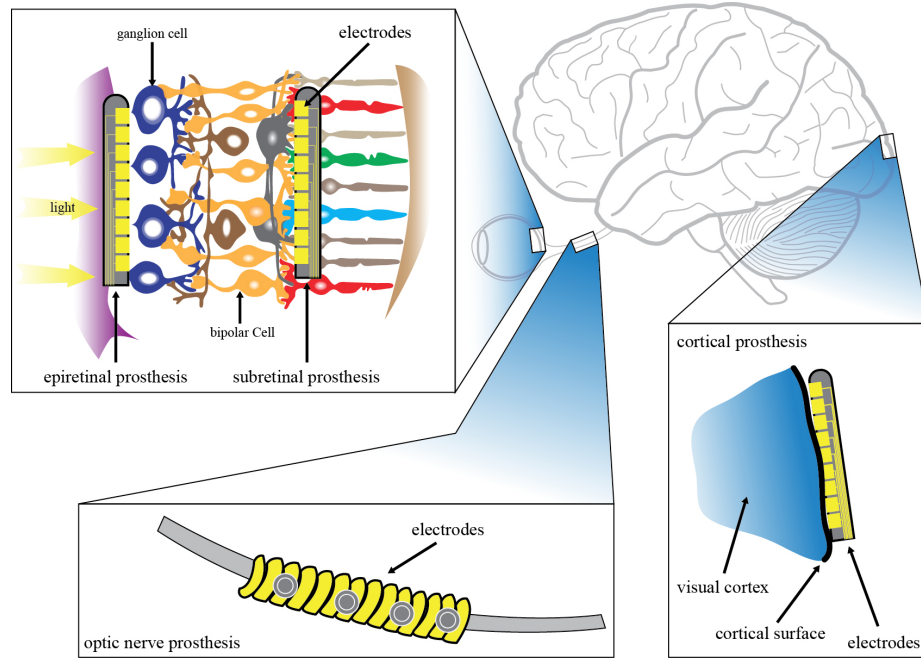


Figure 3.1: Different approaches of retinal prostheses and their placements.

3.1 Extraocular prostheses

3.1.1 Surface cortical prosthesis

The visual cortex is located in the occipital lobe at the back of the brain and plays a role in processing visual information (Schmolesky, 2014). To restore vision in the blind, this area is stimulated by using an electrode array implanted in the skull, and the perceived visual perception, called phosphenes, allows the blind to navigate the world. The phosphenes emitted during the stimulation of electrodes to visual neurons are simple spots or flashes of light. Dobbie implanted 50 electrodes in the occipital lobe of volunteers to restore visual perception via the visual cortex

(Dobelle, 2000). After a brief training period, volunteers were able to recognize six-inch square characters at five feet and count fingers as well as use this device to travel alone on the city metro (Javaheri *et al.*, 2006). Moreover, no epileptic symptoms or systemic problems were observed after implantation into six other volunteers, but the device had to be removed because of the risk of infection (Weiland and Humayun, 2003; Foerster, J and Javaheri, 2006). However, it was difficult for the patients to recognize large characters due to the ‘bottleneck’ caused by information exceeding the limit of the visual tunnel. Other patients also perceived ‘halos’ surrounding phosphenes or recognized distinct phosphenes in addition to being unable to control the number of phosphenes. Consequently, researchers in this field moved on to intracortical stimulation (Dobelle, 2000; Uhlig *et al.*, 2001; Weiland and Humayun, 2003; Foerster, J and Javaheri, 2006). The limitations of surface cortical stimulation are expected to be overcome by means of two projects, namely the Illinois Intracortical Visual Prostheses project and the Utah Electrode Array. In these projects, smaller electrodes were used for closer contact with the target neurons and lower stimulating current. In particular, 152 intraocular microelectrodes were used in the Illinois device and 100 electrodes in the Utah device (Uematsu *et al.*, 1974; Maynard, Nordhausen and Normann, 1997; Margalit *et al.*, 2002). In studies of animal and short-term human implants, these prostheses presented the ability to produce colour phosphenes and operated

regardless of the damaged parts of the early visual system (e.g. the retina) (Weiland and Humayun, 2006).

3.1.2 Optic nerve prostheses

This type of prosthesis compensates for the disadvantages of cortical prostheses by covering a large cortical area by focusing on a small area connecting the retina and the brain, i.e. the optic nerve. In this prosthesis, a spiral cuff is used to stimulate the optic nerve and create visual sensations (Brindley, 1965). This prosthesis is depicted in Figure 3.2: a cuff wraps around the optic nerve (A) and stimulates it based on the signal received by a camera (B). In practice, Veraart et al. performed this type of prosthesis on blind volunteers and obtained encouraging results. Patients were able to perceive multiple phosphenes and interact with the environment by demonstrating basic pattern recognition skills, such as recognition of different shapes, line orientations, and even letters in some cases (Veraart *et al.*, 1998, 2003; Troyk *et al.*, 2003; Chader, Weiland and Humayun, 2009).

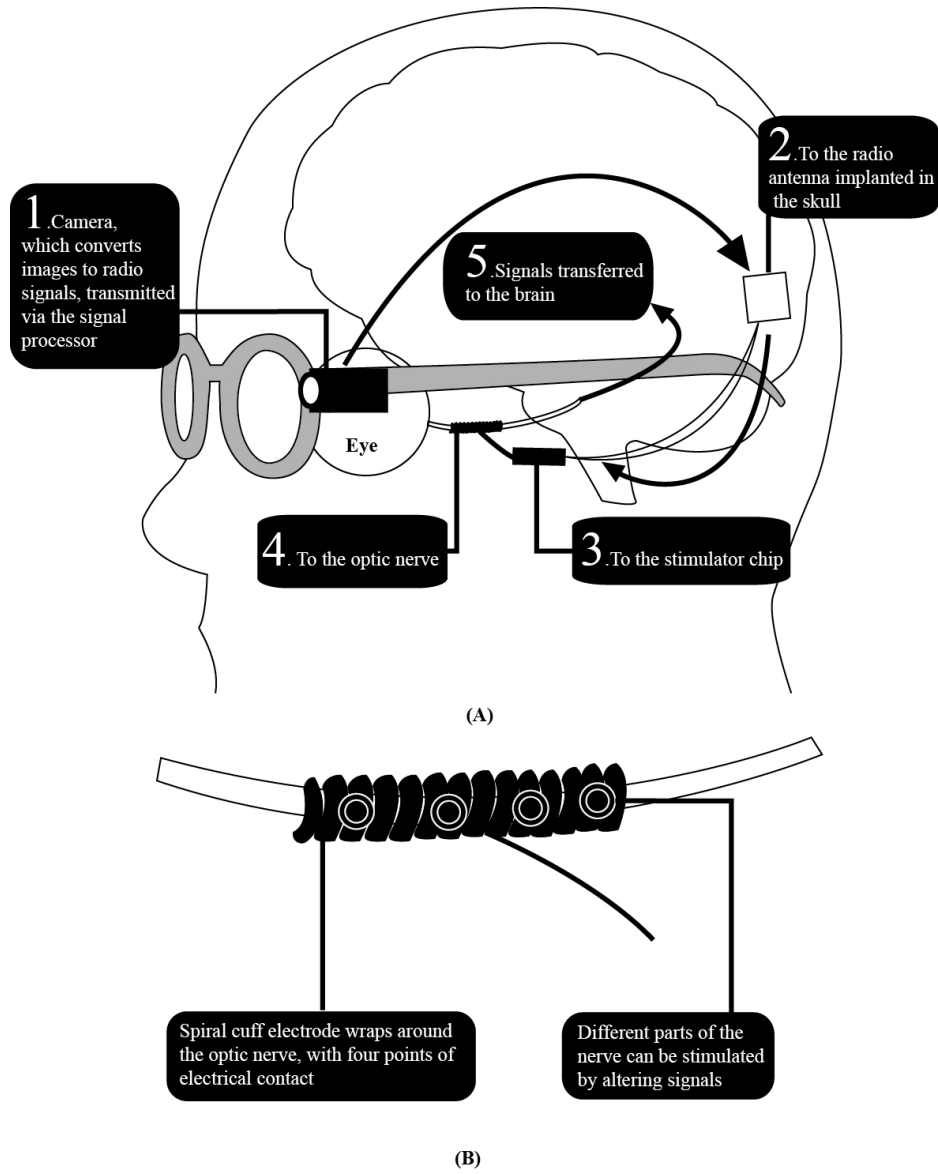


Figure 3.2: The optic nerve prosthesis. Reproducing with permission (Weiland, Liu and Humayun, 2005)

Despite some encouraging advantages, the optic nerve prosthesis has one significant problem, i.e. it needs a large number of contacts to the optic nerve; this

leads to the risk of infection in the central nervous system and hinders blood flow inside the optic nerve. Moreover, stimulation and the implant must be operated precisely and properly due to the density of the axons in the optic nerve (Brindley, 1965).

3.2 Intraocular

3.2.1 Epiretinal prostheses

The intraocular prostheses are implanted inside the eye, instead of outside; this is done using various technologies such as microelectronics, microelectronics packing, power and data telemetry as well as computer vision and image processing. Generally, intraocular prostheses are classified into two major categories, epiretinal and subretinal, based on the location of the implants.

An epiretinal prosthesis is implanted on the inner part of the retina and is in close contact with the ganglion cells (Oozeer *et al.*, 2006). A processing component processes visual signals acquired from an external camera and converts those signals into electrical signals for a stimulator component to stimulate the ganglion cells. This procedure requires power and data telemetry to transfer data and power from the outside to the intraocular parts. Various designs of epiretinal prostheses have been proposed and tested in animal and human trials to achieve the goals of maximizing the functionality of the remaining retinal tissue, while minimizing power consumption and the number and size of devices implanted in the eye.

Arguably, the most mentioned epiretinal prosthesis is the intraocular retinal prosthesis (IRP) by Mark Humayun, from the University of Southern California and the private company Second Sight Medical Products, Inc. (Ahuja *et al.*, 2008; Caspi *et al.*, 2009; Weiland, Cho and Humayun, 2011).

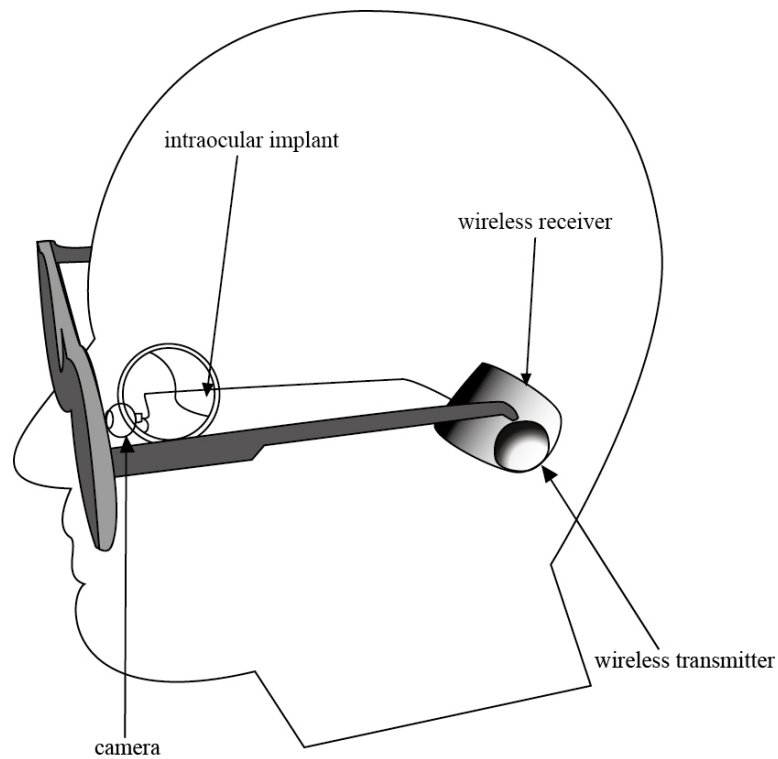


Figure 3.3: The schematic of the prosthesis. Reproducing with permission (Weiland, Liu and Humayun, 2005).

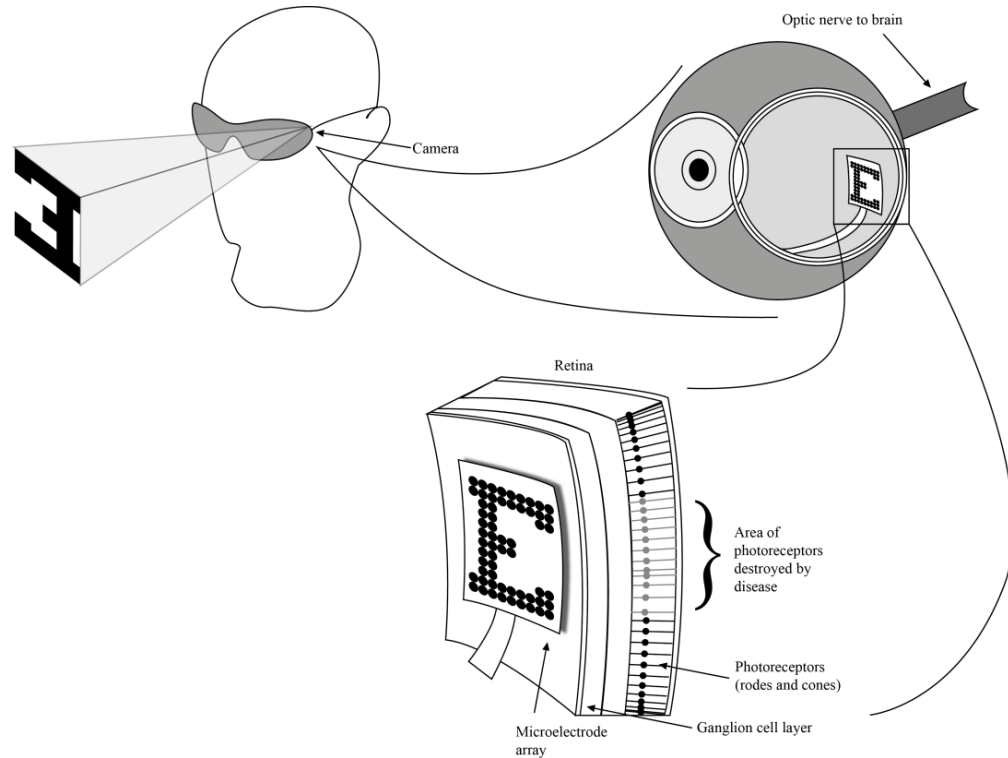


Figure 3.4: The detail of the intraocular implant. Reproducing with permission (Weiland, Liu and Humayun, 2005).

Two major parts of the prosthesis are an external camera mounted on a pair of glasses, and an intraocular unit as depicted in

Figure 3.3. The intraocular unit is an image processing unit, and its functionality consists of processing visual signals recorded by the camera. The processed data is then transmitted to the stimulator unit, which consists of 16

platinum microelectrodes to stimulate the inner retinal neurons (Weiland and Humayun, 2005; Yanai *et al.*, 2007). This process has been illustrated in Figure 3.4.

The first version of this prosthesis, Argus I, was tested on humans after experimentation on animals, which yielded some encouraging results. In terms of the required threshold current to elicit visual responses, 10 out of 16 electrodes remained constant, whereas three required an increased current and three required a decreased current. Interestingly, the size of the phosphenes also increased corresponding to the higher current (Humayun *et al.*, 1999). In terms of visual responses, phosphenes were perceived, and after two and a half months of training, the patients were able to discriminate the perception pattern of phosphenes from the different stimulating patterns; thus, they were able to interact with the surrounding world and tackle complex tasks such as differentiating brightness levels or direction of motion of objects (Humayun *et al.*, 1996; Nanduri *et al.*, 2008). However, the patients also noted four different colours of phosphenes and a perceived ‘halos’ effect as well.

The second version of the device (Argus II)(Ahuja *et al.*, 2008; Chader, Weiland and Humayun, 2009) incorporated some significant changes in hardware.

The improvements are listed below:

- 60 electrodes instead of 16;
- Wireless data transfer; and
- MEMS components for better fixing of the device in the eye ball.

In addition, in this device, the visual field is increased to 20°, and human trials testing this device have yielded positive results, with patients capable of differentiating basic forms of motion, perceiving light and dark environments, and even shooting baskets (Humayun *et al.*, 2012). With these results, the Argus II device was approved by FDA in February 2013, and it became commercially available in Europe in March 2011 and in USA in January 2014. The next-generation Argus III is under development, with the number of electrodes increased to more than 200 units, with the aim of reducing the processing time to less than 3 seconds as in Argus II (Weiland, Cho and Humayun, 2011; Fernandes *et al.*, 2012; Humayun *et al.*, 2012). With an increase in the number of electrodes, the future device is expected to provide more information that is meaningful through ‘pixelated vision’ because increased stimulation in the retinal cells would lead to increased visual signals transferred to the brain. To achieve this, many obstacles need to be overcome, such as minimizing the size of the electrode, reducing the crosstalk effect between electrodes, or mapping the electrode to ganglion cell population. Based on these challenges, experiments are being conducted to determine the optimal method to manufacture and implement the next-generation devices. This thesis will focus on the last obstacle, i.e. determining the optimal method to map the electrodes to the ganglion cells by studying and experimenting with the connectivity of retina in general and the ganglion cells in particular to

elucidate the relationship between visual processing mechanisms and different patterns of connecting retinal cells.

Joseph Rizzo and John Wyatt at the Harvard Medical School introduced another device in this type of prosthesis, with an external part consisting of a camera mounted on a pair of glasses, processing unit, and battery (Grumet, Wyatt and Rizzo, 2000; Rizzo *et al.*, 2003). The intraocular prosthesis contains an electrode array that connects to the retinal ganglion cells, which is controlled by a stimulating chip. Instead of using a cable for data telemetry as in Argus I (Kelly *et al.*, 2009), this prosthesis uses a laser pulse to transfer the processed signal from the processing unit to the stimulating chip.

Different experiments have been conducted on three types of electrode arrays (Rizzo, 2003) to examine the operations of different electrode configurations:

- 10×10 array of 50- μm diameter electrodes, with an inter-electrode spacing of 220 μm
- 8×10 array of 50- μm diameter electrodes, with an inter-electrode spacing of 220 μm
- 4×5 array of 100- μm diameter electrodes, with an inter-electrode spacing of 620 μm

The results obtained in five patients in Joseph Rizzo and John Wyatt's study were similar to those of Humayun *et al.*'s study. Three patients perceived phosphenes when the stimulating current was above the threshold, and higher

threshold was applied to stimulate the other two patients with worse vision (Rizzo, 2003). With this device, eight hypotheses were examined in blind patients, and Rizzo et al. observed that consistent phosphenes were elicited in patients in whom the electrode array was placed above the intact retinal surface and who required lower threshold (Javaheri *et al.*, 2006). However, Rizzo et al. found that the actual threshold range used in the blind patients was 0.16–80 mC/cm², which was different from the range (0.28–2.8 mC/cm²) that their device was designed for. Moreover, they found that no patients matched the lower threshold range, and the retinal cells were subject to heat damage from using the higher threshold range. To explain this, Rizzo et al. pointed out some constraints such as planar electrode, sequential stimulation, and stimulation frequencies. Due to this disparity, Rizzo et al. have abandoned the epiretinal prosthesis and focused on the subretinal device (Javaheri *et al.*, 2006).

The third attempt in epiretinal prosthesis is the learning retina implant, which was proposed and developed by Rolf Eckmiller and his colleagues since 1995 (Eckmiller, 1997; Eckmiller, Hünemann and Becker, 1999). This device contains a camera, retinal encoder part for signal processing, and retinal stimulator. The encoder consists of 256 tunable temporal filters in order to simulate the receptive field in the ganglion cells of the retina, and each receptive field receives input from an array of photo sensors with a resolution of approximately 340 × 290 pixels. The retinal stimulator (RS) is the intraocular component that is placed on the epiretinal

surface, where contact is established with the ganglion cells. It contains an array of 100 electrodes with diameter ranging from 100 to 360 μ m to stimulate one or more ganglion cells. The retinal encoder is designed to be carried as a pocket processor, which provides an integrative perception-based dialogue between the RE and human subject, besides stimulating the complicated mapping operation of parts of the neural retina. The dialogue, which involves patients fine-tuning parameters of the encoding process, helps provide ganglion cells with interpretable codes for epiretinal stimulation (Rizzo *et al.*, 2003).

Some encouraging results were obtained on testing this device on animals such as rabbits and primates (Eckmiller, 1997; Walter *et al.*, 1999; Hornig and Eckmiller, 2001), but retinal detachment was found in human trials. Eckmiller *et al.* adopted a dialogue-based RE tuning approach to tackle the issue of information processing in the retina, the brain, and retinal prosthesis and developed an effective man-machine interface for blind patients (Abbott, 1999; Gutierrez and Marder, 2013). Based on experiments with this device, Eckmiller indicated that to achieve a good dialogue between the retinal encoder and the central visual system, the stimulation to elicit neural signals in ganglion cells must be determined properly. Besides, signals generated by the retinal encoder and retinal stimulator must be clear and unambiguous (Destexhe, 1997; Izhikevich, 2004), and the time rate course must be over more than 100 ms to generate the desired percepts at the central visual system. In particular, ganglion cells need to be stimulated properly, because the ganglion

cells will not be able to convert the electrical signal into visual percepts if the electrical stimulus is not applied at the correct location and affects neighbouring cells. For instance, many patients reported that they had unspecific phosphene-like or cloud-like percepts because it is not possible to stimulate a single ganglion cell without affecting its neighbouring cells. Eckmiller tackled this issue by studying the stimulating pattern in ganglion cells through the Retinal Encoder Dialogue Module that could be adjusted according to the perceived vision in normal people. In other words, this prosthesis addressed the question of information processing between the device and ganglion cells by tuning an ‘artificial’ receptive field to determine the proper stimulation, and the tuning was performed by comparing elicited vision from stimulating signals to the percepts of a person with normal vision. This approach is different from other approaches, in which the receptive field is adjusted to create corresponding pulse trains for adaptive stimulation of ganglion cells.

The last approach is EPIRET-3, developed by Klauke et al., which contains an extraocular and an intraocular component and data is transmitted wirelessly (Klauke *et al.*, 2011; Maidenbaum, Abboud and Amedi, 2013). The intraocular part consists of a receiver coil, receiver chip, stimulation chip, and a microelectrode array. All these components are implanted inside the eye, with only the electrode array in contact with the retinal cells. The receiver coil is responsible for receiving the wireless signal, a radio signal in this case, and transferring it to the receiver chip

for processing. Then, these processed signals are transformed into electrical stimuli by the stimulation chip. These stimuli then transfer to the retinal cells via the array of microelectrodes, and they form the visual perception in the brain. The electrodes array in this design has 25 electrodes, which are arranged in a hexagonal shape; each electrode has a diameter of 100 μm with a gap of 500 μm between them. On the other hand, the extraocular part consists of a camera, computer system, and transmitter coil placed in front of the eye. The computer system is used for encoding spatial signals from the camera and transferring these signals to the coil to transmit to the intraocular component. The placement of this prosthesis is shown in Figure 3.5.

The EPIRET-3 device is now undergoing a clinical trial in Europe on six patients who have been blind for an average of five years, with visual acuity ranging from completely blind to hand movement perception. This trial is being conducted to examine the compatibility of the device with the eye after device implantation. The results show that in all cases, the retinal cells are attached to the electrode array, and the cornea is cleared with intraocular parts in position. Besides, only one case shows optic atrophy in which the optic nerve is deteriorated and no longer sends nerve signals to the brain. In another case, the optic disk changed to a pale colour from the original orange colour, and in yet another case, the vessels had become narrow. In terms of visual acuity, two patients have perception of hand movements, two others have light perception, and the rest have neither light perception nor hand

movement perception. After an acute clinical study, this device is now awaiting a chronic study, which will be followed by further improvement of the design and implantation.

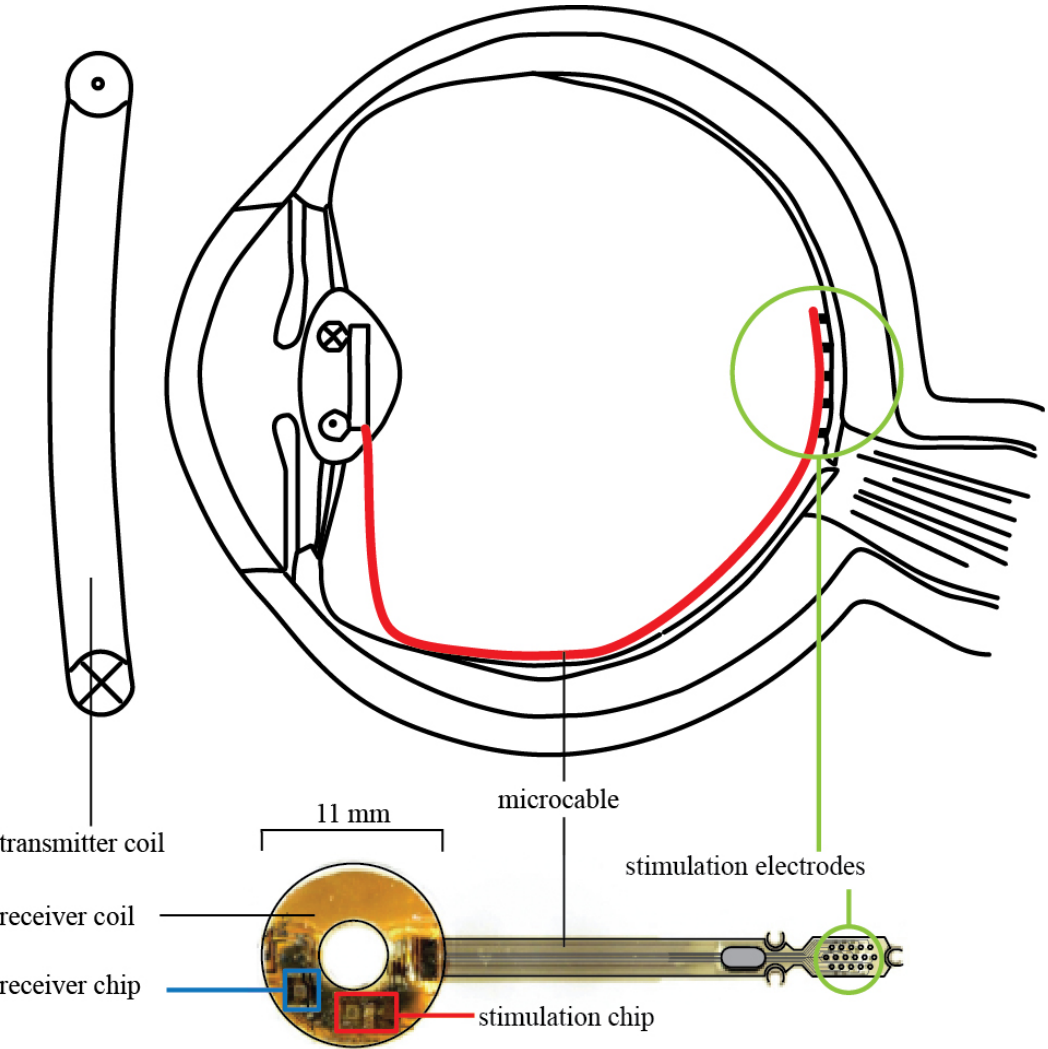


Figure 3.5: EPIRET-3 retinal prosthesis. Reproducing with permission (Klauke *et al.*, 2011).

3.2.1.1 Advantages and disadvantages of epiretinal prostheses

- Advantages

The first advantage of the epiretinal approach is that the electrical device is mostly placed outside the retinal surface, keeping the heat at the retinal surface at low levels and making the prosthesis virtually harmless to the eye (Piyathaisere *et al.*, 2003).

The second advantage is that the surgical process is easier. The surgical procedures involving the vitreous cavity are generally straightforward. Moreover, the device may be placed on the entire vitreous cavity to minimize disruption to the retina (Weiland and Humayun, 2006).

The last advantage is that the approach does not require the remaining retinal cells (e.g. bipolar, horizontal, or amacrine cells) for information processing. This means this prosthesis is suitable for patients with only ganglion cells remained in the retina therefore the chance of using this device to restore vision in the blinds could be increased.

- Disadvantages

The first disadvantage of the epiretinal prosthesis is that the remaining retinal neural cells are not used to process the information (Chow *et al.*, 2004). This generally means that an external camera is required to allow some degree of pre-processing to substitute for what would have been done automatically if the information had

been passed through intact neurons, such as bipolar and amacrine cells. Moreover, the image processing performed by the retina must be replicated in order for the ganglion cells to be stimulated with meaningful signals (Piyathaisere *et al.*, 2003).

Secondly, to increase comfort and reduce retinal damage, the shape and material of the electrode array substrate poses several challenges. The electrode array must be carefully fixed to the curved retinal surface for the stimulation to be consistent and to avoid retinal tearing (Piyathaisere *et al.*, 2003).

Finally, due to the need for an external camera and data transfer from a camera to the stimulation component, the epiretinal device needs more power to operate. Moreover, the camera is also fixed on the glass, which requires the patient to use their head movement to adjust the direction of vision.

3.2.2 Subretinal prostheses

Unlike an epiretinal prosthesis that is placed in contact with the ganglion cells, a subretinal prosthesis is located between the bipolar and photoreceptor cells. Because of the location of its placement, the structure of this device, especially the stimulator part, is different from that of an epiretinal device. In detail, the number of electrodes is higher because the number of retinal cells in the photoreceptor layer is higher than the number of ganglion cells. The first subretinal device—the Artificial Silicon Retina (ASR) (Chow *et al.*, 2004) - was developed by Chow et al. It consists of a stimulator made from a thin silicon plate, approximately two to three

millimetres in diameter and 50–100 μm in thickness. On the silicon plate, there are 5000 subunits with a size of $20 \times 20 \mu\text{m}$, and each subunit consists of a micro-photodiode that is capable of converting light to electrical signals and an electrode to stimulate the bipolar cells. In addition, the micro-photodiodes are used to provide energy to the stimulating electrodes with the integrated solar cells (Chow and Chow, 1997; Chow and Peachey, 1998; Peyman *et al.*, 1998; Chow *et al.*, 2002). Furthermore, the subunits are arranged with a density of 1100 subunits per μm^2 to stimulate a comparably large number of retinal bipolar cells.

The subretinal prostheses were implanted in six patients, and the results were reported as follows (Javaheri *et al.*, 2006):

Patient	Eye Ability	Results
1	Light Perception in both eyes.	Capable of perceiving light without heading to the light source.
2	Light Perception in left eye only.	Capable of seeing shadows of people with the right eye.
3	Had visual acuity of hand moving.	Capable of using night light for navigating and seeing movement on television.
4	Had visual acuity of hand moving in both eyes.	Capable of navigating the yard and locating light sources.
5	Had visual acuity of counting fingers at 1 or 2 ft. in both eyes.	Capable of differentiating paper money, using utensils for eating and recognizing faces.
6	Had a preoperative visual acuity of hand moving in both eyes and equal visual function in both eyes.	Sometimes capable of recognizing denominations of paper money, distinguishing traffic lights, locating cars as well as finding a coffee cup at meals.

Table 3.1: Result from testing an Artificial Silicon Retina. Reproducing with permission (Chow *et al.*, 2004).

Some weaknesses of the device were noted, although encouraging results have been achieved in human clinical trials (Chow and Chow, 1997; Zrenner, 2002). The major drawback of this device is that the micro-photodiode does not transmit sufficient energy to stimulate the retinal cells, due to its limited light sensitivity. Although this limitation can be improved by using an external energy source for the stimulating retinal cells, Chow et al. have abandoned the notion that the ASR Microchip is a prosthetic device and have listed this prosthesis as a therapeutic device. This implies that this device can help patients when required and turned off after use or used in patients who are not completely blind; thus, it is not a true retinal prosthesis. In other words, users can use this device whenever they want but, unlike a visual prosthesis, they do not depend on it for performing daily activities. Although Chow et al.'s concept of a subretinal prosthesis has been discontinued, this device has been noted as the first of its kind and has inspired other researchers to develop better versions of subretinal prostheses.

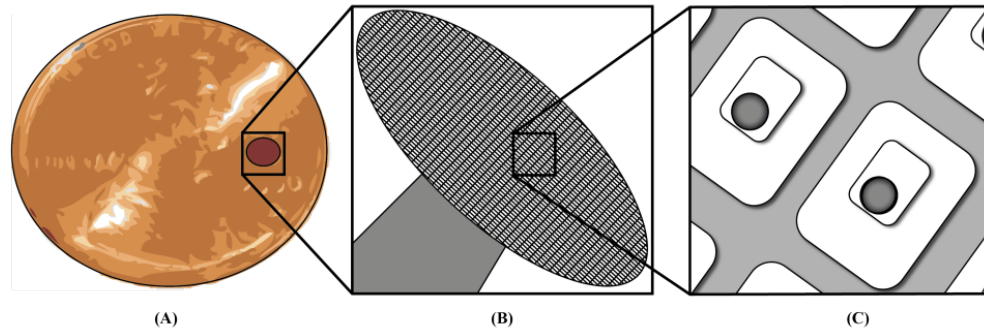


Figure 3.6: The Artificial Silicon Retina (ASR). Reproducing with permission (Chow *et al.*, 2004). (A) ASR compared to a penny; (B) The ASR Microchip in closer view; (C) An ASR electrode.

Zrenner *et al.* developed another design for a subretinal prosthesis consisting of a micro-photodiode array, three millimetre in diameter and 50 μm in thickness, containing 7000 microelectrodes in a checker-board pattern; furthermore, each micro-photodiode is designed to be both insulating and permeable to light (Stett *et al.*, 2000; Eckhorn *et al.*, 2006; Wilke *et al.*, 2011). An external source is used to provide sufficient power to the subretinal implant. The parameters used to define the micro-photodiodes were examined on various animal models of a degenerated retina to stimulate the retinal cells adequately. These parameters were later used to develop a new prosthesis to be implanted in future animal experiments. The goals of the latter experiments were to detect stimulation of the visual cortex (as a result of prosthetic stimulation) and test the long-term bio-compatibility as well as stability of the prosthesis (Wilke *et al.*, 2011).

After 14 months of implantation, angiography and histology studies revealed no rejection reactions or inflammation in the tested subjects (Wilke *et al.*, 2011). Zrenner *et al.* also recorded the cortical evoked potentials during light flash experiments and compared them to responses from not only subretinal but also epiretinal devices with regard to certain aspects of spatial resolution to determine the outcome of the device implanted. The results showed that the spatial resolutions from both devices are sufficient for blind patients to recognize objects, and these resolutions could be increased up to 0.5° visual angle if the electrode was made from a material with a higher charge transfer capacity. With this result, the implant is processed, and currently, in one relatively successful human trial, the blind patient was capable of identifying letters and a clock face, and was able to move around a room independently (Stingl *et al.*, 2013). Unlike epiretinal implants, this approach does not require an external camera. New versions of this prosthesis have been focusing on gathering the device components beneath the skin and providing energy as well as data to the prosthesis through the skin via an external device (Wilke *et al.*, 2011). The new devices are expected to provide the ability to recognize objects, read letters, and recognize people (Stingl *et al.*, 2013).

A third type of subretinal prosthesis is being developed by Rizzo and Wyatt *et al.*, a research effort that goes by the name Boston Retinal Implant Project (Grumet, Wyatt and Rizzo, 2000; Kelly *et al.*, 2009; Freeman, Rizzo and Fried, 2011). As seen in Figure 3.7, the prosthesis consists of a micro-fabricated thin-film electrode

array, controller microchip, power supply components, and power and data receiver coils. The controller microchip and the power supply components are on one module, and the power and data receiver coils as well as electrode array is placed on the other module. These two modules are connected by a biocompatible flex substrate. The energy and data of the prosthesis are wirelessly transferred via the power and data coils through inductive coupling (Kelly *et al.*, 2009).

However, this is just the first generation of the prosthesis and has some significant disadvantages, including the following (Weiland, Cho and Humayun, 2011):

- Small receiver coil, which makes the data and power transfer more difficult;
- Silicon coating, which is not suitable for a long-term trial (e.g. 10 or 15 years);
- Implantation procedure is difficult as the coil is in the way; and
- Little data is available about the long-term survivability of the electrode array.

Therefore, a second-generation prosthesis was developed in order to overcome the drawbacks of the first-generation prosthesis. The second-generation prosthesis has the following advantages (Weiland, Cho and Humayun, 2011):

- A larger coil is used, which is also more comfortable for the eye;

- The circuitry is enclosed in a hermetic, ceramic case; and
- The electrode array is inserted in its own quadrant in a manner that allows for an easier implantation process. The number of electrodes is increased to 200 electrodes, with the diameter reduced to 200 μm , instead of 100 electrodes with a diameter of 400 μm in the first generation. According to Rizzo and Wyatt et al., the number of electrodes in this device is less than those in other devices, but these electrodes are fully controlled individually based on patient feedback, in contrast to the lack of individual control in other approaches.

According to Figure 3.8, the coil is wound on a steel sphere so that it can match the curvature of the eye. There are two coils: the primary coil is used for power telemetry and the second coil is used for data transferring. The prosthesis also contains a CMOS chip to receive incoming stimulation data, which it then decodes and uses to stimulate the electrodes. The electrical stimulation is provided to the retinal nerve cells via a micro-fabricated array of sputtered iridium oxide film (SIROF) electrodes. By encasing and placing the electronic components outside the eye, only the electrode array inside the eye and one contact with the retina; therefore, a retinal tack is not required to attach the array to the retina as in the epiretinal approach (Rizzo, 2011). In particular, in the epiretinal approach, the electrode array must remain in contact with the ganglion cell layer; therefore, it is located in the vitreous chamber and a tack is required to keep the array in a fixed

position. In contrast, the electrode array for a subretinal prosthesis is inserted between the retina and the choroid; therefore, the array is fixed by the natural force of the retina and choroid.

This prosthesis was tested on two Yucatan mini-pigs. The result showed consistency in electrode response and good stability over long-term pulsing (Rizzo, 2011). Human testing has also been conducted in a series of six experiments and shows that the prosthesis provides sufficient electrical currents to the retina. Some patients are capable of seeing and distinguishing small spots of light, and perceiving lines, in spite of the fact that they may have been classified as legally blind for decades (Weiland, Cho and Humayun, 2011; Fernandes *et al.*, 2012).

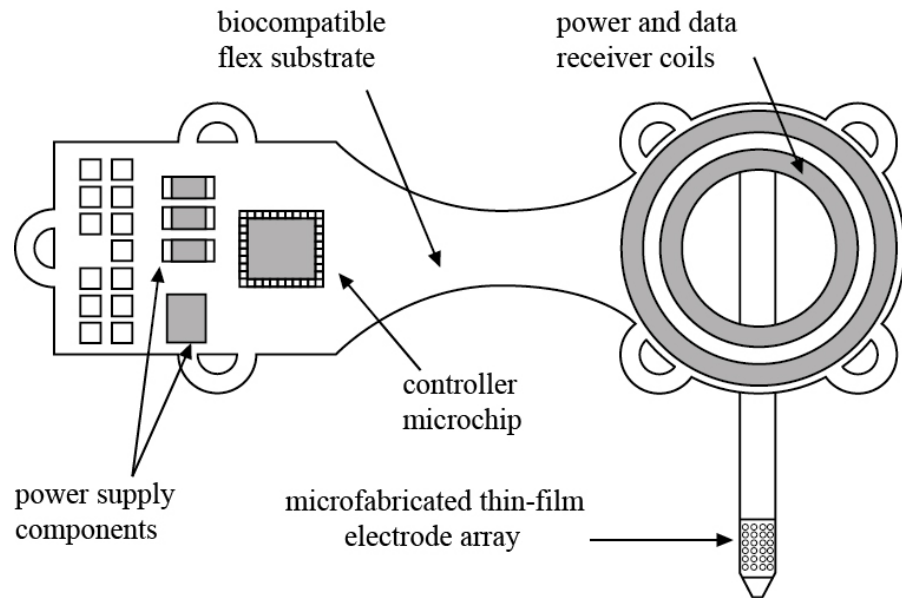


Figure 3.7: The first generation of the retinal prosthesis. Reproducing with permission (Rizzo, 2011).

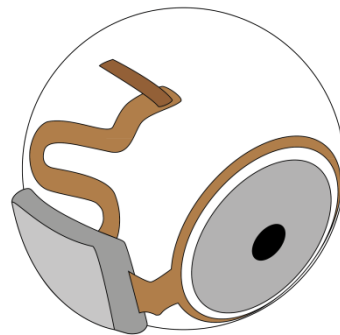


Figure 3.8: The hermetic implant in the second generation of the prosthesis. Reproducing with permission (Rizzo, 2011).

On the downside, few negative effects have been reported in connection with the conjunctiva, which is a thin, clear, and moist membrane that coats the inner surfaces and the outer surface of the eye. The angle formed between the conjunctiva and the coil edge causes tension in the thin conjunctiva. In addition, the hermetic

case is placed too far on the anterior side of the eye, increasing tension in the conjunctiva. These issues can be addressed by redesigning the flex circuit that connects the coil and the case as well as the way the case is sutured to the eye in order to ensure that the case remains in place (Weiland, Cho and Humayun, 2011).

The latest subretinal prosthetic device is the Alpha-IMS. An acute clinical trial of the first-generation Alpha-IMS was conducted in 11 subjects in 2005. Unlike other approaches that use a camera for recording, this device was implemented with a micro-photodiode array consisting of 1500 micro-photodiodes that capture and transform the light directly into an electrical signal. Using the micro-photodiode array, the signal-processing component can be integrated as an intraocular part and placed inside the skull with the stimulation component. This solves the problem of data transfer between the intraocular and extraocular components and increases the speed of processing as the data is now processed inside the intraocular component itself. Power was transferred to the intraocular component through RF telemetry wireless transmission. The device is shown in Figure 3.9.

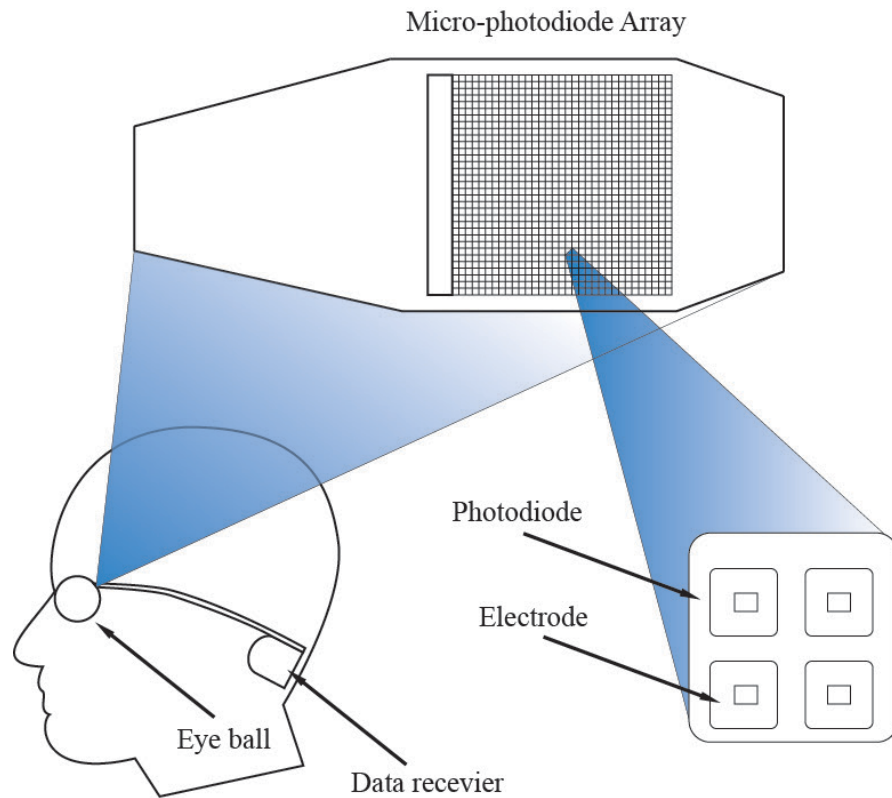


Figure 3.9: Alpha-IMS retinal prosthesis. Reproducing with permission (Stingl *et al.*, 2013).

The first-generation Alpha-IMS device was implanted and tested on three blind patients. The results show that the device can help blind patients perceive light and reliably respond to a flash of light and recognize certain subjects such as cups or saucers on a table (Foerster, J and Javaheri, 2006; Benav *et al.*, 2010; Wilke *et al.*, 2011; Kusnyerik *et al.*, 2012; Stingl *et al.*, 2013). Especially, one patient with subfoveal implantation of the micro-photodiode array was able to recognize the geometric shapes and read large letters and formulate simple words. This result not only encourages the use of the new prosthetic device but also demonstrates

potential development of the MPDA in designing the prosthesis. The second-generation subretinal prosthetic device has an improved design and was implanted in 10 patients for a 3–9 month trial. With the help of this device, these patients could recognize individual letters spontaneously even under low-contrast conditions and demonstrated a visual acuity of 20/546. However, a subretinal bleed with high intra-ocular pressure occurred in one patient, and a damaged optic nerve was reported during implantation in another patient.

In summary, subretinal prostheses include the Artificial Silicon Retina (ASR) with 5000 electrodes, Zrenner group's prosthesis with 7000 micro-photodiode arrays, Boston Retinal Implant Project with 200 individually controlled electrode arrays, and Retinal Implant AG with 1500 micro-photodiodes. The stimulation components in all the devices are implanted in the subretinal area between the retina and choroid. Among these devices, only the device developed by the Boston Retinal Implant Project requires an external camera to acquire visual images; all other devices used micro-photodiodes to transform incoming light into electrical current. With regard to data telemetry, the Boston device used wireless data transfer, whereas the Alpha-IMS and Zrenner group used cables for transferring data and power. In addition, the ASR uses power from the current converted from the micro-photodiode, causing a power problem, leading to the discontinuation of the device. Other prostheses continue to be implanted and approved for human trials or even commercial use, e.g. Alpha-IMS is used in Europe.

3.2.2.1 Advantages and disadvantages of subretinal prostheses

- **Advantages**

The first advantage of the subretinal prosthesis is that the remaining retinal tissues can be used for information processing (Javaheri *et al.*, 2006). Apart from the advantages pertaining to information compatibility with the rest of the visual system, the use of intact retinal circuits decreases the need for external processing and decreases the amount of power required.

Secondly, it is easier for a subretinal prosthesis to remain in place and avoid retinal detachment. This mechanical stability avoids damaging the surrounding tissue, maintains the prosthesis, and retains the consistency of the communication channels between the prosthesis and the intact neurons (Piyathaisere *et al.*, 2003).

- **Disadvantages**

Firstly, the distribution of the nutritional supply between the choroid and the retina may be disrupted because of the placement of the device. In other words, if the electrical device is not placed properly, it may accidentally disrupt nutritional flow inside the eye and cause further damage to the retina (Piyathaisere *et al.*, 2003).

Secondly, power stability is an issue because light absorption in the solar cells is neither sufficient nor consistent. Therefore, an external power source must be provided to ensure that the prosthesis functions reliably.

Thirdly, the inter-neurons on which the prosthesis is relying (i.e. bipolar and amacrine cells) might be heavily re-organized as a consequence of retinal damage, and as a consequence, the information conveyed to the ganglion cells might not be interpretable.

3.3 Summary

The above retinal prosthesis review presented the concept and application of epiretinal and subretinal prostheses as well as the advantages and disadvantages of each device. Both devices consist of a stimulation component and a visual processing unit, with power supply depending on the design of the prosthesis. The epiretinal prosthesis focuses on stimulating the ganglion cell layer, whereas the subretinal prosthesis focuses on the bipolar cell layer. In epiretinal devices, an external camera is required for direct stimulation of the ganglion cells, whereas in subretinal devices, an external camera is optional and micro-photodiodes are used to convert light energy to electrical signals. Thus, in epiretinal prosthesis, a power source is required to supply energy to the camera as well as the stimulation and processing components. The epiretinal devices are suitable for eyes with significant retinal damage and intact ganglion cells, whereas subretinal prostheses are suitable for retinas with a damaged photoreceptor layer only. On the other hand, optic nerve and extraocular prostheses do not need the retina to operate; however, these prostheses are expensive, difficult to implant, and yield poor-quality vision.

CHAPTER 4

RETINAL MODELING REVIEW

In the previous chapter, different approaches in manufacturing and implanting retinal prostheses were reviewed. Besides retinal prosthesis, retinal modelling has also received the attention of many researchers in order to simulate the behaviour of the retina under various conditions. In general, a retinal model is a set of equations that describes the biological properties and connectivity inside the retina based on the anatomy of the retina. Through these equations, scientists can simulate the processing that occurs inside the retina and predict its output under different scenarios. The simulations focus on different levels in the retina from single cells such as photoreceptors (Huang and Robinson, 1998; Kourennyi *et al.*, 2004), horizontal cells (Hateren, 2005; Publio, R. Oliveira and Roque, 2006), bipolar cells (Smith and Vardi, 1995; Publio, R. Oliveira and Roque, 2006; Paninski, Pillow and Lewi, 2007; Raudies and Neumann, 2010), amacrine cells (Ohshima, Yagi and Funahashi, 1995; Paninski, Pillow and Lewi, 2007), and ganglion cells (Lankheet, Molenaar and van de Grind, 1989; Destexhe, 1997; Feller *et al.*, 1997; Abbott, 1999; Benison *et al.*, 2001; Izhikevich, 2004; Sheasby and Fohlmeister, 2013) to a group of cells such as the OPL layer (Publio, R. Oliveira and Roque, 2006; Hateren, 2007), IPL layer (Zhijun Pei and Qingli Qiao, 2010; Decuyper and Capron, 2011; Suh, 2012), or the whole retina (Kenyon *et al.*, 2005; Wohrer and Kornprobst, 2009). Although different models are used to simulate the processing inside the

retina with different purposes, the purpose of all the models is the same, that is, to replicate the retinal cells, and this method differs between models. However, the models can be classified based on their characteristics: conductance-based models, threshold-fire models, compartment models, and white-noise models. In this section, each type of model and the application of these models in case of modelling the retina is discussed to present a state-of-the-art view of retinal modelling.

4.1 Conductance-based models

The name of this model is based on the fact that the opening and closing state of ionic channels inside the neurons may lead to a change in their conductance. These changes can be described using a set of differential equations. This section will describe the Hodgkin–Huxley model and its variations and their applications in retinal modelling.

4.1.1 Hodgkin–Huxley model

The Hodgkin–Huxley model is based on the Hodgkin–Huxley equation, which was proposed by Hodgkin and Huxley in 1952, to simulate the action potential of the neuron based on their experiments with the axon of a giant squid. They determined that the action potential is a combination of component currents such as Na^+ and K^+ currents, which are based on the flow of Na^+ and K^+ through the cell membrane. A leakage Cl^- current is also developed, but the greatest contribution to the action

potential is the Na⁺ and K⁺ current. The Hodgkin–Huxley equation can be described using a set of differential equations as follows:

$$I = C_m \frac{dV_m}{dt} + g_K(V_m - V_K) + g_{Na}(V_m - V_{Na}) + g_L(V_m - V_L) \quad (4.1)$$

Where I is the total membrane current, C_m is the membrane capacitance, g_K and g_{Na} are potassium and sodium conductance, respectively. V_K and V_{Na} are the potassium and sodium reversal potentials, respectively, and g_L and V_L refer to the leak conductance per unit area and leak reversal potential, respectively. The time-dependent elements of this equation are V_m , g_{Na} , and g_K , where the last two conductances depend explicitly on voltage.

By successfully simulating the action potential of the neuron, the Hodgkin–Huxley equation is widely used in modelling neurons as a single compartment or a network of compartments. Fohlmeister, Coleman, and Miller used the Hodgkin–Huxley equation to simulate the repetitive firing of the ganglion cells in the retina of a tiger salamander (Fohlmeister, Coleman and Miller, 1990), after Barnes and Hille simulated the ionic channels of the inner segment of its cone photoreceptors (Barnes and Hille, 1989). Moreover, Fohlmeister and Miller and Sheasby developed a realistic five-channel spiking model based on the Hodgkin–Huxley model to replicate the bursting behaviours of the retinal ganglion cells of a tiger salamander (Sheasby and Fohlmeister, 2013) and its morphologies (Barnes and

Hille, 1989). Skaliora et al. used the model to simulate the properties of K^+ conductances in cat retinal ganglion cells (Skaliora *et al.*, 1995). Besides Skaliora and their colleagues, Benison et al. also modelled the postnatal retinal ganglion cells of a cat in terms of temporal behaviour using the Hodgkin–Huxley equation and the data from the experiments of Huang and Robinson (Huang and Robinson, 1998; Benison *et al.*, 2001). Besides the ganglion cells, Kourennyi and Liu et al. simulated the light response and the calcium dynamics in rod and cone photoreceptors (Kourennyi *et al.*, 2004; Liu and Kourennyi, 2004). This work by Kourennyi was followed by that of Publio and Oliveira and Roque and presented a realistic model of rod photoreceptors and ON rod pathway in 2006, which include the rod, bipolar, and ganglion cells in the vertebrate retina (Publio, R. Oliveira and Roque, 2006; Publio, Oliveira and Roque, 2009).

4.1.2 Morris–Lecar model

The Morris–Lecar model is a simplified version of the Hodgkin–Huxley model, but it still maintains the biologically meaningful characteristics though its parameters. In this model, Morris and Lecar added an instantaneously responsive voltage-sensitive Ca^{2+} conductance for excitation and a delayed voltage-dependent K^+ conductance for recovery. The equations for this model are as follows:

$$\begin{aligned} CV' &= -g_{Ca}M_{ss}(V)(V - V_{Ca}) - g_KW(V - V_K) - g_L(V - V_L) + I_{app} \\ W' &= (W_{ss}(V) - W)/T_W(V) \end{aligned}$$

$$M_{ss}(V) = (1 + \tanh\left[\frac{V - V_1}{V_2}\right])/2 \quad (4.2)$$

$$W_{ss}(V) = (1 + \tanh\left[\frac{V - V_3}{V_4}\right])/2$$

$$T_W(V) = T_0 \operatorname{sech}\left[\frac{V - V_3}{2V_4}\right]$$

Where V is the membrane potential, W is recovery variable, and I_{app} is the applied current stimulus. The value W is equal to the instantaneous value of the probability that a K^+ ion channel is in its open state. The second equation is the relaxation process, where the protein channels undergo conformational transitions between ion-conducting and non-conducting states and $M_{ss}(V)$ and $W_{ss}(V)$ represent the function of open-state probability.

Compared to the Hodgkin–Huxley equation, the Morris–Lecar model requires only two dynamic variables, instead of four, to describe the two voltage-gated channels (Na^+ and K^+) and a leakage current (Cl^-), and this improvement reduces the cost for computation by up to 50% (Destexhe, 1997). Moreover, the Morris–Lecar model also introduced the concept of voltage oscillation in the neuron due to the resonance. Because of this advantage, the Morris–Lecar model is used widely in neuroscience to simulate spiking neurons, especially fast-spiking neurons and spiking neurons with the property of oscillation. Siegel et al. used and modified the Morris–Lecar model to infer that the Ca^{2+} concentration depends on both electrical activity and cell morphology (Siegel, Marder and Abbott, 1994). Jacobs, Roska,

and Werblin have implemented the Morris–Lecar model to construct a cellular neural network and create a physiologically detailed model of the vertebrate retina (Jacobs, Roska and Werblin, 1996). Agmon-Snir, Carr and Rinzel later created a model using the Morris–Lecar equation to simulate the coincidence-detector neurons in the auditory system of mammals and birds and showed that the computational ability of these neurons depends on their cell morphology and spatial distribution of the inputs (Agmon-Snir, Carr and Rinzel, 1998; Murakoshi and Nakamura, 2001). Sekerli and Butera applied the Morris–Lecar equation to field programmable analogue arrays to create an electronic neuron and showed that the neuron is able to describe biologically relevant dynamics in real time (Sekerli and Butera, 2004). Breakspear and Stam modified the equation and implemented it in a multi-scale dynamic neural framework, and the dynamics at each scale was determined by the non-linear oscillators (Breakspear and Stam, 2005). Veredas, Vico, and Alonso simulated the two mono-synaptically connected neurons to measure changes in correlated firing and found that the time course of excitatory postsynaptic potential affected the precision of correlated firing generated by strong mono-synaptic connections in the visual pathway of cats (Veredas, Vico and Alonso, 2005). In 2006, Tsaneva-Atanasova et al. used a modified Morris–Lecar model to simulate the diffusion of calcium and metabolites and study the synchronization of the pancreatic islets. In addition, Prescott et al. have studied the effect of changes in conductance on spiking activity in pyramid neurons using the

Morris–Lecar model as a phase plane model (Prescott *et al.*, 2006; Tsaneva-Atanasova *et al.*, 2006). In 2007, Behn *et al.* used a Morris–Lecar relaxation oscillator to produce a model involving the neural dynamics underlying sleep-wake behaviour in mice (Behn *et al.*, 2007). In 2009, Hennig *et al.* studied the early-stage waves in the retina using a biophysically realistic model adopted from the Morris–Lecar model (Hennig *et al.*, 2009). In the next year, Almeida and Ledberg implemented a biologically plausible model that contained a set of bi-stable units that could switch from one state to the other at random times and showed its consistency with time-scale invariant behaviour over a substantial range of intervals (Almeida and Ledberg, 2010). In 2013, Gutierrez and Marder presented a five-cell model, with each cell based on the Morris–Lecar equation, to simulate a pattern-generating neuronal network to investigate the change in behaviour of a small neuronal network from the rectifying electrical synapses (Gutierrez and Marder, 2013).

4.1.3 Advantages and disadvantages

Through the implementation of the Hodgkin–Huxley and Morris–Lecar models, the conductance-based model simulates the ionic currents to help scientists investigate issues related to neuronal dynamics as well as determine biophysically meaningful parameters that could be adjusted and measured in experiments. A disadvantage of this model is that the cost for computation is high and it warrants knowledge about

the biophysical properties of a neuron to adjust the parameters of the model. Therefore, the conductance-based model is only suitable for simulating a small number of neurons, when the computational cost and time required for simulation is not an issue.

4.2 Threshold-fire models

According to its name, in this model, the post-synaptic neuron accumulates all signals from the pre-synaptic neuron and fires when the summation exceeds a pre-defined threshold. After firing, the signal of the post-synaptic neuron will be reset to the resting state and accumulate again. The integrate-and-fire model and its variants are reviewed as an example.

4.2.1 Integrate-and-fire

The integrate-and-fire model was presented in 1907 by Lapicque (Abbott, 1999) and is based on the RC (resistor-capacitor) circuit, as shown in Figure 4.1:

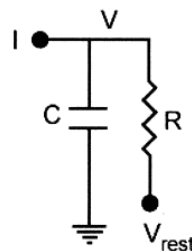


Figure 4.1: A neuron as an RC circuit. Reproducing with permission (Abbott, 1999).

Using the RC circuit shown above, Lapicque described the spiking mechanism in the neuron by replicating the membrane resistance and capacitance with capacitance C and resistance R . At the resting state, the membrane potential V_{mem} is maintained stable as V_{rest} and under the input current I , the membrane potential increases until it reaches the threshold level, generating an action potential and subsequently resetting to a stable state. In the first model, there is no time-dependent memory, which would increase the membrane voltage to the threshold point for firing when the applied current is below the threshold. Moreover, the variations in the Na^+ and K^+ current are not well utilized, thus preventing the production of phasic spiking or bursting spiking (Izhikevich, 2004). To overcome this drawback, a leakage channel has been added to the original integrate-and-fire model by facilitating the diffusion of ions through the membrane so that the membrane potential does not continue to increase. After the addition of the leakage channel, the leaky integrate-and-fire model assumes the following form:

$$I(t) = \frac{u(t)}{R} + C \frac{du}{dt}$$

$$\tau_m \frac{du}{dt} = -u(t) + RI(t) \tag{4.3}$$

$$\text{Where } \tau_m = RC$$

In terms of retinal modelling, in 1989, Lankheet, Molenaar, and van de Grind implemented a model to simulate the spiking neuron and explain the mechanism of spiking generation in cat retinal ganglion cells (Lankheet, Molenaar and van de Grind, 1989). In 1992, Levine used this model to simulate the spiking of ganglion cells in the vertebrate retina in order to examine the variability of the firing rate (Levine, 1992). Five years later, Feller et al. used the leaky integrate-and-fire model to simulate and explain the mechanisms behind the highly correlated activity generated by the retinal waves in the mammalian retina (Feller *et al.*, 1997). In the same year, Rudd and Brown studied the gain control in the retinal ganglion cells of the toad *Bufo marinus* using the integrate-and-fire model (Rudd and Brown, 1997). In 2004, Jolivet, Lewis, and Gerstner presented the model using the integrate-and-fire equation to simulate fast-spiking cortical neurons (Jolivet, Lewis and Gerstner, 2004). In the same year, Sun, Rüttiger, and Lee used this model to compare the spatial-temporal precision of ganglion cell response with moving gratings (Sun, Rüttiger and Lee, 2004). One year later, Federici implemented the integrate-and-fire model in a neuronal network that can regenerate and continue performing spiking in case of cell loss (Federici, 2005). Later, in 2007, Capela, Tomás, and Sousa introduced a stochastic integrate-and-fire model that included additive white noise in order to create a model and provide a training method to fit this model to the real data for simulating a human visual system (Capela, Tomás and Sousa, 2007). In 2008, Wu et al. used the same integrate-and-fire model to implement a

spiking neuronal network that can segment the object and form the shapes of objects using local excitatory lateral connections (Wu *et al.*, 2008). Four years later, Bichler *et al.* proposed a neural network based on this model and were able to extract complex and overlapping temporally correlated features from a spiking silicon retina (Bichler *et al.*, 2012). In the same year, Bugmann used the leaky integrate-and-fire model to conduct a multilayer network for fast learning along the dorsal pathway from primary visual areas to pre-motor cortex (Bugmann, 2012). In 2013, Zhou *et al.* utilized this model to theoretically determine the effects of the dynamics of the sub-threshold membrane potential in the soma on dendritic integration (Zhou *et al.*, 2013). In early 2014, Cho and Choi simulated an integrated-and-fire neuron based on this approach to replicate the receptive field of the retinal ganglion cells (Cho and Choi, 2014).

4.2.2 Spike Response Model

In 1993, Gerstner proposed another model adapted from the integrate-and-fire model, called the Spike Response Model, to provide a different view of the spiking neurons. In this model, the concept of the integrate-and-fire model is retained, i.e., the neuron will fire when the accumulated voltage exceeds the threshold. The difference between this model and the integrate-and-fire model is that this model can capture the refractoriness property of the neuron, where the spiking frequency is reduced by preventing it from firing for a specific time (Gerstner and van

Hemmen, 1992; Gerstner, Ritz and van Hemmen, 1993). With this feature, the spike response model has an advantage over both the leaky and integrate-and-fire models (Jolivet *et al.*, 2008), and this model has been proven to be a generalization of the leaky integrate-and-fire model (Jolivet, Lewis and Gerstner, 2004). The equation for the Spike Response Model is as follows:

$$u(t) = \eta(t - \hat{t}) + \int_0^{\infty} \kappa(t - \hat{t}, s) I(t - s) ds \quad (4.4)$$

Where \hat{t} is the firing time of the last spike of neuron, η describes the form of action potential and its spike after-potential, $u(t)$ is the stimulating current, and K is the linear response to an input pulse.

Keat *et al.* used this model to predict every single spike in a spike train in retinal ganglion cells in salamanders, rabbits, and cats (Keat *et al.*, 2001). In 2004, Northmore implemented this model in a spiking neuron network that reflects the retino-tectal-motor system in fish and has the ability to extract the information from the environment for navigation with minimal resources (Northmore, 2004). Two years later, Jolivet *et al.* used this model to predict the spike timing of neocortical pyramidal neurons and found that a simple threshold process could capture most of the non-linearities (Jolivet *et al.*, 2006). Carandini, Horton, and Sincich used this model in 2007 to verify that the geniculate spike train could be predicted from retinal spike trains on the basis of postsynaptic summation (Carandini, Horton and Sincich, 2007). In 2008, Pillow *et al.* fit the physiological data to this model to

provide a general framework for understanding the correlated activity in populations of neurons and indicated that the noise in the spike train is reduced when encoding at the population level compared to responses from individual neurons (Pillow *et al.*, 2008). In 2010, Lazar, Pnevmatikakis, and Zhou presented a framework containing spiking neurons modelled with a Spike Response Model as an encoder for population spiking, and this framework can reconstruct a natural video scene (Lazar, Pnevmatikakis and Zhou, 2010). One year later, Glackin et al. created a supervised and fuzzy reasoning spiking neuronal network with the Spike Response Model approach for each neuron to develop a biologically plausible network that could tune itself based on biological principles (Glackin *et al.*, 2011). In 2012, Ghani et al. used this model to develop a network of spiking neurons to evaluate the output of a CMOS-based synapse (Ghani *et al.*, 2012).

4.2.3 Izhikevich model

In 2003, Izhikevich proposed a spiking neuron model to provide a flexible framework for neuroscientists to easily construct spiking neurons with different types of dynamics, using a simple differential equation with a minimal cost of computation (Izhikevich, 2003). In particular, the equation of this model is a reduction of the Hodgkin–Huxley model to a two-dimensional system of an ordinary differential equation:

$$\begin{aligned} \frac{du}{dt} &= 0.04u^2 + 5u + 140 - w + I \\ \frac{dw}{dt} &= a(bu - w) \\ \text{if } u &\geq +30mV, \text{ then } \begin{cases} u \leftarrow c \\ w \leftarrow w + d \end{cases} \end{aligned} \quad (4.5)$$

Due to the simplification of the model, many spiking neurons have been constructed based on the Izhikevich model. Durackova and Grega developed a computational neuronal network for image processing, with each element implemented using the Izhikevich model (Durackova and Grega, 2006). In 2009, Gjorgjieva, Toyozumi, and Eglen replicated the retinal waves in the lateral geniculate nucleus. They found that by integrating pre- and post-synaptic bursts, irrespective of their firing order, over a second-long timescale, the burst-time-dependent plasticity can guide On/Off segregation robustly without normalization (Gjorgjieva, Toyozumi and Eglen, 2009). In 2011, Rasch et al. used this model to simulate the response of the primary visual cortex (V1) area in the lateral geniculate nucleus and showed that the model can generate realistic spiking activity despite its simplifications and abstractions. Rast et al. implemented this model in a neuromimetic chip to support hetero-generous simulations of biological mechanisms in real time (Rasch *et al.*, 2011). Stodilka et al. also simulated the cortex to examine the effect of extremely low-frequency electromagnetic fields on brain tissue through the transduction mechanism (Stodilka *et al.*, 2011). In 2012, Wacongne, Changeux, and Dehaene presented a neuronal model of auditory cortex

based on predictive coding to simulate the mismatch negativity (Wacongne, Changeux and Dehaene, 2012). Wijekoon and Dudek also implemented the Izhikevich model to a Very Large Scale Integration integrated circuit to simulate the neocortical neuron (Wijekoon and Dudek, 2012). In 2013, Cassidy, Georgiou, and Andreou applied the Izhikevich model to design a neuromorphic chip that contains millions of spiking neurons and Spike Timing Dependent Plasticity learning using Field Programmable Gate Arrays (Cassidy, Georgiou and Andreou, 2013). In the same year, Cevikbas and Yildirim used this model to develop a simplified visual cortex model used for digit recognition, whereas Ratnasingam and Robles-Kelly implemented this to create a spiking network to discriminate colours that was invariant to the illuminance (Cevikbas and Yildirim, 2013; Ratnasingam and Robles-Kelly, 2013).

4.2.4 Advantages and disadvantages

The advantage of the threshold-fire model is the capability to simulate a large number of neurons with a reasonable computational cost, as shown in Table 4.1. The reason for this is the simplicity of the model in which the biological firing properties are simulated using the time derivatives of the law of capacitance. On the down side, if the model receives a sub-threshold signal at any time, it will retain the accumulation until it gets fired again.

4.3 Compartment model

A compartment model is a system that replicates the biological neuron by dividing the neuron into multiple components, where each neuron is treated either as one or multiple compartments, depending on the details of the model. Each component in the system can simulate the behaviour of neurons and interact with other compartments using appropriate differential equations. The neuron is treated as an electrical circuit as follows:

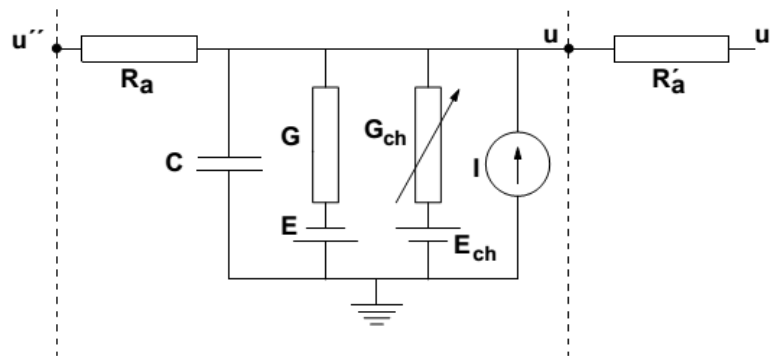


Figure 4.2: A neuron cell as compartment circuitry. Reproducing with permission (Coelho and Gerais, 2005).

The corresponding equation for the above circuitry is as follows:

$$C \frac{du}{dt} = (E - u)G + \sum_{ch} (E_{ch} - u)G_{ch} + \frac{(u' - u)}{R'_a} + \frac{(u'' - u)}{R_a} + I \quad (4.6)$$

According to the above equation, u is the membrane potential that propagates along the membrane capacitance C and causes a current flow through the resistance

R_a/R_a' into or out of the circuit. This leads to a difference in membrane potential between two compartments marked as $u-u''$. The membrane conductance is described as G_{ch} , and the battery represents the corresponding equilibrium potential. In addition, the leakage conductance G and associated equilibrium E are close to U_{rest} , and external input is shown as I .

In 1995, Ohshima, Yagi, and Funahashi presented a compartment model of H1 horizontal and red cones for simulating the spatio-temporal response of the light induced with regard to membrane impedance, strength of chemical synapse, and coupling resistance (Ohshima, Yagi and Funahashi, 1995). Smith and Vardi also simulated AII amacrine cells as a compartment to study noise removal in amacrine cells when combining the signal from rods in the mammalian retina (Smith and Vardi, 1995). In 1996, Kamiyama, Ogura, and Usui also studied the ionic current in vertebrate rod photoreceptors using the compartment model (Kamiyama, Ogura and Usui, 1996). In 1999, Egelhaaf and Warzechat used this model to simulate the receptive field of the direction-selective cells in the fly and showed its role in encoding the time-dependent optic flow (Egelhaaf and Warzechat, 1999). One year later, Protti, Flores-Herr, and Gersdorff modelled the bipolar cell in the vertebrate retina to study the evoked Ca^{2+} spike in bipolar cells under light stimulation (Protti, Flores-Herr and von Gersdorff, 2000), and in 2002, Marian and Reilly proposed a computational biological model of motor control of directions (Marian and Reilly, 2002). Two years later, Sisak, Banin, and Blumenthal modelled the human retina

as a simple system with two compartments - the inner and outer retina - for enhancing the understanding of retinal pathologies (Sisak, Banin and Blumenthal, 2004), whereas in 2006, Publio, Oliveira, and Roque explored deeper into this field by continuing to use the compartment model to create a realistic model of rod photoreceptors with a direct current injection instead of the photo-transduction process, thus reducing the computational cost of modelling (Publio, R. F. Oliveira and Roque, 2006). In 2007, Neumann, Yazdanbakhsh, and Mingolla created a single-compartment model of neurons with non-linear interaction for determining the mechanism of surface perception to identify and discriminate objects (Neumann, Yazdanbakhsh and Mingolla, 2007). In 2010, Raudies and Neumann also studied surface perception with regard to discriminating objects in front from those in the background using the compartment model and indicated the role of V1 response variations (Raudies and Neumann, 2010). Kampeter et al., on the other hand, used the compartment model to experiment with the intraocular concentration of triamcinolone acetonide over an 8-month period in rabbits (Kampeter, Cej and Jonas, 2008), whereas Rattay, Paredes, and Leao studied the extracellular and intracellular stimulation of cell membranes in terms of the strength–duration relationship (Rattay, Paredes and Leao, 2012). In 2013, Lu and Madhukar developed the stimulation of synthesized photovoltaic nanoscale cellular prostheses to induce repetitive action potential under continuous light (Lu and Madhukar, 2013), whereas, in early 2014, Chang and He studied the role of bipolar cell

terminals in response latency to light adaptation of ganglion cells using an 8-compartment model of cone bipolar cells (Chang and He, 2014).

4.3.1 Advantages and disadvantages

In general, this model maintains computational accuracy in terms of biological meaning by treating a neuron as having multiple compartments with each compartment having its own membrane potentials. This allows the model to be tuned and fitted into different neuron types according to their biological structures. The limitation of this model is the number of assembled compartments to simulate a network of neurons because the more accurate the model the more compartments are required, which will increase the computation cost of the model.

4.4 Linear-Non-linear-Poisson model

The linear-nonlinear-Poisson (LNP) model was developed to capture the stimulus-response relationship and relevant neuronal dynamics. As described below, in Figure 4.3, the LNP model contains a spatial linear filter $L(x, y)$, temporal non-linear filter $N(t)$, and Poisson process $P(t)$. The spatial linear filter is accountable for the spatial integration of the input stimulus, whereas the temporal non-linear filter used for simulating the spike rate and the Poisson process is applied to generate the spike train.

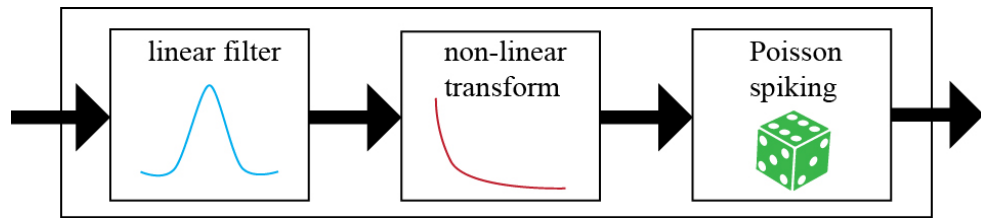


Figure 4.3: Linear-Non-linear-Poisson model. Reproducing with permission (Ostojic and Brunel, 2011).

In 1986, Hunter and Korenberg proposed a linear–non-linear system and its variants for simulating a non-linear biological system (Hunter and Korenberg, 1986). Shah and Levine applied the LNP model without the Poisson process to simulate the retina that accounts for the processing in a primate cone system and validated it with data from experiments conducted in monkeys, thus showing the role of the LNP model in simulating an artificial retina (Shah and Levine, 1993). Keat et al. in 2001 used this model to predict the response of ganglion neurons in the retinas of salamanders, rabbits, and cats (Keat *et al.*, 2001). In 2005, Zaghloul, Boahen, and Demb modelled such a spike when studying the spiking behaviour in contrast sensitivity of ON and OFF ganglion cells (Zaghloul, Boahen and Demb, 2005). In the same year, Kenyon et al. used this method to model the whole retina and found that the spiking oscillations encode the overall size of the stimulus (Kenyon *et al.*, 2005). In 2006, Schwartz et al. analysed the spike-triggered stimulus ensemble to characterize the LNP model (Schwartz *et al.*, 2006). In 2007, Paninski, Pillow, and Lewi discussed the use of the LNP model to adapt and optimize the stimuli presented to the cell on a trial-by-trial basis as well as suggested the optimal

model parameters (Paninski, Pillow and Lewi, 2007). In 2008, Shlens, Rieke, and Chichilnisky also simulated synchronized firing in the ON and OFF parasol cells in primates by using the LNP model (Shlens, Rieke and Chichilnisky, 2008). Haefner and Cumming also created an energy model to predict the response of neurons to nonphysical left and right image pairs and indicated the presence of multiple excitatory and suppressive spatiotemporal subunits within V1 receptive fields (Haefner and Cumming, 2008). Baccus et al. also used this model to simulate the retina, with the capability to compute object motion (Baccus *et al.*, 2008). Beaudoin et al., on the other hand, simulated the ‘contrast gain control’ mechanism in retinal ganglion cells using the LNP model (Beaudoin, Manookin and Demb, 2008). In 2009, Wohrer and Kornprobst proposed a complete model of the biological retina with contrast gain control with all five cell types, such as photoreceptors, horizontal cells, bipolar cells, amacrine cells, and ganglion cells (Wohrer and Kornprobst, 2009). In 2010, Shinomoto used the LNP model to create a stochastic model of neuronal spiking and fit that model to biological data and found that this stochastic model can predict the precise times of individual spikes evoked by fluctuating current (Shinomoto, 2010). Zhijun and Qingli also used the LNP model to simulate the processing inside the retina, but without a contrast gain control mechanism (Zhijun Pei and Qingli Qiao, 2010). In contrast, in 2011, Decuyper et al. implemented the LNP approach in their model to simulate the contrast gain control mechanism in mesopic design through the rod-cone gap

junction (Decuyper and Capron, 2011). In 2012, Suh captured the spiking behaviour in parallel On and Off ganglion cells using the LNP model (Suh, 2012). In 2013, Maravall et al. studied the adaptation of the barrel cortex firing rate to the variance of a whisker stimulus, whereas Vasserman, Schneidman, and Segev studied the adaptation of colour-contrast coding in ganglion cells, and they found that the retina adjusted the red and blue stimulus inputs to balance them (Maravall *et al.*, 2013; Vasserman, Schneidman and Segev, 2013). Moreover, in 2013, Garvert and Gollisch simulated the retina using the LNP model to explore the local and global contrast adaptation in retinal ganglion cells (Garvert and Gollisch, 2013). In early 2014, Dhruv and Carandini used this LNP model to emphasize the cascade effects of spatial adaptation in the lateral geniculate nucleus and V1 areas of mice (Dhruv and Carandini, 2014).

4.4.1 Advantages and disadvantages

Compared to the other models, the advantage of the LNP model is the simplification in implementation and computational cost, especially in spike analysis. By taking into account spatial and temporal filters for the responses of neurons, the computation is reduced but the biological meaning is still preserved at the abstract level for modelling retinal neurons (i.e. in simulating the centre-surround and saturation effect of the eyes). This advantage is also the drawback because the biological meaning determined from this model will lack accuracy. However, this

model is suitable for simulating the responses of retinal neurons because the visual signal is processed as spatial and temporal responses in sequence.

4.5 Discussion

According to the structure and function of the retina, only ganglion cells and some bipolar and amacrine cells have the ability to generate spiking activity, whereas most other cells only propagate grade potential without spiking. This leads to the consideration of the following spiking models for ganglion cells in conductance-based, threshold-fire categories: Hodgkin–Huxley, Morris–Lecar, integrate-and-fire, and Izhikevich. Among these models, Hodgkin–Huxley and Morris–Lecar have the advantage of being able to describe the details of the processing mechanism and biological parameters compared to the integrate-and-fire and Izhikevich models. However, the major disadvantage of these two models is that they cannot be implemented as a large-scale model, due to the computational cost and time involved. In particular, it takes 600 and 1200 FLOPS (Floating Point Operations per Second) for Morris–Lecar and Hodgkin–Huxley, respectively, compared to 5 and 13 FLOPS for the integrate-and-fire or Izhikevich approaches (Izhikevich, 2004). Therefore, the most suitable model for simulating the ganglion cells is either the integrate-and-fire and Izhikevich model. Between these two models, the integrate-and-fire model and its variants can simulate the spike faster than the Izhikevich model can. However, compared to the Izhikevich model, the

integrate-and-fire model is limited with regard to model variance as this model cannot simulate the tonic bursting spikes in the retina (Izhikevich, 2004). The Izhikevich model is better than the integrate-and-fire model in this regard and provides a wide range of options for simulating spiking neurons as well as lower computational cost (5 FLOPS compared to 13 FLOPS). Therefore, the Izhikevich model has been selected to simulate the ganglion cells and spiking process in the model proposed in this thesis.

Model	Tonic Bursting	Mixed Firing (Spiking & Bursting)	Floating Point Operations per Second (FLOPS)
Hodgkin–Huxley	Yes	No	1200
Morris–Lecar	No	No	600
Integrate-and-fire	No	No	13
Izhikevich	Yes	Yes	5

Table 4.1: FLOPS comparison of different retinal models.

For the other cells in the retina such as the photoreceptors, horizontal cells, bipolar cells, and amacrine cells, either the compartment or LNP approach can best describe the activity of these non-spiking neurons. The compartment model has the same problem as the conductance-based model in that the cost and time for computation are not conducive to large-scale modelling; moreover, this thesis does not focus too deeply on the biological aspect of the retina; instead, the focus is on the implementation of a biologically reasonable and effective model to reflect and explain image processing mechanisms inside the retina. Based on the above-mentioned facts, the LNP model has been used to model the other cells in the retina.

The LNP model has the advantage of replicating the spatial and temporal responses of the retinal cells in both spiking and non-spiking phases, and the time for operation is acceptable for simulation in a large neuronal network (Dhruv and Carandini, 2014). The structure and detail of the retinal model will be described and explained in the methodology section.

4.6 Summary

In this chapter, a complete review of different approaches to model the retinal circuitry has been presented. In the review, the models were categorized and discussed based on their biological and image-processing aspects. In each category, the equation of the model and its applications in different fields are presented. The strength and drawback of each type of model have been discussed to justify the selection of the appropriate model to simulate the retinal circuitry in this thesis.

CHAPTER 5

SYSTEM MODELING

5.1 The retinal model

As discussed in CHAPTER 4, retinal modelling review, the LNP model (Dhruv and Carandini, 2014) is selected for modelling the retinal cells, except the ganglion cells. This was done by applying a linear filter followed by a non-linear filter to the spatial input to the retinal cell. This section will describe these filters in detail and explore the integration of these filters into a system that models retinal processing.

5.2 Linear–non-linear system

Dhruv and Carandini argued that the LNP model is a standard model used for modelling of retinal processing (Dhruv and Carandini, 2014) because of its ability to replicate the behaviour of the retinal cells both spatially and temporally. By applying a spatial filter followed by a static non-linear temporal filter, the linear and non-linear processing of the retinal cells is captured as observed in the biological retina (Schwartz and Rieke, 2011). The linearity property is an important factor in predicting the response of neural cells to an arbitrary spatial input by using the spatial response function (Shapley and Lennie, 1985).

The mathematical description of this approach is expressed in the following equation:

$$Output(x, y, t) = TF(I(x, y) * SF(x, y), t) \tag{5.1}$$

In the above equation, I is the visual input of an image to the retina at time t , fully stated as $I(x, y)$, while $SF(x, y)$ and $TF(x, y, t)$ are spatial and temporal filters applied to the input I , respectively. The symbol $*$ stands for the convolution operation to apply a filter to the input image I . From equation 5.1 above, the input image I is first convolved by a spatial filter SF ; the corresponding result is subjected to another filter TF to achieve a temporal response. The equations for the spatial and temporal filters are as follows:

$$TF(t, \omega) = \begin{cases} 0 & \text{if } t < 0 \\ \frac{1}{\tau} \exp\left[\frac{-t}{\omega}\right] & \text{if } t > 0 \end{cases} \quad 5.2$$

$$SF(x, y, \sigma) = \frac{1}{2\pi\sigma^2} \exp\left[\frac{-|x^2 + y^2|}{2\sigma^2}\right]$$

In temporal filter equation above, τ is length of the filter and ω is the intensity of input signal at time t . On the other hand, the variable σ in spatial filter defines the size of the spatial filter applied to $I(x,y)$. In detail, the spatial filter is a simplified version of the spatial low-pass filter or Gaussian filter, and the temporal filter is a variation of the exponential function. On the other hand, the exponential function may be applied to simulate the suppression of the retinal cell after a certain time, whereas the low-pass function models the distributed processing of the retinal cells according to their population in the retina. The retinal cells consist of different groups of cells and these groups respond to visual input differently based on different formations, and this formation was first described as a receptive field by

Rodieck in 1965 (Rodieck, 1965). The Gaussian filter is applied because of its advantage in simulating optical blur in vision and the blurring vision is a result of information processing of the retina as discussed in CHAPTER 2. This receptive field has been described in detail in the next section.

5.3 Model receptive field

According to Rodieck, the receptive field of the retina is separated into two types: centre and surround, and retinal cells inside each type respond differently, and the final output is the sum of both centre and surround responses (Rodieck, 1965). There are different types of retinal receptive fields exist, but, in general, a receptive field contains a centre and surround area as illustrated in Figure 5.1.

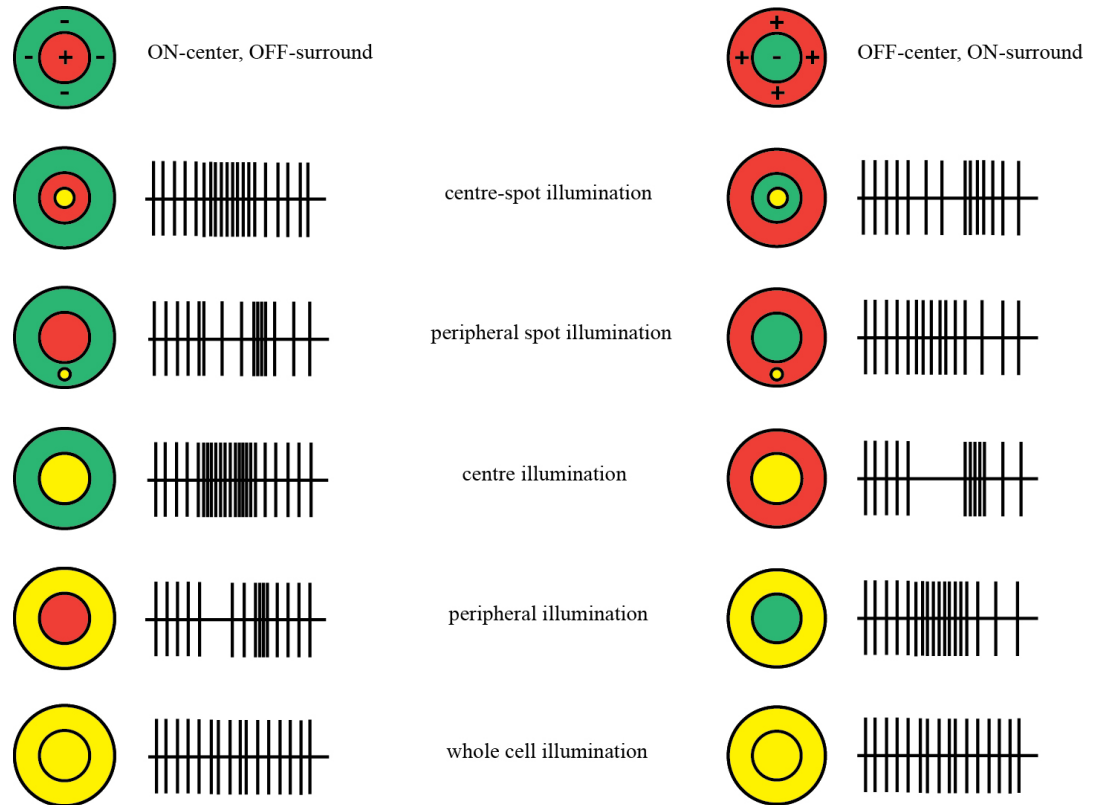


Figure 5.1: The response of receptive field of ganglion cells to different stimulus (Wohrer and Kornprobst, 2009).

In the figure above, cells in the centre and those surrounding the receptive field respond in different ways to stimuli, depending on the coverage of the stimuli on the cell surface. Thus, two major types of receptive fields are categorized: ON-centre and OFF-centre receptive fields. As illustrated in Figure 5.1 above, for the receptive field in ganglion cells, the ON-centre ganglion cell fires rapidly when the light stimulus is on the centre only and does not fire when light is projected on the surround area. No firing occurs when no light is projected on the whole receptive

field, and the cell fires with lower frequency when the light covers the whole cell. In contrast, no firing occurs when the light stimulus covers the centre area, but rapid firing occurs when the surround area is covered in OFF-centre ganglion cells. In case of the whole cell, covering the OFF-centre ganglion cell elicits the same response as the ON-centre ganglion cell, that is, it fires with normal frequency. Based on this property, the information entering the retinal cell is filtered and reduced; however, the cell can still process the input with the remaining information. An example for this concept is the edge detection mechanism in edge-detecting ganglion cells (Figure 5.2), in which the receptive field functions as a spatial filter to extract the edges from the visual input (Huk, 2014).

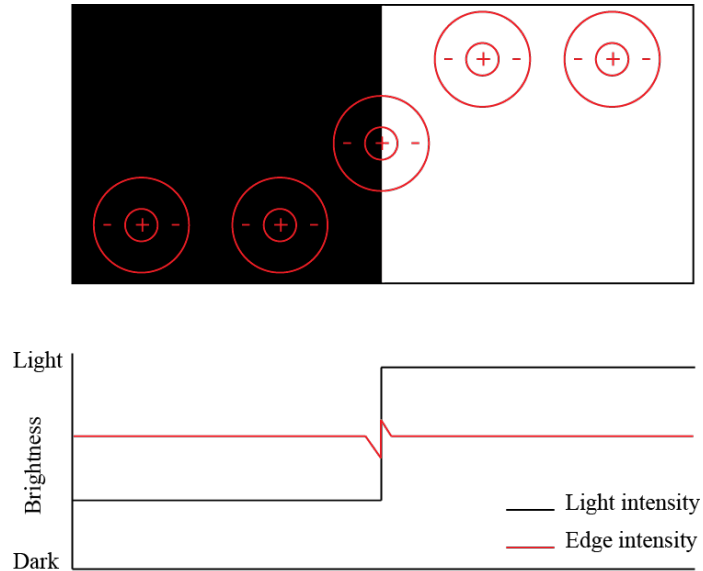


Figure 5.2: Edge detection as a result from receptive field(Corney and Lotto, 2007).

The receptive field is an important factor for information processing in the retina, and this factor must be implemented in the proposed model. Equation 5.3

describes how the information is processed through the receptive field for the model proposed in this thesis.

$$Bipolar_{ON\ CONE} = \sum_{x,y=0}^{R_{Center}} \frac{Cones(x,y)}{\varphi^{C_{Cones}}} - \sum_{x,y=0}^{R_{Surround}} \frac{Horizontal(x,y)}{\varphi^{S_{Horizontal}}} \quad 5.3$$

$$Bipolar_{OFF\ CONE} = \sum_{x,y=0}^{R_{Surround}} \frac{Horizontal(x,y)}{\varphi^{S_{Horizontal}}} - \sum_{x,y=0}^{R_{Center}} \frac{Cones(x,y)}{\varphi^{C_{Cones}}}$$

From the equation above, at the OPL layer, there are photoreceptors, bipolar cells, and horizontal cells involved in the processing pathway, and the processed signals from the photoreceptors and horizontal cells are passed on to the bipolar cells as output. According to the biological retina, at the OPL layer, the signals from the horizontal cells act as surround information, whereas the signal from the photoreceptors act as centre information. The combined signals from the centre and surround information are transferred to the bipolar cells for further processing. On the other hand, at the IPL layer, the signals from the bipolar cells are used as centre signals while the surround signals are obtained from amacrine cells and the output signals are transmitted to the ganglion cells. In addition, the difference in the combination of the centre and surround signals create different processing pathways such as the ON and OFF pathways. The ON pathway includes centre

signals, without any surround signal, whereas the opposite is true for the OFF pathway.

Several receptive fields have been described in the literature in addition to the receptive field with symmetry and circular formation for centre and surround signals as described below. A receptive field proposed by Conway (Conway *et al.*, 2010) is shown in Figure 5.3. The variations in receptive field formation show that the processing pathway inside the retina can differ according to the purpose. This shows that the role of the receptive field formation in retinal information processing is still an open question for many researchers. This issue is also addressed in later sections of this thesis by proposing a receptive field with a different weight distribution for centre and surround cells and verifying the proposed receptive field through the Hermann grid.

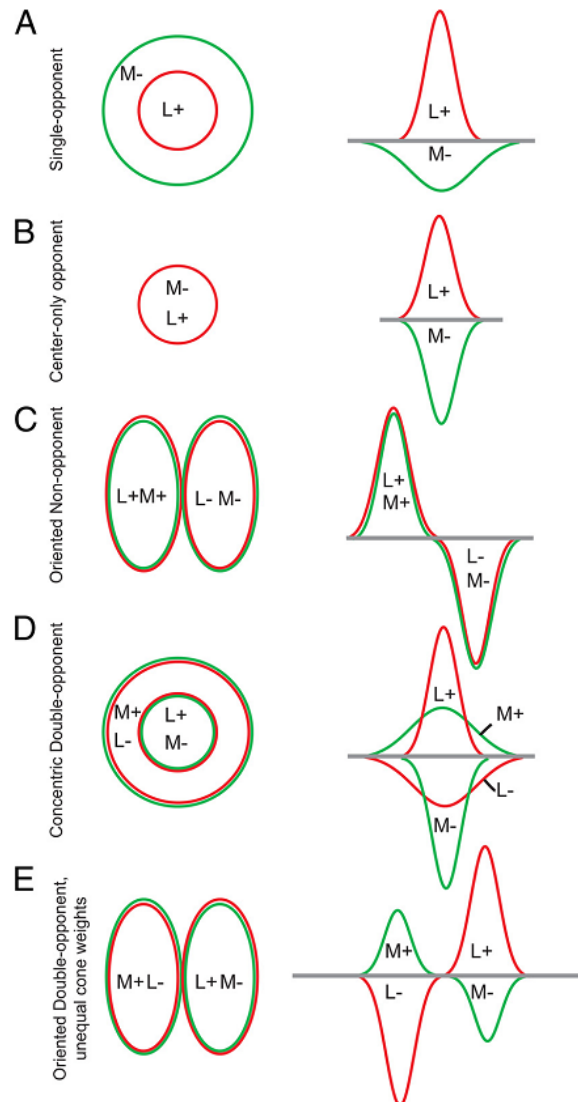


Figure 5.3: Different types of receptive fields. Obtained with permission from Conway et al. (Conway *et al.*, 2010).

5.4 ON and OFF pathways

As mentioned above, the different combination of signals in the receptive field creates two different pathways called the ON and OFF processing pathways in the

retina. The roles of these pathways are not completely understood, and they are still being investigated. The ‘push–pull’ mechanism has been proposed to explain the origin of the OFF pathway based on the ON pathway and vice-versa. In this proposal, the OFF ganglion cell signal is believed to originate from the ON pathway ganglion cell signal, and this mechanism is controlled by the amacrine cells in the retina. In a later section of this thesis, this mechanism is used to explain colour processing of the retinal model, with the involvement of the amacrine cells. In the proposed model, the ON and OFF pathways are separated, and in each pathway, the connection differs based on the processing involved.

5.5 Cone and rod pathway

In addition to separate processing in the ON and OFF pathways, two other important factors must be considered: the rods and cones for each pathway are responsible for vision under specified conditions such as night and day, respectively. Therefore, the roles of cones and rods in these pathways are discussed here in detail as well as their implementation in the proposed model.

5.5.1 Cone pathway

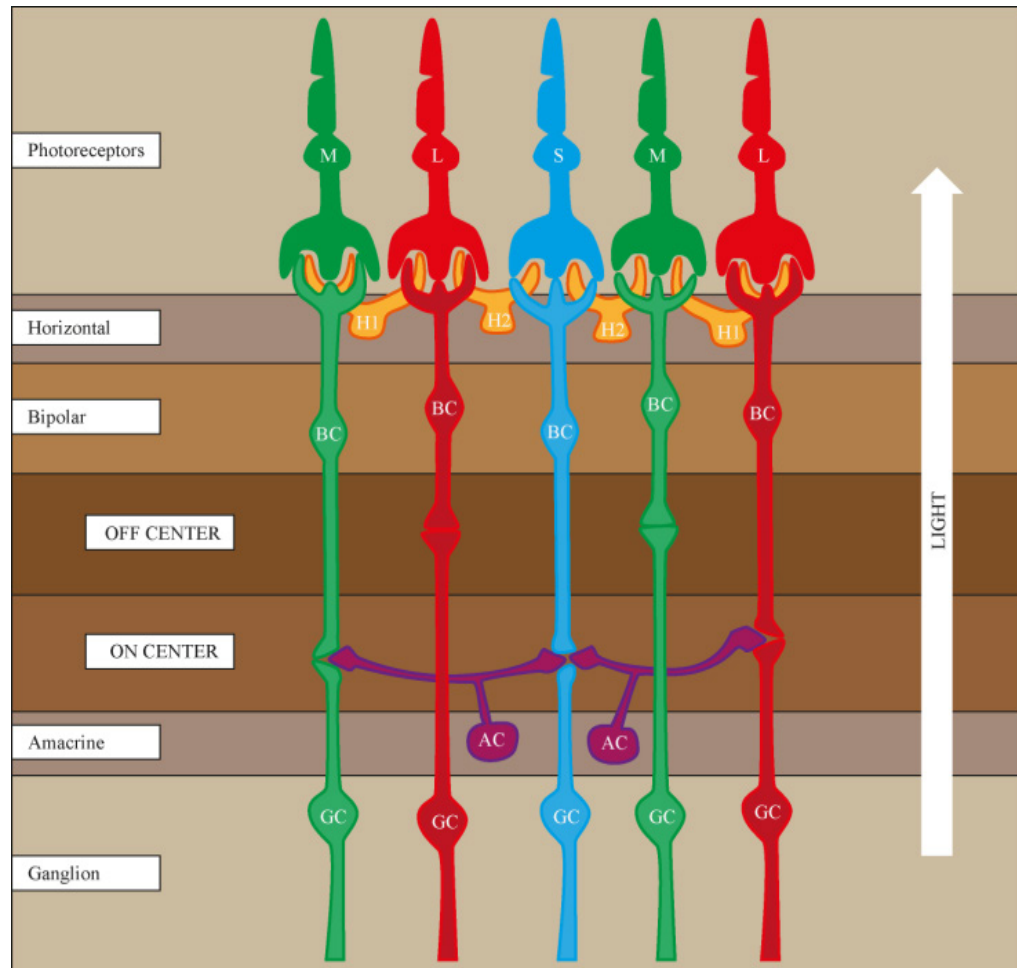


Figure 5.4: Cone pathway in retina.

Figure 5.4 depicts the cone system in the photoreceptor layer of the primate retina. Three different types of cones are found: red (long, L), green (medium, M) and blue (short, S). Each type of cone has its own connectivity and results in the L-on/L-off, M-on/M-off, and S-on pathways. For instance, the L-cone will connect to H1 horizontal cells to form the L-on and L-off pathways, and the same connectivity is

applied to M-cone ON and OFF pathways. On the other hand, in the S-on pathway, S-cones are connected to H2 horizontal cells. As a result, this creates five different pathways to the ganglion cells through the bipolar cells. Another horizontal cell, H3, connects only to the L-cone and M-cone, but as mentioned in CHAPTER 2, this cell is not discussed here because of the lack of knowledge regarding it. The bipolar cells discussed here are the midget bipolar cells, which are shown to contribute to high-acuity colour vision. L, M, and S midget bipolar cells connect to L, M, and S cones, respectively, as well as to the H1 and H2 horizontal cells. The connection pattern is based on centre-surround antagonism, which determines the receptive fields of these bipolar cells. Photoreceptors provide centre signals, whereas horizontal cells provide surround feedback to bipolar cells. According to Figure 5.4, L and M midget bipolar cells receive centre signals from L and M cones and surround signals from H1 horizontal cells. In the S midget bipolar cell, a small change occurs, and the surround signal is obtained from H2 instead of H1. Corresponding to these bipolar cells are six different types of ganglion cells: Red-ON/Green-OFF, Red-OFF/Green-ON, Green-ON/Red-OFF, Green-OFF/Red-ON, Blue-ON/Yellow-OFF, and Blue-OFF/Yellow-ON. These ganglion cells integrate photoreceptor signals via bipolar cells and project to the brain via the lateral geniculate nucleus in the thalamus. This pathway is responsible for processing colour information in the retina and is explored in detail in CHAPTER 8 in the model proposed for processing colour enhancement.

5.5.2 Rod pathway

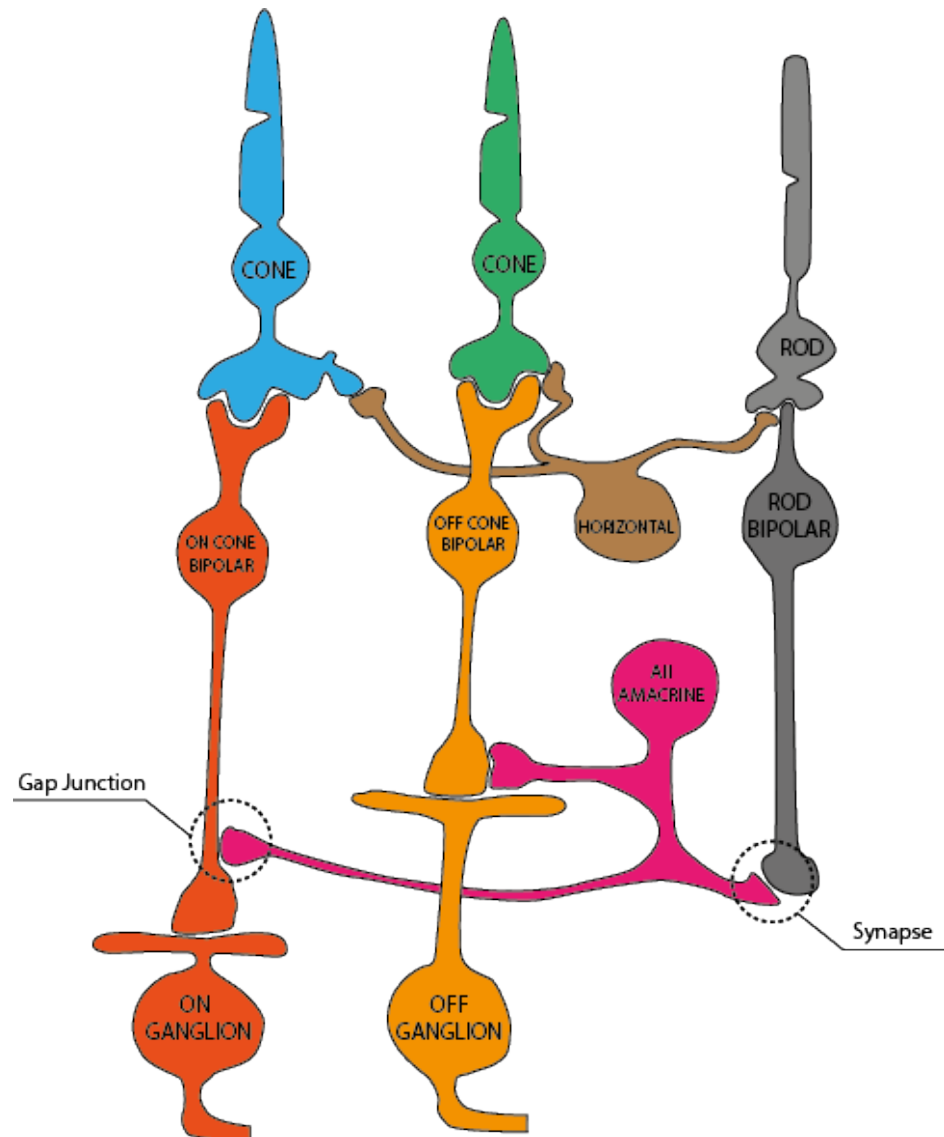


Figure 5.5: Rod pathway in retina.

In contrast to the cone system, the rod system plays a role in perceiving the visual scene in low-light conditions such as night or mesopic conditions. Unlike the cone system, which comprises three different types of cones, only one type of rod is

present. This rod is connected to a specific bipolar cell called the rod bipolar cell as well as horizontal cells as described in the receptive field section. The rod bipolar cell then synapses to the AII amacrine cell, and this amacrine cell in turn connects to the cone bipolar cell through the gap junction. This pathway is responsible for processing visual signals in conditions of low light such as dusk or night time. In CHAPTER 7, this pathway is implemented in the model and utilized for processing contrast in low-light conditions.

5.6 Implementation in the proposed model

A model for retinal processing was constructed based on the linear–non-linear approach based on the knowledge of the receptive field, ON/OFF pathways, and rod/cone pathways. The details of this model are illustrated in Figure 5.6:

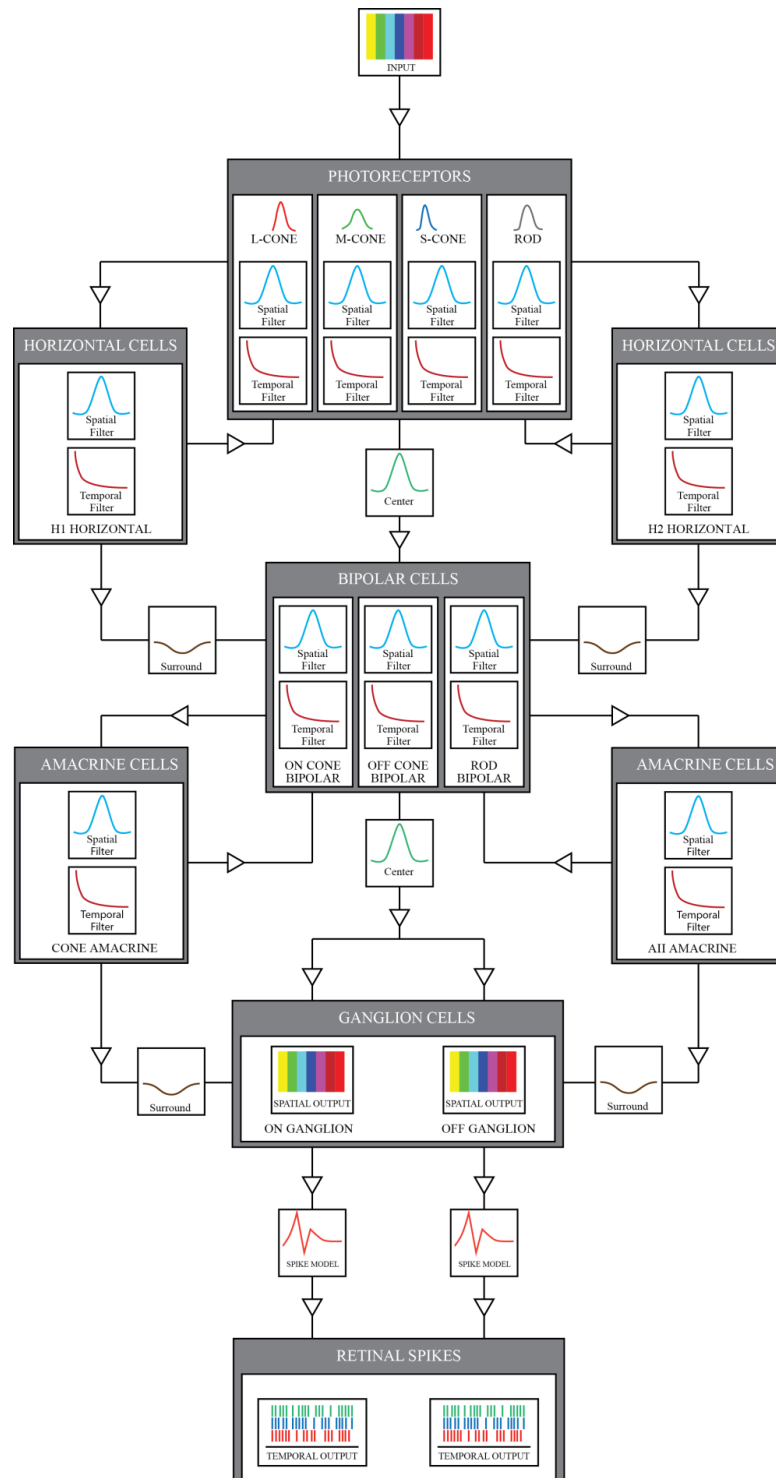


Figure 5.6: Proposed retina model

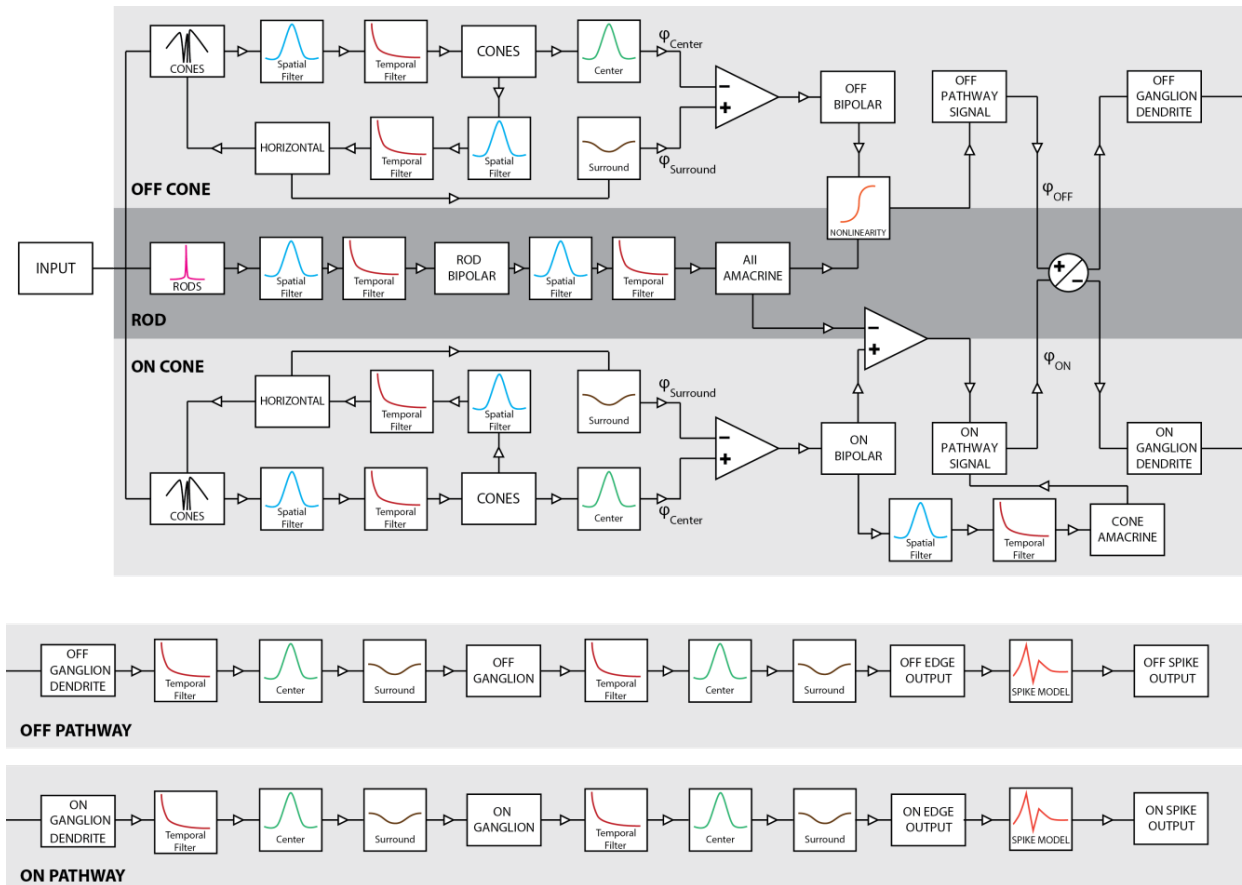


Figure 5.7: Rod pathway circuitry in the model.

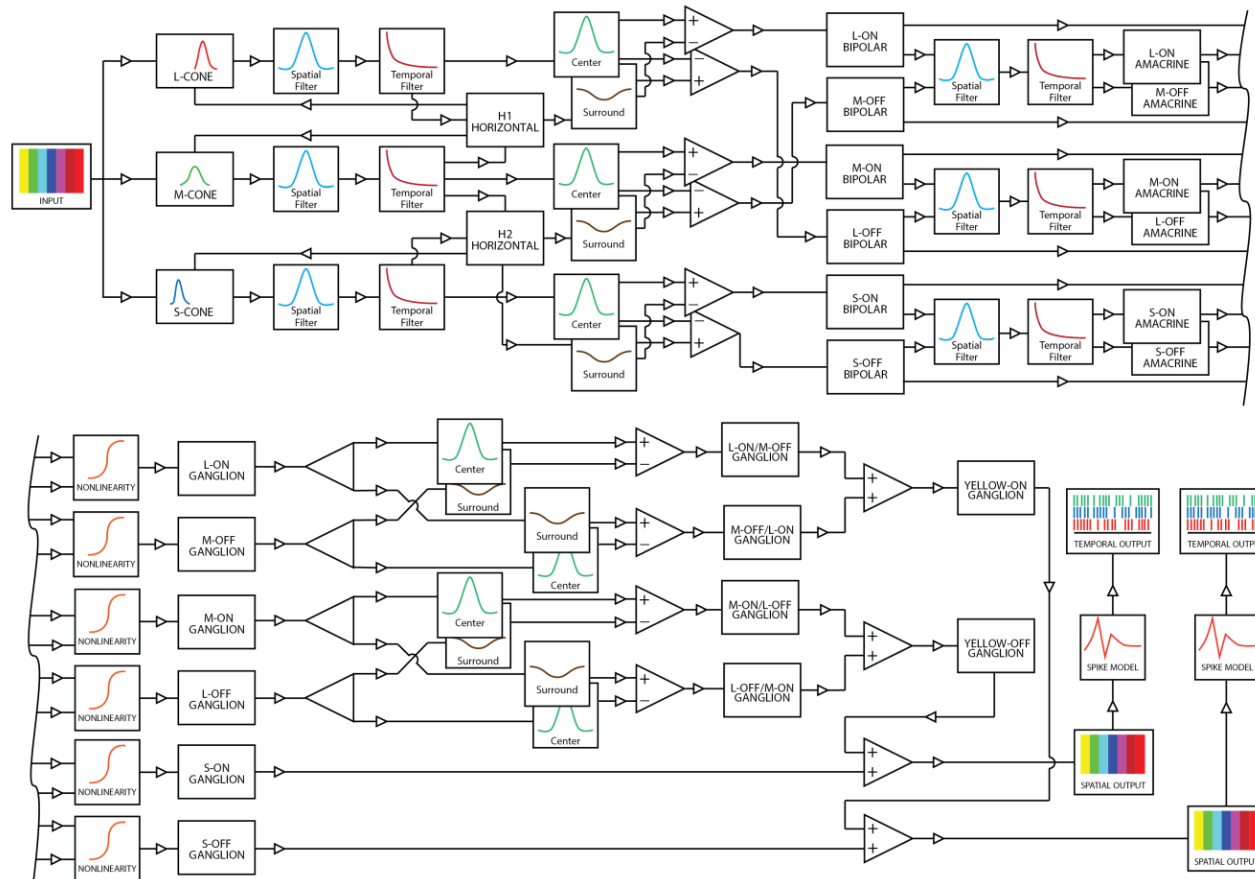


Figure 5.8: The cone pathway in the model.

The definitions for the block diagram in the illustrations above are:

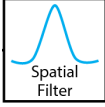
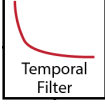
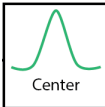
Symbol	Definition	Equation
	Spatial filtering operation: Applying spatial filter to input signal.	$TF(t, \omega) = \begin{cases} 0 & \text{if } t < 0 \\ \frac{1}{\tau} \exp\left[-\frac{t}{\tau}\right] & \text{if } t > 0 \end{cases}$
	Temporal filtering: Applying temporal filter to input signal.	$SF(x, y, \sigma) = \frac{1}{2\pi\sigma^2} \exp\left[-\frac{ x^2 + y^2 }{2\sigma^2}\right]$
	Receptive field computation in center: Compute center output signal of receptive field.	$Bipolar_{ON\ CONE} = \sum_{x,y=0}^{R_{Center}} \frac{Cones(x,y)}{\varphi_{CCones}} - \sum_{x,y=0}^{R_{Surround}} \frac{Horizontal(x,y)}{\varphi_{SHorizontal}}$
	Receptive field computation in surround: Compute surround output signal of receptive field.	$Bipolar_{OFF\ CONE} = \sum_{x,y=0}^{R_{Surround}} \frac{Horizontal(x,y)}{\varphi_{SHorizontal}} - \sum_{x,y=0}^{R_{Center}} \frac{Cones(x,y)}{\varphi_{CCones}}$
	Nonlinearity computation: Applying non-linearity computation to input signals.	$GDS_{ON}(t) = \varphi_{ON} * S_{ON} + \varphi_{OFF} * S_{OFF}$ $GDS_{OFF}(t) = \varphi_{ON} * S_{ON} + \varphi_{OFF} * S_{OFF}$ $Ganglion = Bipolar^{2.2Amacrine - 1}$
	Spiking computation: Applying Izhikevich model to input signals to generate spiking signals.	$\begin{cases} v' = 0.04v^2 + 5v + 140 - u + I \\ u' = a(bv - u) \end{cases}$ $\text{if } v \geq 30\text{ mV, then } \begin{cases} v \leftarrow c \\ u \leftarrow u + d \end{cases}$

Table 5.1: Processing block and its definition in proposed model.

In the illustrations above, the retinal cell is indicated by a block with specific name such as bipolar cell, horizontal cell, ganglion cell...while processing block is indicated by different block as shown in Table 5.1. Initially the input image will be split into rod and cone signals then applied spatial and temporal filters in sequent to generate responding signals of horizontal cells. The applying of spatial and temporal filters is the convolution operation where the input image is convolved

with a predefined kernel. This operation is repeated to generate signals of bipolar and amacrine cells while the nonlinearity process is applied at amacrine cell level to compute contrast and colour information as discussed in later section. At ganglion cell level, Izhikevich spiking model is applied to bipolar output signal generate spiking response of ganglion cell. According to Wilson, the spatial filter is used to simulate the response of the retinal cells inside a receptive field, and the response of the spatial filter is different between cells of a different configuration (Wilson *et al.*, 1981). In addition, the cell responses are weighted with different weights for centre and surround, since centre and surround cells respond differently, depending on their cell concentrations. The temporal filter is used to simulate the suppression of retinal cells after a certain time and the decrease in output signals from the retinal cells over time, before reaching the ganglion cells, are mostly graded potential. Although the spatial processes inside the retina are non-linear in major cells, spatial linear filters were used in this model for the following reasons. Tranchina et al. stated that the visual signals in the retina at the photoreceptor layer are not affected by the non-linearity distortion (Tranchina *et al.*, 1981), whereas Halupka confirmed the accuracy of the linear–non-linear model in predicting the cortical responses with simultaneous electrical stimulation (Halupka, 2014). According to Rodieck, the recording made at the output of ganglion cells has shown that linear filters in both space and time were able to approximate their behaviours

and the neurons were subject to a temporal undershoot in neurophysiologic experiments (Rodieck, 1965). Although the linear filter is sufficient to accurately estimate the firing rate of a single ganglion cell, this approach fails to match the actual retinal output recording when more sophisticated stimuli are presented. To overcome this, a non-linear stage is added after the linear filter to reproduce the behaviour of the biological retina more accurately. Therefore, the spatial and temporal filters are applied repeatedly at every cell layer, except the ganglion cell layer as mentioned above, in this model. In terms of signal summation, excitation is indicated by the plus (+) symbol, whereas inhibition is indicated by the minus symbol (-). On the other hand, the surrounding signal is taken from the horizontal cells and amacrine cells in the OPL and IPL layer, respectively, and the signal is combined with the centre signal to form ON and OFF pathways.

The model described here is the basic processing pathway in the retina, and connections for contrast and colour processing have been specified as shown in Figure 5.7 and Figure 5.8, respectively. In the cone pathway, the same method for signal integration is applied for each cell type, but there are five different streams for five different colour pathways, as mentioned in CHAPTER 2. A non-linearity step is performed to process the colour information between bipolar and amacrine cells at the IPL layer. The details of this non-linearity are later discussed in CHAPTER 8. On the other hand, the rod pathway is implemented with rod bipolar

cells, AII amacrine cells, and ganglion dendrites to process signals for contrast enhancement. This configuration will be discussed in CHAPTER 7.

5.7 Spiking neurons

CHAPTER 2 stated that the output signals in the retina are graded potential and action potential, with action potential generated at the ganglion cell layer and graded potential at the other cells. Furthermore, as discussed in CHAPTER 4, the ganglion cells in this model are simulated with the Izhikevich model, and this spiking generation is added after the linear–non-linear processing in the previous layer of the model. This method is similar to the linear-non-linear-Poisson model for generating action potential, but here, spiking generation is replaced by the Izhikevich model and the linear–non-linear processing step occurs in previous layers as described above. The model for spiking based on the Izhikevich model is described below:

$$\begin{cases} v' = 0.04v^2 + 5v + 140 - u + I \\ u' = a(bv - u) \end{cases} \quad 5.4$$

if $v \geq 30 \text{ mV}$, *then* $\begin{cases} v \leftarrow c \\ u \leftarrow u + d \end{cases}$

Where $a = 0.02, b = 0.2, c = -65 \text{ mV}$ and $d = 2$

According to Izhikevich, equation 5.4 is a two dimensional system of ordinary differential equations that is reduced from Hodgkin-Huxley model using bifurcation methodologies (Izhikevich, 2003). In this equation, parameter a is the time scale of the recovery variable u , b is the sensitivity of the recovery variable u

to the membrane potential v , c is the after-spike reset value of membrane potential v and d is the after-spike reset of the recovery variable u caused by slow high-threshold Na^+ and K^+ conductances.

As shown in the model diagram, the outputs from spatial and temporal filters are fed to the Izhikevich model as input current I , and from this, the voltage V is integrated through time to obtain the corresponding spikes. Similar to the bipolar cells, the ganglion cells are also gathered into a group and form the receptive field in ganglion cell layers with the centre derived from bipolar and surroundings derived from amacrine cells. This forms a spike train from the ganglion cell networks, and these spikes are analysed to assess the response of the retina in encoding information in different situations. The analysis of the ganglion cell spiking activity is presented in CHAPTER 7 and CHAPTER 8 in experiments of contrast and colour encoding of the retinal model in specific cases.

5.8 Model simulation

The model is implemented in C/C++ language and uses libraries such as OpenCV (Open Computer Vision) (Bradski, 2000) and CUDA (Compute Unified Device Architecture) platforms for image acquisition and parallel processing, respectively (Bradski and Kaehler, 2008; Nickolls *et al.*, 2008). OpenCV is an open source library for computer vision that is created by Intel and supports many programming languages, while CUDA is a framework to utilize a GPU (Graphics Processing

Unit) for computing information in parallel instead of just the CPU (Central Processing Unit). Both OpenCV and CUDA support C/C++; therefore, various mathematical functions provided in these frameworks can be invoked directly without using any code wrappers. On the other hand, parallel computing is useful for processing many visual signals at the same time, as described in Figure 5.7 and Figure 5.8. This reduces the operating time, and thus, the visual output can be observed continuously during the operation of the model. In this model, the visual inputs are acquired as still images and converted to an OpenCV structure called `cv:Mat` for computation. By using this structure, the visual inputs with dimension $W \times H$ are treated as matrices with W columns and H rows; thus, the computations function as matrix computations in mathematics. This model differs in that all the proposed algorithms are designed to run on a GPU by passing the matrices to the GPU for computing and transferring them back to the CPU for the purpose of being displayed. This is made possible by copying data from the CPU memory to GPU memory repeatedly, using functions implemented in the CUDA library.

Another feature of this model is the spiking generation function that converts visual inputs to neuronal spikes using the differential equation stated in section 5.7. To achieve this, the model is simulated using iteration for integrating the potentials in ganglion cells and the pseudo code for this iteration is as follows:

```

while run_error > stop_error
    V_out(t,:) = reset_voltage;
    I_out(t,:) = I_steady;
    I_state = spike_occurance*synapse_weight + I_state.*synapse_decay_rate;
    I_current = I_state + I_steady + ganglion_spatial_output(t,:)*synapse_weight;

    v = v + dt * (0.04*v.^2+5*v+140-u+I);
    u = u + dt * a.*(b.*v-u);

    fired = find(v >= 30);
    if ~isempty(fired)
        v(fired) = c(fired) ;
        u(fired) = u(fired)+d(fired) ;
    end;
    run_error = RMSE(ganglion_spatial_output, ideal_spatial_output);
    t = t + 1;
end;

```

As a result, the computing cost of the model running on GPU is reduced and the processing time is speeded up and this allows the model to be simulated many times within the same time compared to CPU. With this advantage, the model can be trained to compute optimized parameters in specific experiments as described in CHAPTER 6, CHAPTER 7 and CHAPTER 8.

5.9 Summary

This chapter provides a closer look of the proposed model and describes the model components in a mathematical way with regard to the linear–non-linear approach. In this model, the spatial and temporal filters are utilized to simulate the responses of the retinal cells with graded potential output. On the other hand, the Izhikevich model is used to simulate the action potential output in ganglion cells for analysing the encoding of the model. The receptive field concept is utilized in the model at the OPL and IPL layers to form the ON and OFF pathways, in addition to the rod

and cone pathways. In addition, the model is modified in cell connectivity for processing in specific cases such as contrast and colour processing. These modifications are presented in the next chapter.

CHAPTER 6

OUTER PLEXIFORM LAYER RECEPTIVE FIELDS AS UNDERLYING FACTORS OF THE HERMANN GRID ILLUSION

6.1 Introduction

A perceptual illusion occurs when a perceived vision contradicts physical measurements consistently in different people. This phenomenon is also known as an optical illusion, and various types of these illusions have been defined, such as motion illusions, luminance and contrast illusions, colour illusions, and geometric and angle illusions (Baumgartner and Levine, 1971). Among them, luminance and contrast illusions have received significant interest from physiologists and psychologists through a famous experiment called the Hermann grid illusion (Schiller and Carvey, 2005). When looking at the Hermann grid, which is an array of equidistant black-filled squares on a white background, one can perceive black or grey dots at the intersections of white bars. This phenomenon is interesting because the illusion is perceived at the peripheral field of the centre of view. Additionally, when inverting the colour of the grid, the perceived illusion is inverted as well; i.e. white or grey dots will appear instead of black or grey dots. The grid and its illusion are illustrated in Figure 6.1.

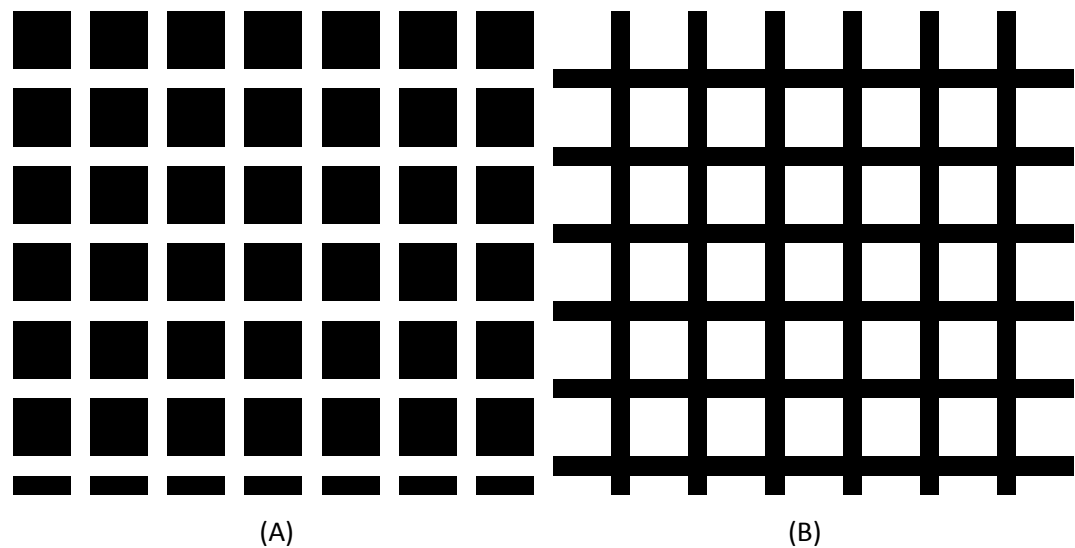


Figure 6.1: The original Hermann grid (A) and its inverted colour version (B).

The underlying neural and computational causes of the illusion have still not been completely determined, although many theories have been proposed (De Lafuente and Ruiz, 2004; Schiller and Carvey, 2005; Geier *et al.*, 2008). This chapter proposes an explanation for the illusion, wherein the outer-plexiform layer (OPL) plays a fundamental role by simulating the retinal response to the Hermann grid, and described different experiments to test this hypothesis. Specifically, the geometric shape of the receptive field in the OPL is proposed to be the factor that forms the illusion. Unlike the circular receptive field used in other works, the proposed receptive field has an asymmetrical shape, and the connectivity through this receptive field is distributed heterogeneously. Various experiments are conducted and discussed on the possibility of this proposed receptive field. The results from these experiments show that this formation can explain the Hermann

grid illusion, thus raising some novel concepts for retinal prosthesis design in terms of stimulating electrode placement.

6.2 The Hermann grid illusion

In 1960, Baumgartner proposed a theory based on the lateral inhibition in the retina to explain the Hermann grid illusion (Baumgartner and Levine, 1971). He also argued that centre-surround antagonism played a major role in creating the illusion, because the ON-centre ganglion cells were more inhibited when placed over the intersection compared to placement over the bar portion of the grid or away from the intersection. One explanation for this finding, illustrated in Figure 7.2, is that the total inhibitory surround area of the receptive field is larger than the total excitatory centre area at the intersection, and therefore the total inhibition signal overwhelms the total excitation signal. This argument is also applied in the inverted colour grid and results in brighter smudges at the intersections. It further explains why people don't perceive the illusion in the centre of the gaze, due to the small receptive fields of the fovea. If the receptive fields are small enough, balance can be achieved between inhibition and excitation, thus abolishing the illusion (Bodkin, 2008).

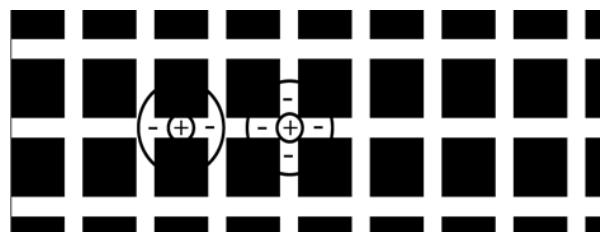


Figure 6.2: Baumgartner's explanation for the Hermann grid illusion.

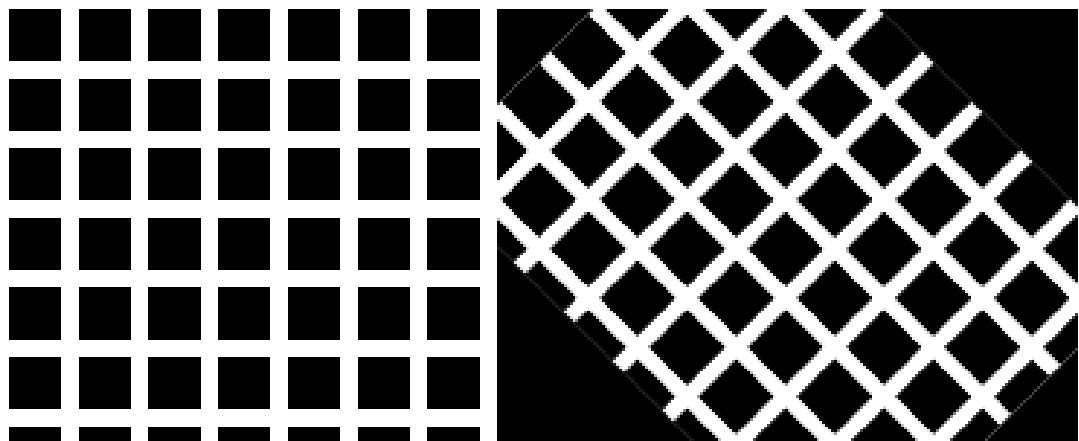
Although Baumgartner's theory has considerable explanatory power, it breaks down in the face of more recent experiments involving variations of the Hermann grid. These variations belong to three main categories, namely orientation, luminance, and distortion.

(A)

(B)

Figure 6.3: The original Hermann grid (A) and grid rotated by 45° (B).

In the first category, Spillmann and Levine observed that the illusion is reduced



when rotating the grid by 45° (Spillmann and Levine, 1971), as illustrated in Figure 6.3. This evidence does not support Baumgartner's theory, in which rotation should not affect the inhibition/excitation imbalance that produces the smudge effect. Recent research shows that when the grid is rotated by 45°, the illusion is at its weakest, which is explained by the involvement of orientation-selective neurons in the cortex according to Hubel and Wiesel (Hubel and Wiesel, 1968; Ash *et al.*, 2003).

In the second category, luminance, the grid is created such that the horizontal and vertical bars are filled with different colours (McCarter, 1979; Levine, Spillmann and Wolf, 1980). In this case, the illusion is still elicited, but the colours of the spots are replaced by the colour of the bars. From this observation, McCarter proposed that the illusion is produced by the double-opponent cell, where the distribution of receptive fields consists of red-ON/green-OFF centre and red-OFF/green-ON surround ganglion cells (McCarter, 1979). According to this theory, the illusion will be stronger if the receptive field is placed at the intersection of green bars on a red background, because excitation is stronger due to more red-on stimulation, and the situation will be reversed with a green background. Oehler and Spillmann also predicted that, in terms of photoreceptors, the illusion is based on red and green cones only; their experiment showed that the intensity of the illusion does not substantially depend on blue cones (Oehler and Spillmann, 1981). Figure 6.4 illustrates how the illusion varies with bar colour.

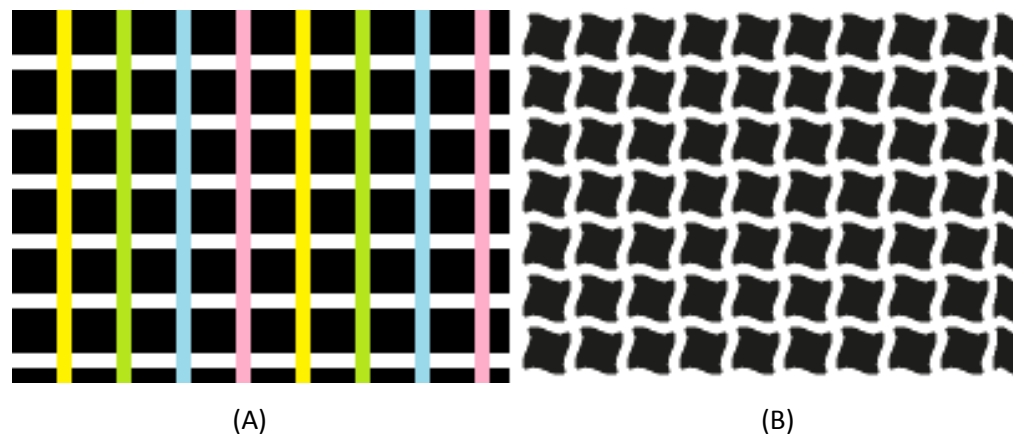


Figure 6.4: Colour variant (A) and distorted (B) versions of the Hermann grid.

In the last category, the Hermann grid is geometrically distorted in different ways, such as the bars taking on a curved shape resulting in a sinusoid grid as in the illustration on the right in Figure 6.4. Based on the finding that the illusion disappears at the intersections of sinusoid bars, Geier et al. concluded that the Hermann grid illusion also depends on straightness. These authors claimed that the role of ON and OFF ganglion cells was not important to the illusion and proposed a new theory to explain the Hermann grid illusion that could account for the elimination of the effect in the distorted case. At the core of this theory lies the ‘radiating edge hypothesis’, which states that a segment of a white-black edge will radiate darkness and lightness on its dark and light side, respectively, with the magnitude of the radiation directly proportional to the straightness of the edge and the direction of the radiation perpendicular to the orientation of the edge (Geier *et al.*, 2008).

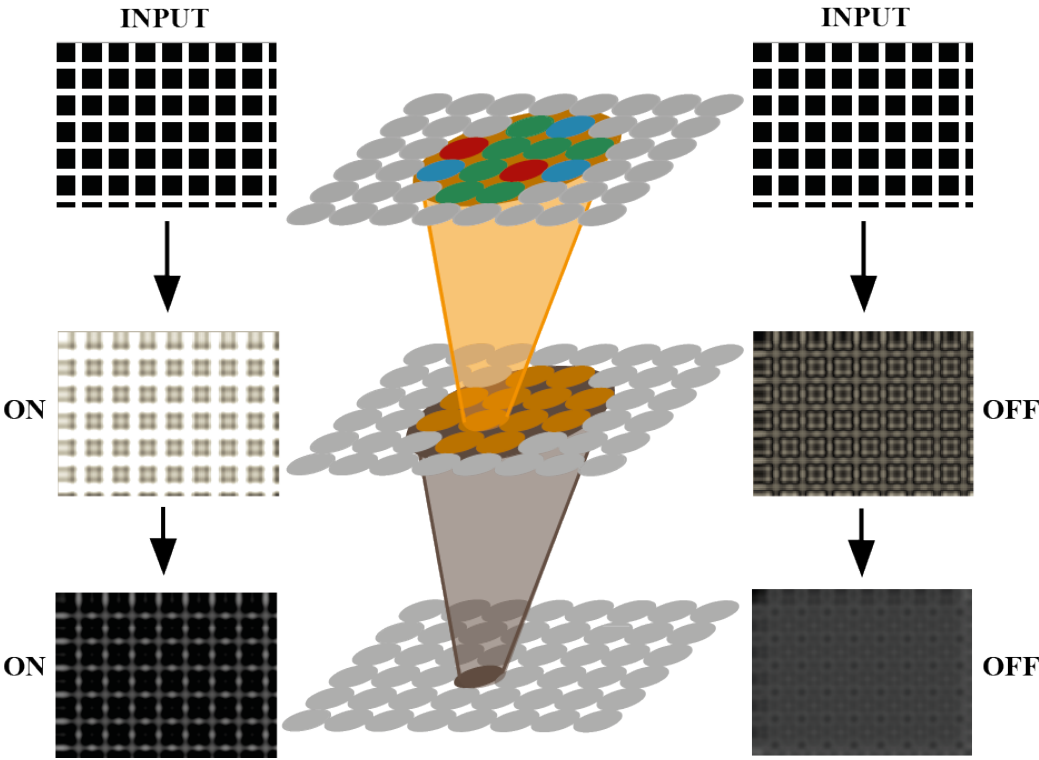
Through various versions of the Hermann grid, many theories have been proposed to explain the origin of the illusion, but there is still no unified model to explain the Hermann grid in all variations (Schrauf, Lingelbach and Wist, 1997; De Lafuente and Ruiz, 2004; Schiller and Carvey, 2005; Cembrowski *et al.*, 2012). This chapter proposes such a unified theory to explain the Hermann grid illusion in which the OPL receptive field plays a fundamental role. This theory shows that the classic receptive field explanation of Baumgartner is still useful after taking into consideration the OPL and a more detailed model of retinal processing.

6.3 A unified model based on Hermann grid illusion

Data is transferred from photoreceptors to ganglion cells by bipolar cells via chemical and electrical synapses. The OPL of many retinas includes complex circuitry involving photoreceptors, horizontal cells, and bipolar cells, exhibiting feedforward, lateral, and feedback computations; mediated via chemical and electrical connections; and implementing diverse computational functions including contrast enhancement, centre-surround antagonism, and colour correction (Barlow and Levick, 1965; Enroth-Cugell and Robson, 1966; Dowling and Ripps, 1973; Barlow, 1981). This chapter focuses on the centre-surround antagonism that was first discovered by Kuffler in ganglion cells and has been claimed to exist in bipolar cell as well (Kuffler, 1953; Werblin and Dowling, 1969; Kaneko, 1970). This study shows that changing the receptive field shape from circular to geometrically heterogeneous can account for some of the modern variations of the effect, in addition to explaining the classic effect. Additionally, the ganglion cell would be able to elicit visual signals when connections between photoreceptors and bipolar cells are limited.

In the retina, small diffuse bipolar cells collect information from 5–7 cones in the centre and 12–14 cones in the surround to form a centre-surround receptive field (Kolb, Nelson and Mariani, 1981). The questions that need to be answered here include ‘How do the connectivity properties of bipolar cells with respect to

photoreceptors affect their receptive field properties?’ and ‘How do bipolar cell receptive fields explain the Hermann grid effect?’ Using the proposed retinal model in this thesis to simulate Hermann grid processing by the retina, tentative answers for these questions and suggestions for future investigations have been developed.



6.4 Proposed model

The model described in CHAPTER 5 encompassing both the OPL and the inner-plexiform layer (IPL) was used to simulate the responses of retinal cells to the Hermann grid and observe whether the outputs from ganglion cells were consistent with the Hermann grid illusion.

Figure 6.5: Simplified illustration of receptive field integration in the retina model.

The original version of the Hermann grid and several variants pertaining to orientation, colour, and geometrical distortion were simulated. The spatial integration of a simplified model between different cell layers involving photoreceptor, bipolar, horizontal, amacrine, and ganglion cells is represented in Figure 6.5. Here, only the major layers involving photoreceptors, bipolar cells, and ganglion cells are illustrated. From top to bottom, the first layer is the photoreceptor layer, which receives the stimulus image and transfers information to horizontal cells (not shown here) and bipolar cells. Horizontal cells feed back to photoreceptors, while bipolar cells, which are in the second layer, receive information from both photoreceptors and horizontal cells and pass the results of their own computations to ganglion cells in the third layer. The ganglion cell layer also receives information from amacrine cells (not shown in this figure), which in turn process information originating from bipolar cells. Note that the highlighted circles in each layer are the cells covered in one receptive field. The Hermann grid images at each layer represent example outputs for each layer. There are two outputs for each of the bipolar and ganglion cell layers, which correspond to ON and OFF cells.

A probability matrix was used to determine the connection between bipolar cells and photoreceptors. In this matrix each value determines the probability of a connection at the corresponding coordinate as:

$$M(x, y) = P_x * P_y$$

In this equation, P_x and P_y are the probabilities of a connection existing between a specific bipolar cell and a photoreceptor at coordinates (x, y). This study used a 10×10 matrix, meaning that the probability of a connection was 10% for each coordinate. This rationale is selected after running the model with different connection probabilities from 0 to 100 to see what is the minimum probability that the model is still able to generate output at bipolar and ganglion cells while maintaining the asymmetrical connectivity pattern. In detail, if the probability is under 10%, there is no output at bipolar and ganglion cells while higher probability leads to uniform pattern as in circular receptive field. On the other hand, if the probability is 100%, the connectivity will be uniformed and the receptive field will have circular shape. Thus, this 10% ratio maintains an average of 10 input connections to each bipolar cell as well as the asymmetrical connectivity pattern in the receptive field.

All ganglion cells exhibit circular receptive fields and can be either ON or OFF. As described in section 5.3, equation 5.3 is used to compute the integration of ON and OFF pathways at bipolar and ganglion receptive fields. The input to the model consists of the original Hermann grid stimulus and its variants. The Hermann grid was generated using Adobe Illustrator. The bar width consisted of 6 pixels and the square was 3 times larger than the bar, as suggested by Schiller and Carvey (Schiller

and Carvey, 2005). In order to make the output images clearer and easy to observe, their contrast was enhanced using histogram normalization and equalization.

6.5 Experiments and results

6.5.1 Line width ratio

This experiment was conducted to examine the spatial responses of the retina to Hermann grids of different sizes. In this experiment, the width of the white bar was changed, while the receptive field size was maintained and vice-versa. The experimental conditions are listed in Table 6.1.

Receptive field size		Ratio			
		1:1		1:3	
		Hermann grid size		Hermann grid size	
<i>Centre</i>	<i>Surround</i>	<i>Line</i>	<i>Square</i>	<i>Line</i>	<i>Square</i>
1-5	2-10	2	2	2	6
1-5	2-10	4	4	4	12
1-5	2-10	6	6	6	18
1-5	2-10	8	8	8	24
1-5	2-10	10	10	10	30

Table 6.1: Ratio test cases

The ratio between the widths of the white bars and black squares was changed from 1:1 to 1:3. The receptive field centre radius was varied from 1 to 5, and the surround radius from 2 to 10. These parameters were selected according to the report by Dacey et al. that the centre radius of diffuse ganglion cells was 2 to 5 times smaller than the surround (Dacey *et al.*, 2000). Additionally, Schiller and

Carvey stated that the effect was reduced for the 1:1 case, compared to the standard 1:3 ratio of the Hermann grid (Schiller and Carvey, 2005). Hence, the Hermann grid ratio was varied from 1:1 to 1:3 while the centre radius was set to two.

Figure 6.6 and Figure 6.7 depict the results of models with and without bipolar cells connected, respectively. The Hermann grid is only visible in the bottom right image in Figure 6.6, where the involvement of bipolar cells in the processing pathway creates a darkening smudge at the intersection of bars. The smudges appear when the grid is set to a 1:3 ratio, and the illusion is strongest when the receptive field centre diameter matches the width of the white bars. The illusion is not visible at the 1:1 ratio, regardless of receptive field size.

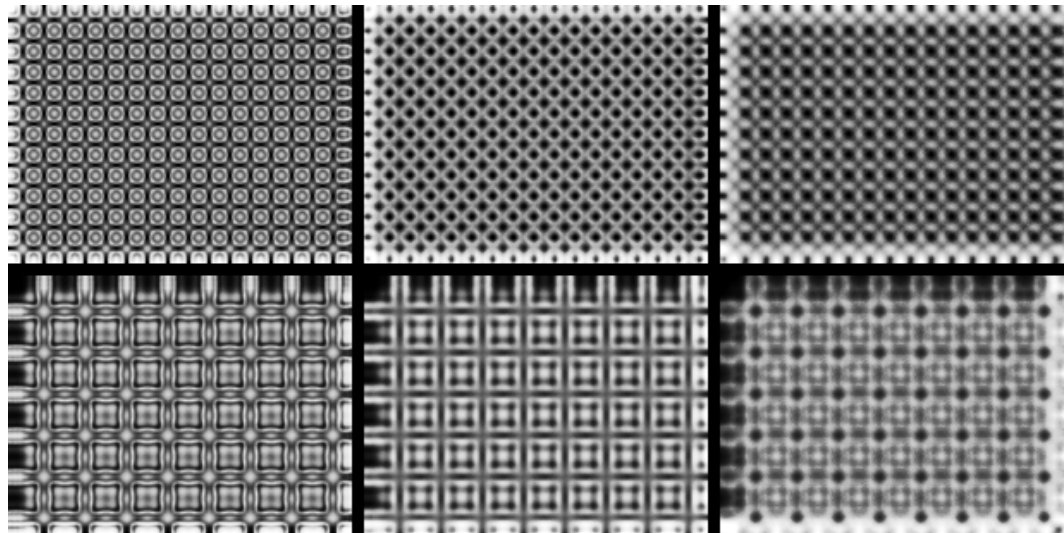


Figure 6.6: The Hermann grid output from the model at different receptive field sizes and a line-width ratio of 1:1 (top row) or 1:3 (bottom row) with bipolar cells connected. At each ratio, the centre:surround receptive field size was changed in range from 1:2 to 2:4 and 3:6, shown from left to right.

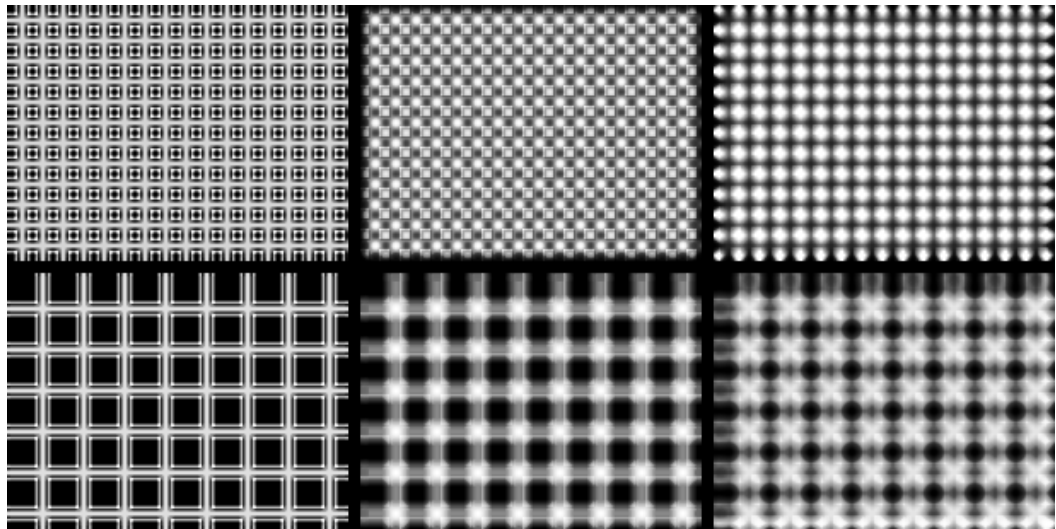


Figure 6.7: The Hermann grid output from the model at different receptive field sizes and a line-width ratio of 1:1 (top row) and 1:3 (bottom row) with no bipolar cells connected. At each ratio, the centre:surround receptive field size was changed in range from 1:2 to 2:4 and 3:6, shown from left to right.

6.5.2 Orientation

The Hermann grid in this experiment was rotated to various angles, namely 15° , 30° , 45° , and 60° . Based on the results of the line-width ratio analysis, the size of the receptive field was established as 6 pixels for the centre and 18 pixels for surround diameters and followed the 1:3 ratio to make the illusion visible for observation, because large white gaps can generate large smudges that are visible to the naked eye. Figure 6.8 and Figure 6.9 depict the spatial outputs from OFF-ganglion cells for circular and non-circular receptive fields, respectively. The intensity of the illusion decreased when the rotated angle was increased up to 45° . At 45° , the intensities of the smudges were smallest, as observed by the naked eye.

When there was no connection from bipolar cells, the illusion did not occur, as in previous experiments.

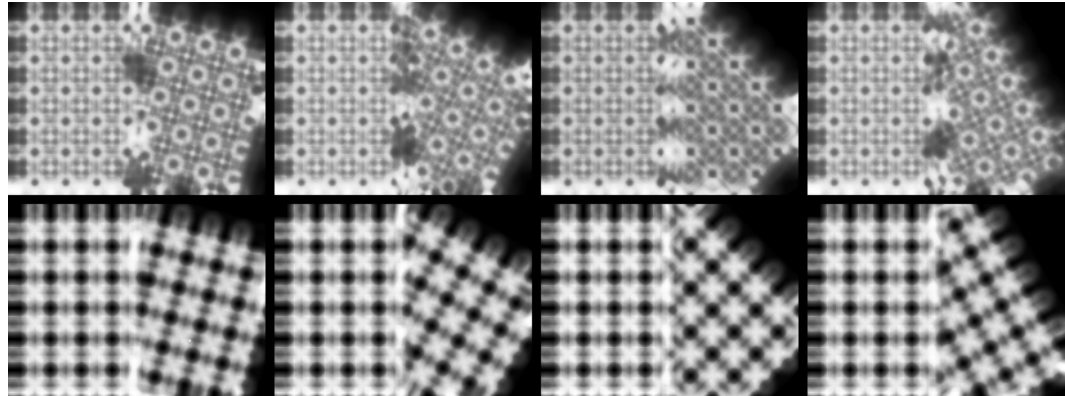


Figure 6.8: Output from the model for grids rotated at 15° , 30° , 45° , and 60° with connectivity calculated using a probability matrix. The output for each angle corresponds to each column in the figure. The top row contains images output from a model with bipolar cells involved, while in the bottom row bipolar cells were not involved. When bipolar cells were not involved (bottom row), the outputs of the model were the same for the original and rotated grids. The receptive field of the bipolar cells in this case was circular.

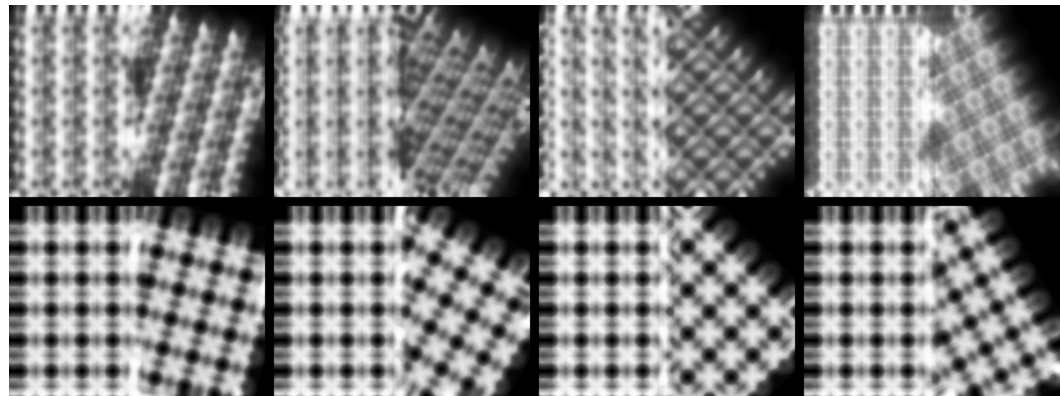


Figure 6.9: The output with the same orientations as in Figure 6.8 but with a non-circular receptive field of the bipolar cells.

6.5.3 Luminance

In this experiment, the white bars in the Hermann grid is changed to different colour to see the responses of the model to colour changes of the grid. The colour of the grid is changed by changing the colours of the white bars and background in sequent. There are eight alternatives for the grid colours in this experiment as described in Table 6.2. These colours pattern are selected to examine the responses of model to single and combined colours in the grid.

Colour	Test case							
	1	2	3	4	5	6	7	8
Bar	Red	Green	Blue	Yellow	Red	Green	Blue	Yellow
Background	Black				Green	Red	Yellow	Blue

Table 6.2: Colour test cases

The responses of the model to different colour grids are described in Figure 6.10. The analyses of these outputs will be discussed in discussion section later.

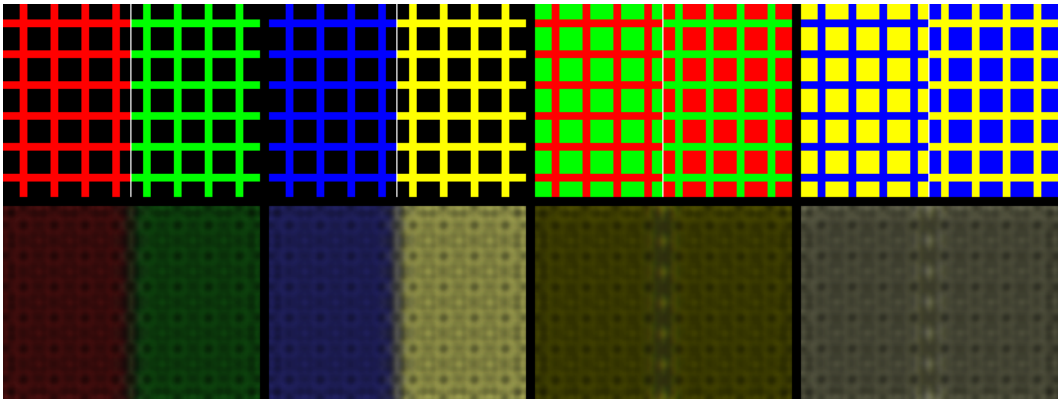


Figure 6.10: The output of model with colour grids. Top row illustrates eight different grids as inputs while bottom row depicts their corresponding outputs. The results show that the model is able to generate smudge with general colour depend on the colour of the grids.

6.5.4 Distortion

In the final experiment, the grid was distorted geometrically to examine the role of the bipolar receptive field in eliciting a Hermann grid illusion with non-straight bars. The distorted Hermann grid and outputs of the model are depicted in Figure 6.11. The input and configuration settings of the model were the same used in the orientation test to maintain the observability of the effect when seen by human eyes. The distortion was set to the same parameters reported by Geier and colleagues (Geier *et al.*, 2008).

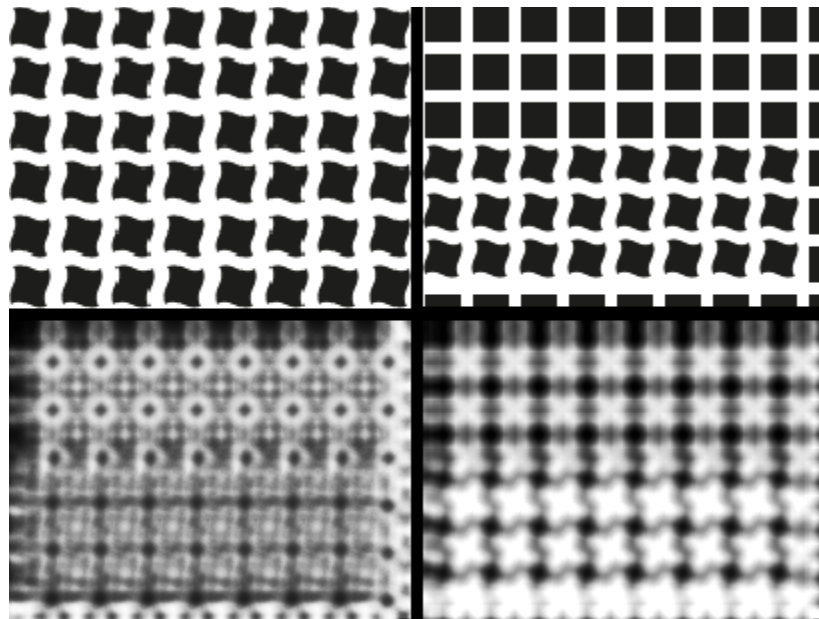


Figure 6.11: Distorted Hermann grid as input to and output from the model. The top right image is the input to the model while the top left is an example of distorted grid, and bottom images correspond to outputs from the model with (bottom left) and without bipolar cell involvement (bottom right).

6.6 Discussion

Based on these experiments on the Hermann grid, some conclusions can be drawn regarding different factors involved in generating the illusion. The first factor is the square-to-bar ratio, which at 1:3 allows the illusion to be easily observed by the human eye. Second, this experiment confirmed the role of bipolar cells in forming the illusion. Specifically, when bipolar cells were disconnected from the model, smudges were no longer present at the output from the ganglion cell layer. Even with the classic Hermann grid, as in Figure 6.6, no smudge appeared when bipolar cells were disconnected, which provides positive evidence of the critical role bipolar cells play in producing the Hermann grid response as seen at the ganglion cell layer.

In rotation experiments, the ‘orientation modulation’ effect of rotated Hermann grids can also be explained by the proposed model, thus emphasizing the critical role of the OPL in the illusion as well as in the spatial responses of ganglion cells. Without bipolar cell involvement, the outputs of the model at the ganglion cell layer show no trace of the ‘orientation modulation’ effect, as discussed by Schiller and Carvey as well as Geier et al. (Schiller and Carvey, 2005; Geier *et al.*, 2008), and when bipolar cells are involved, the ‘orientation modulation’ effect is clearly visible. To emphasize this experimental result, the mean square error (MSE) was

used to measure the difference between the output from the rotated grid and the rotated output from the original grid (Table 6.3).

Orientation	Mean Square Error
15°	2.1840
30°	16.9023
45°	27.8667
60°	15.12146

Table 6.3: MSE between the output from a rotated Hermann grid and the rotated output from the original grid.

The MSE results imply that the sparse connectivity between photoreceptors and bipolar cells, which in turn leads to heterogeneous and asymmetrically shaped receptive fields, can explain the orientation modulation effect. This thesis at the very least provides strong evidence in favour of the previously unrecognized critical role of bipolar cells and suggests that the effect is due to the heterogeneous shape of bipolar cell receptive fields. However, the precise relationship between the orientation modulation effect and the geometrical properties of bipolar cell receptive fields is still open for further investigation. Figure 6.12 depicts an example of receptive field connectivity, in which white pixels represent the presence of a connection between a photoreceptor and bipolar cell.

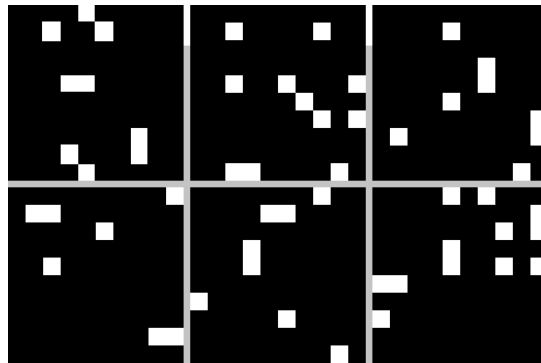


Figure 6.12: Binary maps of connectivity in bipolar receptive field.

The output from the rotation experiment shows the impact of a non-circular receptive field, illustrating how responses differ according to the use of receptive fields with circular and non-circular shapes. In the event that receptive fields are perfectly circular, the orientation modulation effect is completely obliterated. For the circular case, the orientation modulation effect is absent, whereas for the non-circular case, the effect is significant, as in the present experiments with bipolar cell receptive fields. This circular vs. non-circular explanation appears to support the hypothesis that bipolar cells contribute towards the orientation modulation effect due to the non-circularity of their receptive fields. The precise geometrical relationships, as mentioned, require further investigation, especially when the overall effect of multiple receptive fields with different shapes is considered.

The heterogeneously shaped receptive field can also explain the appearance of ‘diagonal smudges’ in a 45°-rotated Hermann grid. This phenomenon was first discussed by Geier et al., as 5–10% of viewers can see these ‘diagonal smudges’ in

the original position, but most subjects see them only in the 45° rotation case (Geier *et al.*, 2008). The responses from the model are consistent with this observation, as depicted in Figure 6.9. While the circular smudges are weak and harder to observe in the 45° rotated grid, the diagonal smudges are visible. These diagonal smudges are not visible when using a circular receptive field. Combining this result and the MSE result above, these results indicate that the rotated Hermann grid illusion can be explained using Baumgartner's theory if bipolar cells with a heterogeneously shaped receptive field are involved.

In the colour experiment, the outputs show that the model is able to generate the smudges at the intersections as well as the colours of the outputs. The colours of the outputs are the mix between the grid colours and background colours as can be seen in Figure 6.10. In particular, the colours of the outputs are the mixed colours of the grids and the background in the grids. For instance, in test case number 5 and 6, the colours of the outputs are mixed between red and green colours and results the yellow colour for the output. The same response is applied for test case number 7 and 8 where white colour is the mixture of blue and yellow colours in the input grids. On the other hand, in first four test cases the colours are mixed between single colour of the grids and black colours of the background thus results in darker colours of red, green, blue and yellow. This result shows that the colours of the smudges are depending on the colours of the grids and the correction of model implementation.

In the final experiment, responses from the model are consistent with visual observations. The role of bipolar cells in the retinal processing pathway is again highlighted through these outputs. When the bipolar cell receptive field is involved, the responses show visible smudges at the intersection in the original grid only. Without involvement of the bipolar cell receptive field, there are no smudges at the intersection, as in the bottom right image in Figure 6.11. According to hypothesis from Geier et al., the straightness of the white bar in the grid determines the appearance of the illusion but that hypothesis did not cover the case where the illusion appear when the grid is rotated 45 degree. This study on the other hand indicates that the asymmetrical connectivity pattern at bipolar cell layer is a main factor underlying the illusion and this hypothesis is valid not only in normal grid but also in 45 degree rotated grid. From this fact, the asymmetrical connectivity pattern hypothesis from this study can be a unifying hypothesis to explain the Hermann grid illusion in term of normal and distorted grid.

The experiments and results in Hermann grid illusion described above show that the retina is still able to process information with least connectivity in the receptive field. The results from orientation experiment indicates that the sparse connectivity receptive field is the factor to make the illusion maintained instead of circular receptive field. These findings have at least two important medical implication with regard to new designs for retinal prostheses (Kien, Maul and Bargiela, 2012). First, the results indicate that by using a receptive field with sparse

connectivity, spatial responses can be formed at the ganglion cell layer. Therefore, future retinal prostheses may be able to stimulate ganglion cells with fewer electrodes by placing these electrodes precisely in optimal positions. The second advantage is the implication that stimulation with fewer electrodes can resolve the issue of crosstalk as well as reduce the heat from electrodes as inter-electrode distances are increased.

One limitation of this model is that it pertains to shading variations of the Hermann grid in which the outputs are not consistent with what human eyes see when the background of the bar is shaded to grey while the intersections remain white. This omission warrants further research in the future and may be addressed by adding more detail to the retinal model to increase its realism.

6.7 Summary

This chapter presents experiments on the Hermann grid in terms of line-width ratio, orientation, and distortion, aimed at determining the effect of bipolar receptive fields on the output from ganglion cells. When bipolar cell receptive fields are not involved, the outputs of the model ganglion cells are consistent with the reports of other researchers and therefore exhibit several subtle inaccuracies. When bipolar cells are added to the model, the outputs of ganglion cells are highly consistent with what human eyes perceive when looking at the Hermann grid. Although the model is still far from matching the richness of the real retina and more test cases are

needed, these experiments show that Baumgartner's explanation of the Hermann grid illusion, when considered in conjunction with a more detailed model of the retina (e.g. OPL and IPL mechanisms), deserves further investigation.

CHAPTER 7

A RETINAL MODEL OF CONTRAST ADJUSTMENT IN MESOPIC CONDITIONS

7.1 Introduction

In the previous chapter, the concepts of asymmetrical and heterogeneous receptive fields were introduced, as well as the role of bipolar cells in the processing pathway inside the retina. These concepts underscore the importance of placing and distributing electrodes to contact ganglion cells efficiently in order to restore spatial vision with minimal damage to the retina. Consequently, retinal prostheses can take advantage of this finding to improve the precision of stimulation in restoring spatial vision. However, many more issues must also be addressed in order to restore vision to the blind with acceptable resolution and quality. As discussed in the review of retinal prostheses in CHAPTER 3, the current device only provides low resolution with black and white ‘pixel-like’ vision due to hardware limitations. In future devices, the resolution may be increased, but this improvement might bring more challenges because the perceived quality must match the high resolution of vision to provide a good experience to users.

One issue highlighted in this thesis is the performance of retinal prostheses in low-light conditions with low contrast sensitivity. It is difficult to perform tasks in low light, because objects with a dim background and low

contrast sensitivity are not distinguishable from background. Contrast sensitivity is related to visual acuity; it is easier to differentiate two points as being separate if those points have high contrast to the background rather than low contrast. Thus, perceiving vision with high acuity under conditions of dim light and low contrast sensitivity is challenging even with high resolution. By enhancing contrast, especially in low-light conditions, retinal prostheses can help to increase visual acuity and thus provide precise information in dim light conditions with low contrast. In this chapter, contrast processing in the retina is explored in the context of connectivity and temporal responses at the ganglion cell layer. The results show that different processing pathways such as the ON and OFF pathways in the retina are utilized to process contrast in mesopic conditions with the involvement of AII amacrine cells.

7.2 Contrast processing in the retina

The role of the retina is to convert visual signals to patterns of spikes by processing, compressing, and encoding the perceived visual signals and then transferring this information to the brain for further processing, ultimately leading to high-level understanding visual information. Colour, luminance, edges, motion, and contrast are examples of the types of information processed and encoded by the retina. This chapter focuses on contrast, i.e. the difference between the brightest and darkest regions in an image spatially or temporally. The bigger this difference, the higher the contrast and vice-versa. Thus the process of enhancing contrast involves increasing the gap between the brighter

and darker portions of a scene in order to differentiate objects with different brightness levels more effectively.

In the context of retinal processing, various cells mediate the contrast enhancement process including cones, rods, horizontal and bipolar cells in the outer-plexiform layer (OPL) and bipolar, amacrine, and ganglion cells in the inner-plexiform layer (IPL). Although some aspects of the contrast enhancement process have been clarified in the previous studies, the detailed roles of various cells involved are still under investigation (Lindsay and Andrew, 1999; Decuypere and Capron, 2011; Maul, Bargiela and Ren, 2011). As introduced in the previous section, this thesis focused on contrast processing in dim light, or mesopic conditions, as opposed to photopic (bright light, e.g. daytime) or scotopic (darkness, e.g. night) conditions. In mesopic conditions both cones and rods are activated. By contrast, although some rods and cones are still activated in both photopic and scotopic conditions, in photopic conditions most cones are activated while rods are de-activated, whereas in scotopic conditions most rods are activated while cones are ‘disabled’ (Stabell, 1967; Sugita and Tasaki, 1988). Although both cones and rods are utilized in mesopic conditions, the findings from this chapter indicate that rods and All amacrine cells are important factors in processing contrast information through separated ON and OFF pathways.

The role of bipolar cells in contrast processing was discussed by Burkhardt and Fahey, while Baccus and Meister discussed several types of retinal cells besides bipolar cells, such as amacrine and ganglion cells in this type of

information processing (Baccus and Meister, 2002; Burkhardt, 2011). Sharpe and Stockman suggested that rods are involved in contrast control via two distinct circuitries: one consisting of the processing pathway from rods to bipolar cells through AII amacrine cells and the other consisting of the interface between cones and rods in the photoreceptor layer (Sharpe and Stockman, 1999). On the other hand, Zaghloul and Burkhardt stated that ON and OFF pathways are important factors in contrast adaptation (Zaghloul, Boahen and Demb, 2005; Burkhardt, 2011). In particular, Zaghloul and his colleagues stated that there are different circuits for ON and OFF pathways involved in contrast processing, while Burkhardt found that these distinct circuits lie at the level of bipolar cells. Moreover, Decuypere utilized the interface between cones and rods in the photoreceptor layer to model mesopic vision (Decuypere and Capron, 2011). In this chapter, a model of the retina including the rod pathway is described, which was constructed based on the current state of knowledge regarding contrast control summarized above. The aim of this model was to investigate and simulate the role of the rod pathway with regard to contrast processing. This model is an updated version of an earlier model containing only an outer retinal layer, which was developed by Maul et al. and shown to be effective in terms of visual functions pertaining to noise, brightness, contrast, saturation, and colour (Maul, Bargiela and Ren, 2011). Kien et al. later developed an outer retinal model with a receptive field concept based on this early version to propose an explanation of the Hermann grid illusion (Kien *et al.*, 2012). Therefore, the model reported in this thesis not only complements

the work of Decuypere et al. on mesopic vision through its inclusion of the rod-AII pathway instead of the interface between cones and rods, but also serves as an extension of earlier retinal models whose main aim was to understand the neural substrates of retinal visual functions.

The results from this model show that contrast adjustment in both low- and high-contrast conditions can be achieved by contributions from the rod-AII amacrine pathway and combined ON/OFF pathways (Sharpe and Stockman, 1999; Zaghoul, Boahen and Demb, 2003). These encouraging results indicate that the retinal model has the capability to modulate contrast in both low- and high-contrast conditions thanks to non-linear computations in the rod pathway, and also has the capability to unify previous researchers' discoveries in contrast control.

7.3 The rod pathway in the retina

Figure 8.1 depicts five major layers in the biological retina with ON and OFF pathways. The function of each cell type is described in section 2.1; thus, this section focuses only on the ON, OFF, and rod pathways in the retina.

According to Figure 7.1, there are certain types of bipolar, amacrine, and photoreceptor cells involved in the contrast control mechanism. This chapter

focuses on rods and the separation of ON and OFF pathways, which have major roles in processing contrast sensitivity in mesopic conditions.

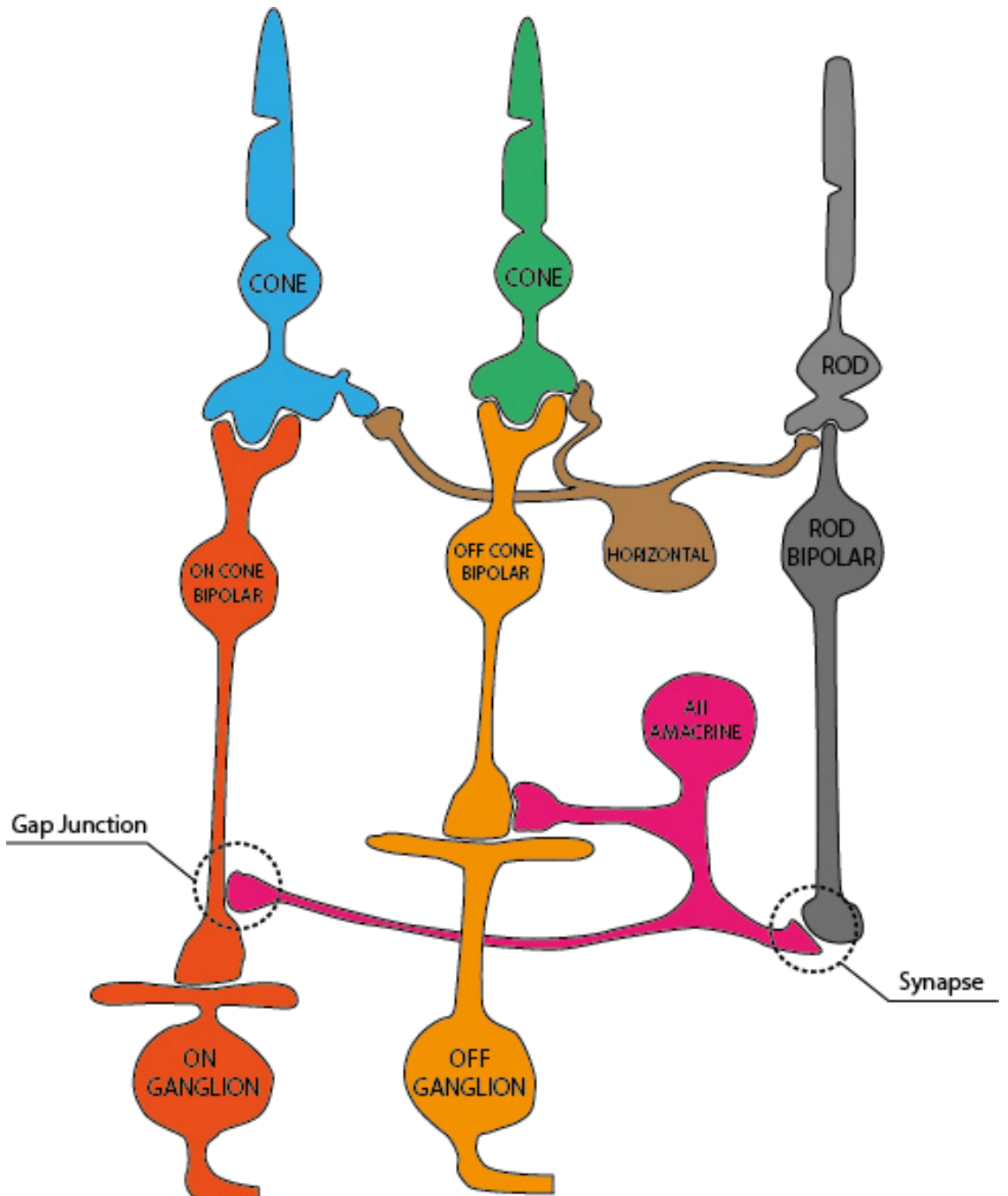


Figure 7.1: The rod pathway in the retina.

In the context of the rod pathway, as mentioned in the previous section, Decuypere et al. constructed a model involving gap junctions between cones and rods in the photoreceptor layer, while the present study has chosen a different circuitry that involves AII amacrine cells (Decuypere and Capron, 2011). According to Decuypere et al., the interface between cones and rods implemented in the previous model provided faster integration but less sensitivity compared to the rod-AII pathway. Hence, in this analysis, the rod-AII circuit was simulated, and the ON and OFF pathways were taken into account in order to elucidate a new contrast control mechanism and a more accurate process, with implications for retinal prostheses and even image processing. On the other hand, the retina has a specific mechanism for switching between these two pathways to deal with contrast in each specific condition. As described in CHAPTER 2, the retina has a mechanism to switch from cone to rod and vice-versa when light is changing from light to dark and this allows the contrast processing changing from rod-cone to rod-AII pathway and vice-versa. Thus, although these two pathways exist in the retina but contrast information is processed in only one of these pathways to maintain the processing transition from cone to rod.

Both cones and rods are implemented with their own pathways in the proposed model. The cone pathway is separated into ON and OFF pathways with cones, horizontal, bipolar, and AII amacrine cells in each pathway. The rod pathway consists only of rods and rod bipolar cells. The ON cone pathway consists of cones, horizontal cells, ON bipolar cells, and ON ganglion cells.

Cones receive light and convert and transfer signals to horizontal and ON bipolar cells. As discussed in section 5.3, the signals from horizontal cells are transferred to the surround receptive field of ON bipolar cells as inhibitory signals (Siminoff, 1980; Curlander and Marmarelis, 1983). By contrast, the centre receptive field of ON bipolar cells receives signals from cones. The information originally embodied in cone signals eventually reaches AII amacrine cells, which generate an inhibitory signal (much like horizontal cells do in the OPL). In the OFF cone pathway, the same type of connectivity is represented, but instead of processing signals in ON cone bipolar cells, signals from cones are passed to OFF bipolar cells. Rod bipolar cells receive signals from rods and then transfer these signals to AII amacrine cells and eventually to ON cone and OFF cone bipolar cells through gap junctions and synapses. Consequently, ON and OFF ganglion cells integrate signals from corresponding bipolar cells and fire to generate spiking signals that are transferred to the brain.

7.4 Rod pathway modelling

The rod pathway is summarized in section 5.5.2 and explored in detail in this section. Figure 5.5 illustrates the different processing pathways of the proposed retinal model. The model takes an input image and processes it through different paths and in different stages, culminating in the final results found in ganglion cells.

Equation 7.1 was used to compute the feedback from AII amacrine cells to OFF cone bipolar cells. This equation simulates the chemical synapses between

OFF bipolar and AII amacrine cells as observed in the biological retina. Besides this synapse, the AII amacrine cells also connect to ON cone bipolar cells via gap junctions, and this connection is depicted in the lower right side of the ON cone block in Figure 5.5. These chemical and electrical synapses are believed to control the hyperpolarization and depolarization of the OFF and ON cone bipolar cells, respectively, in the rod pathway (Wilson and Kim, 1998; Meylan, Alleysson and Süssstrunk, 2007).

$$S_{OFF}(t) = \frac{Bipolar_{OFF\ CONE}(t)^n}{Bipolar_{OFF\ CONE}(t)^n + Amacrine_{AII}(t)^n} \quad 7.1$$

In equation 7.1, $Bipolar_{OFF\ CONE}(t)$ refers to the output from OFF cone bipolar cells, and $Amacrine_{AII}(t)$ refers to the output from AII amacrine cells. $S_{OFF}(t)$ refers to the output signal in the OFF pathway before reaching ganglion cells through ganglion cell dendrites. Equation 7.1 is considered to reflect the non-linear interaction between amacrine cells, bipolar cells, and ganglion cells in the IPL layer (Graham, Hood and Finkelstein, 1979; Geisler, 1981; Adelson, 1982; Walraven *et al.*, 1984; Hood, Finkelstein and Boff, 1986; Webster and Mollon, 1991; Wilson and Kim, 1998; Field and Rieke, 2002; Valeton, van Norren and van Wyk, 2006; Demb, 2007; Naka and Rushton, 2012). Moreover, some authors have also utilized this type of equation for the circuitry in the OPL and even in the photoreceptor layer (Meylan, Alleysson and Süssstrunk, 2007; Decuypere and Capron, 2011). The parameter used in this chapter was set to 1, as in other works of Meylan *et al.* and Decuypere (Meylan, Alleysson and Süssstrunk, 2007; Decuypere and Capron, 2011).

This thesis proposes a model of interaction between signals from ON and OFF pathways prior to the generation of spiking signals. This proposal is supported by Schnapf et al., who mentioned the different mechanisms of contrast adaptation in higher mesopic light (Verweij, Hornstein and Schnapf, 2003; Hornstein, Verweij and Schnapf, 2004; Hornstein *et al.*, 2005). Schnapf et al. indicated that besides the feedback from horizontal cells coupling to photoreceptors, the contrast processing mechanism occurred through either gap junction coupling between rod and cone or electrical coupling between red and green cones. Kim and Rieke also stated that adaptation occurs at the ganglion cell dendrite level before the generation of spikes (Kim and Rieke, 2001). Based on these findings, the adjustment of the weight between ON and OFF signals at the dendrites of ganglion cells is believed to generate different contrast outputs.

$$\begin{aligned} GDS_{ON}(t) &= \varphi_{ON} * S_{ON} + \varphi_{OFF} * S_{OFF} \\ GDS_{OFF}(t) &= \varphi_{ON} * S_{ON} + \varphi_{OFF} * S_{OFF} \end{aligned} \tag{7.2}$$

Equation 7.2 indicates the combination of different weights of ON and OFF pathways to create signals at ganglion cell dendrites for ON and OFF ganglion cells (symbolized as $GDS_{ON}(t)$ and $GDS_{OFF}(t)$), respectively. φ_{ON} and φ_{OFF} are the weights of the ON and OFF pathways, respectively, and S_{ON} and S_{OFF} are the ON and OFF pathway signals, as depicted in Figure 5.5.

Again, a concentric receptive field was implemented at the ganglion cell layer for ON and OFF ganglion cells. A simple model for generating spiking signals was applied after this step as described in equation 7.3. This model was employed in this chapter because it is robust, and the spiking signals are easy

and efficient to compute. Moreover, as mentioned above, this study focuses on how contrast is processed at the bipolar-ganglion cell dendritic interface, rather than how the spiking mechanism affects the contrast process.

$$Ganglion_{SPIKE}(t) = \begin{cases} 1 & \text{if } r\Delta t > x_{rand} \\ 0 & \text{if } r\Delta t \leq x_{rand} \end{cases} \quad 7.3$$

In this equation, $r\Delta t$ is the probability of firing within a short interval, and x_{rand} is a random number from zero to one.

7.5 Experimental setups

In order to investigate the contrast enhancement mechanism of the proposed retinal model, four experiments were conducted, and four images were used as input to each experiment. These images were created from one sample image obtained in RAW format from Bychkovsky et al. (Bychkovsky *et al.*, 2011) using Adobe Bridge Camera Raw to adjust image contrast, thus producing four different versions with the following contrast levels: low, medium low, medium high, and high. Each input image of a specified contrast level was fed into the model to generate output signals from bipolar and ganglion cells. The contrast levels in sample images were already calibrated, which provided ideal images for comparison purposes.

A contrast measurement method called Retinal-like Sub-sampling Contrast (RSC) was adopted from Rizzi et al. to compare the contrast between output images and ideal images. This method is selected because of its ability to

measure the perceptual contrast of digital image with high accuracy (Rizzi, Simone and Cordone, 2008). In other words, this method is able to convert the contrast to a number thus makes it is easier to compare contrast in output images. Equation 7.4 indicates the measurement of contrast intensity.

$$C^{RSC} = \alpha \cdot C_L^{RSC} + \beta \cdot C_a^{RSC} + \gamma \cdot C_b^{RSC} \quad 7.4$$

In equation 7.4, α , β , and γ are the weight for each colour channel, and C^{RSC} is the local contrast measurement based on a DOG (Difference of Gaussian) neighborhood. A DOG model was used due to its success in describing the receptive field and responses of retinal ganglion cells (Simone, Pedersen and Hardeberg, 2012). The C^{RSC} value was used to determine the contrast of output images. This value is high in the case of low contrast and vice-versa. Hence, the aim of the experiments was to reduce this value in the case of low contrast, and increase it in the case of overly high contrast.

In the first simulation, the dataset was applied with different contrast levels; these results are depicted in Figure 7.4 and Table 7.1. The second simulation focused on the optimization/tuning of parameters. The optimal parameters were then applied to the model and simulated in the third experiment, which focused on the spatial and temporal output from ganglion cells, with results depicted in Table 7.2 and Figure 7.5. Additionally, a dataset containing 10 images was used to simulate and compare the contrast levels between inputs, outputs, and ideal images in the first and second simulations. Image number 5 in that dataset is shown in Figure 7.4, Figure 7.5, and Figure 7.6.

7.6 Results

Figure 7.4 depicts the spatial responses of ON and OFF pathways compared to ideal responses. The results indicated that outputs from the OFF and ON pathways provided better contrast for the low- and high-contrast inputs, respectively. In the case of low contrast inputs, contrast was visibly increased, and the details in the images could be seen clearly, especially in the OFF pathway (in which the grey fog is reduced). This effect was measured and confirmed by the RSC values, as shown in Table 7.1. In the case of high-contrast inputs, the contrast was not reduced significantly, and differences between the outputs and ideal images were not readily apparent. The RSC values in this case were consistent with these observations, with only the values for case number 5 increased at medium-high and high contrast (Table 7.1). To determine whether the ON and OFF pathways were separately responsible for high- and low-contrast inputs, both ON and OFF pathways were examined using two parameters, φ_{ON} and φ_{OFF} , in equation 7.3 to adjust the integration in each pathway. The second simulation was conducted in order to find the optimal values for these parameters.

In the second simulation, the integration of ON and OFF pathways at ganglion cell dendrites was examined. The model was simulated exhaustively in order to select suitable values for φ_{ON} and φ_{OFF} in the range of -1.0 to 1.0 to verify whether the output from cone and rod bipolar cells was visible or not. All visible outputs were compared using the above-mentioned measurement

technique in order to select the optimal values for φ_{ON} and φ_{OFF} . This selection was made based on the root mean square error (RMSE) distance between RSC values in output images and corresponding values in ideal images. After running simulations on eight sets of images (with each set containing four different contrast levels), the optimal parameters for φ_{ON} and φ_{OFF} were found to be 1.0 and -0.1 for ON ganglion cells with high-contrast images and 0.0 and 1.0 for OFF ganglion cells with low-contrast images. The RMSE for each value from -1 to 1 pertaining to ON and OFF bipolar cell weights for each of the image contrast levels used in Figure 7.4 is illustrated in Figure 7.2 and Figure 7.3. The circles indicate the error for each pair of φ_{ON} and φ_{OFF} values. Figure 7.5 and Table 7.2 illustrate the results of dendritic integration in ON and OFF ganglion cells, with the optimal weights mentioned above, and their corresponding RSC contrast measurement.

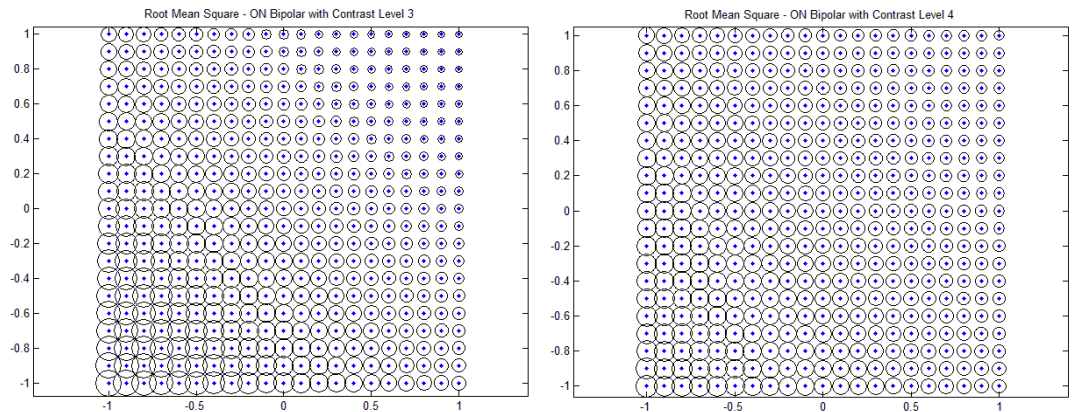


Figure 7.2: The root mean square error pertaining to ON ganglion cells for contrast levels 3 (left) and 4 (right) (i.e. medium-high and high contrast levels). The x-axis corresponds to φ_{ON} , and the y-axis refers to φ_{OFF} .

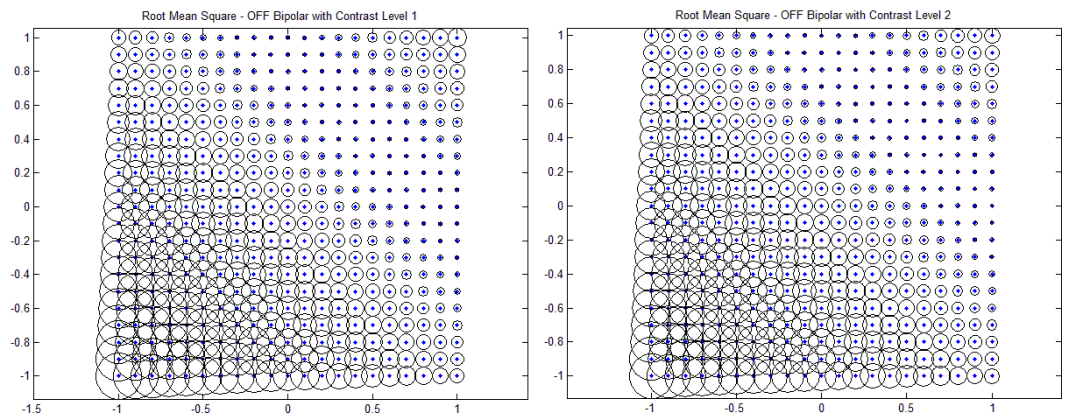


Figure 7.3: The root mean square error pertaining to OFF ganglion cells for contrast levels 1 (left) and 2 (right) (i.e. low and medium-low contrast levels). The x-axis refers to φ_{ON} , and the y-axis refers to φ_{OFF} .



Figure 7.4: Without ON/OFF integration. Outputs from the ON and OFF pathways for the following contrast levels (from top to bottom): low, medium-low, medium-high, and high. The “ideal images” in the right-most column consist of pre-calibrated images with ideal scene contrast. At first glance, the model outputs in the ON and OFF pathways appear the same, and both achieve better contrast in low-contrast conditions. For the high-contrast case, it is difficult to note, by visual inspection alone, any changes in either the ON or OFF pathways. The images shown in this figure correspond to test case number 5 in the dataset.



Figure 7.5: With ON/OFF integration. The results of dendritic integration in ON and OFF ganglion cells for the following contrast levels (from top to bottom): low, medium-low, medium-high, and high. Applying the weights to the ON and OFF pathways led to significant changes in the high-contrast case. The improvement in contrast in the ON pathway compared to the outputs in Figure 7.4 can be easily seen. The images shown in this figure correspond to test case number 5 in the dataset.

The main finding of this simulation was that the ON outputs enhance contrast under medium-high- and high-contrast conditions. For example, the detail of the building behind the electronic panel can be noted by visual inspection in Figure 7.5. This result was then evaluated again in the data listed in Table 7.2. From the RSC table, one can easily see that the RSC values are increased, bringing them closer to the RSC values of ideal images, for most images with the highest contrast levels in the ON pathway compared to the OFF pathway. For the medium-high-contrast case, improvement also occurred in the ON pathway, but not as significantly as in the high-contrast case (case number 1, 3,

5 and 7). For the low-contrast cases, the RSC values from both ON and OFF pathways were decreased, but the decrease in the OFF pathway was closer to the RSC values of the ideal images.

In the third experiment, the integration of ON and OFF bipolar cell inputs at ganglion cell dendrites was used to determine how the relative weights of these bipolar cell inputs can lead to different contrast processing results. Dendritic computation in ganglion cells can be seen as occurring in two ‘stages’, the first being responsible for contrast modulation and the second for edge detection. Van Wyk et al. reported this type of edge detection ganglion cell as X-cells/ β -cells with the smallest receptive field in rabbit (van Wyk, Taylor and Vaney, 2006), cat, mouse, guinea pig (Xu *et al.*, 2005; Zeck, Xiao and Masland, 2005; van Wyk, Taylor and Vaney, 2006; Berry *et al.*, 2013), and primate retinas (Rodieck and Watanabe, 1993).

A RETINAL MODEL OF CONTRAST ADJUSTMENT IN MESOPIC CONDITIONS

Test Cases	Low contrast			Medium-low contrast			Medium-high contrast			High contrast			Ideal Images
	Input	ON Pathway	OFF Pathway	Input	ON Pathway	OFF Pathway	Input	ON Pathway	OFF Pathway	Input	ON Pathway	OFF Pathway	
1	51.943	44.409	44.381	49.255	43.690	43.759	44.126	42.335	42.355	41.997	41.269	41.261	46.659
2	60.054	52.384	52.293	58.616	52.367	52.229	55.115	52.062	52.046	53.521	50.636	50.637	56.945
3	44.340	40.325	40.315	42.038	39.953	39.972	38.908	38.697	38.661	37.932	38.111	38.005	40.305
4	54.678	50.247	50.306	53.408	50.273	50.186	51.251	49.504	49.434	50.570	49.034	49.193	52.266
5	43.666	41.371	41.341	41.361	40.121	40.200	37.748	37.757	37.750	36.777	37.321	37.329	39.323
6	52.493	47.803	47.855	49.889	47.854	47.906	45.230	46.370	46.468	43.651	45.187	45.254	47.582
7	52.262	49.911	49.880	49.549	49.387	49.316	43.851	48.268	48.260	41.503	47.064	47.121	46.595
8	50.137	48.074	48.048	48.479	47.310	47.320	45.851	44.859	44.829	45.039	44.060	44.029	47.040
9	54.587	50.506	50.491	53.355	50.501	50.642	51.155	49.882	49.890	50.319	49.522	49.511	52.213
10	65.131	56.750	56.732	64.079	57.253	57.297	61.489	57.793	57.808	60.185	56.426	56.408	62.881

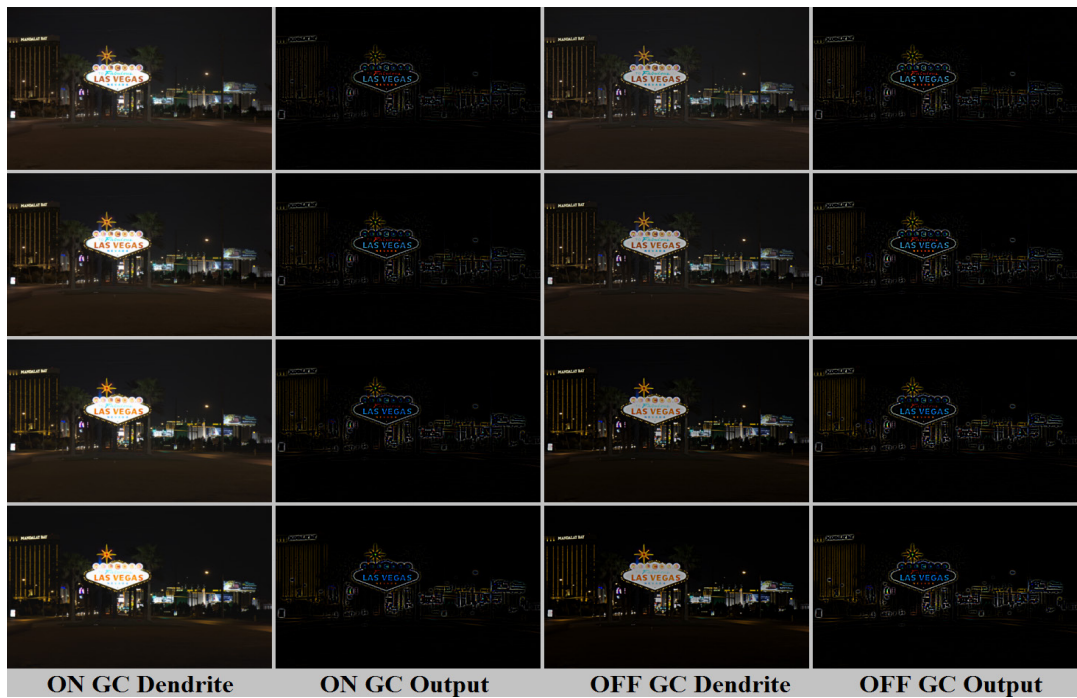
Table 7.1: Without ON/OFF integration. RSC contrast measurements corresponding to the ON and OFF pathway outputs from 10 test images varying from low to high contrast. The green cells indicate an increase, while red cells indicate a decrease of RSC compared to that of the input images. The scope of the model is to improve contrast by decreasing the RSC value in low-contrast images and increasing it in high-contrast images, but both ON and OFF RSC values are nearly the same for all cases shown here. For example, in low and medium-low contrast, the changes between RSC values in input and model output are significant with 1 failure case (highlighted in red cell) while in medium-high and high contrast there are only 4 pass cases (highlighted in green cell).

A RETINAL MODEL OF CONTRAST ADJUSTMENT IN MESOPIC CONDITIONS

Test Cases	Low contrast			Medium low contrast			Medium high contrast			High contrast			Ideal Images
	Input	ON Pathway	OFF Pathway	Input	ON Pathway	OFF Pathway	Input	ON Pathway	OFF Pathway	Input	ON Pathway	OFF Pathway	
1	51.943	42.950	45.012	49.255	42.331	44.509	44.126	43.501	40.971	41.997	42.571	39.966	46.659
2	60.054	49.387	54.666	58.616	49.255	54.816	55.115	55.770	48.314	53.521	54.091	46.719	56.945
3	44.340	39.952	40.607	42.038	39.557	40.283	38.908	39.353	38.046	37.932	38.805	37.414	40.305
4	54.678	48.576	52.014	53.408	48.359	51.817	51.251	51.476	46.993	50.570	51.516	46.453	52.266
5	43.666	40.792	41.905	41.361	39.678	40.685	37.748	38.319	37.296	36.777	38.218	36.677	39.323
6	52.493	45.932	47.676	49.889	44.002	46.903	45.230	48.116	42.283	43.651	46.351	41.290	47.582
7	52.262	44.805	48.089	49.549	43.683	47.157	43.851	44.139	40.171	41.503	42.261	39.056	46.595
8	50.137	46.636	48.913	48.479	45.571	48.000	45.851	45.944	42.878	45.039	45.534	42.157	47.040
9	54.587	49.460	51.932	53.355	49.357	52.070	51.155	51.549	48.225	50.319	51.817	47.092	52.213
10	65.131	53.496	59.284	64.079	53.484	59.907	61.489	62.243	52.601	60.185	60.969	51.233	62.881

Table 7.2: With ON/OFF integration.RSC contrast measurements corresponding to the ON and OFF pathway outputs from 10 test images varying from low to high contrast. From the table one can see that the outputs from the ON and OFF pathways significantly changed after applying the ON/OFF integration weights. The rate of success (improvement) for medium-high contrast increased significantly to 60%, whereas for high cases it increased to 80%.

Figure 7.6: ON and OFF ganglion cell processing results for contrast control



and edge detection.

Figure 7.6 depicts both these stages in both ON and OFF ganglion cells. According to the model diagram in Figure 5.5, the first ‘stage’, which deals with contrast processing, is mediated by the integration of ON and OFF bipolar cell inputs at ganglion cell dendrites, whereas the second ‘stage’, which deals with edge detection, is mediated by centre-surround antagonism. Although these different computations are discussed here as distinct and sequential stages, their spatial and temporal relationships in ganglion cell dendrites may be much more complex than what this study implies. In the proposed model, the result from edge detection was used to compute spike patterns at the final stage.

A RETINAL MODEL OF CONTRAST ADJUSTMENT IN MESOPIC CONDITIONS

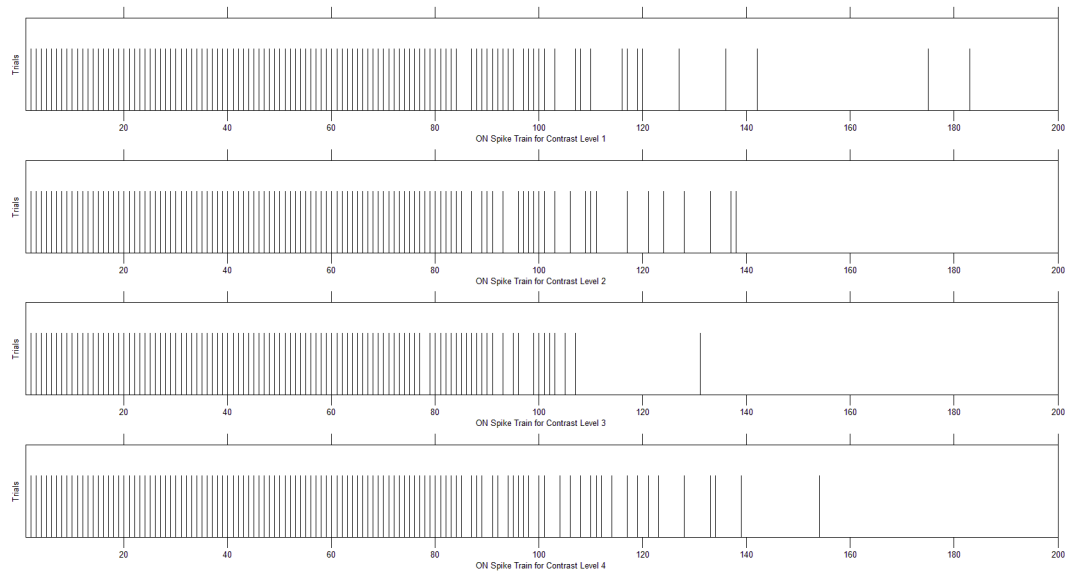


Figure 7.7: Responses from ON ganglion cells for each contrast level from 1 (top) to 4 (bottom) (i.e. low contrast, medium-low contrast, medium-high contrast, and high contrast).

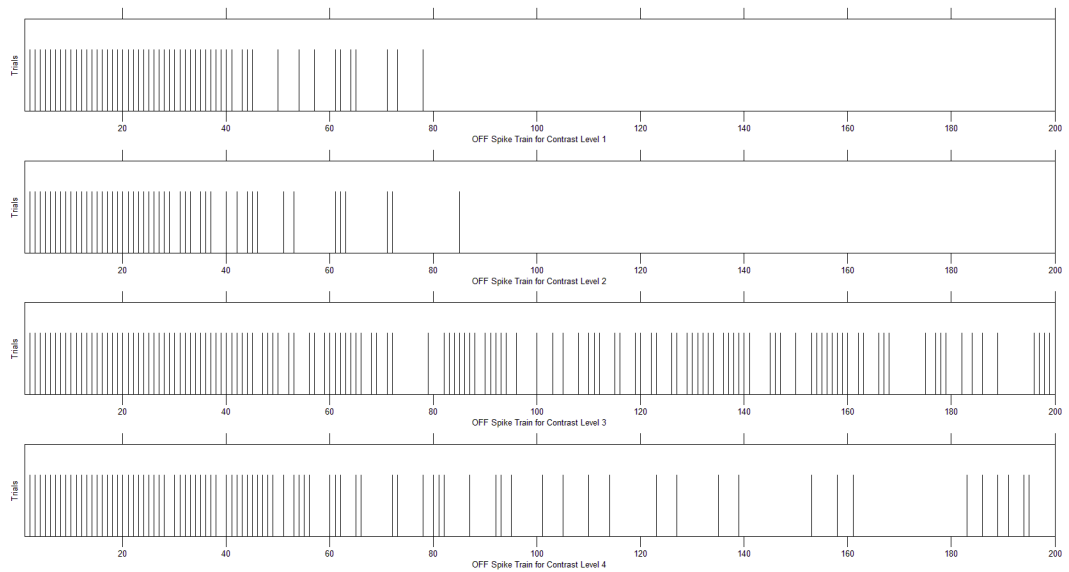


Figure 7.8: Responses from OFF ganglion cells for each contrast level from 1 (top) to 4 (bottom) (i.e. low contrast, medium-low contrast, medium-high contrast, and high contrast).

In the final experiment, the spike train responses from ON and OFF ganglion cells for all contrast levels are illustrated in Figure 7.7 and Figure 7.8. This spiking responses are generated using equation 7.4 at ganglion cell level. After

applying the nonlinearity equation to bipolar and amacrine processing pathways, the output from this equation is applied to equation 7.4 to simulate the responses of ganglion cells in ON and OFF pathways as can be seen in Figure 7.7 and Figure 7.8.

7.7 Discussion

7.7.1 Different processes in ON and OFF pathways for contrast control

In the second simulation, in case of high-contrast inputs, the outputs from the ON pathway exhibited more detail (i.e. better contrast) than the outputs from the OFF pathway, while with low-contrast inputs, the dendritic integration results of OFF ganglion cells were closer to the corresponding ideal images compared to the integration results of ON ganglion cells. These results were confirmed through the RSC measurements for both pathways, as seen in Table 7.2. For the low-contrast inputs, the RSC values of the OFF pathway were closer to those of the corresponding ideal images, while, conversely, for the high-contrast images, the RSC values in the ON pathway were increased significantly compared to those from the OFF pathway. The non-linearity of AII amacrine cells may be one explanation for these enhancements.

Due to this non-linearity, the rod pathway allows signals from rod bipolar cells to manipulate signals from OFF cone bipolar cells in the case of both low and high contrast. In the low-contrast case, rod bipolar cell non-linearity is limited due to the fact that light levels are decreased and cone information is relatively suppressed, while rods and AII amacrine signals are

stronger. According to equation 7.3, the increase of rod signals and decrease of OFF cone bipolar signals will lead to the decrease of signals in the OFF pathway, because AII amacrine cell signals are inversely proportional to the OFF pathway output. This result is consistent with findings from other authors regarding hyperpolarization in the OFF pathway and depolarization in the ON pathway at low contrast (Famiglietti and Kolb, 1975; Pourcho and Goebel, 1985; Muller, Wässle and Voight, 1988; Wässle *et al.*, 1995). However, these findings correspond to photopic conditions. Therefore, under mesopic vision, the present study hypothesizes that due to the non-linearity of equation 7.3, the OFF pathway signals are still decreased but not completely hyperpolarized, which will lead to both ON and OFF pathway signals being present and adjusted with their corresponding weights in later processing (which is discussed in next section). For a high-contrast case, the rod signals will be relatively suppressed, and thus from equation 7.3 the signals in the OFF pathway will tend to become saturated (i.e. closer to 1). This saturation will in turn lead to the contrast modulation role being passed to the ON pathway. In other words, when mean light levels are higher and therefore image contrast tends to be higher (Famiglietti and Kolb, 1975; Bühren *et al.*, 2006; Werblin, 2010), the retina has lower contrast sensitivity, whereas when mean light levels are lower (darker mesopic conditions) and image contrast tends to be lower, retinal contrast sensitivity is higher. Retinal non-linearities as expressed by equation 7.3 have been studied by other researchers in rod bipolar (Field and Rieke, 2002) and cone bipolar cells (Werblin, 2010) using psychophysical paradigms, and the

current study expands this approach to AII amacrine cells in the rod pathway, as mentioned by Freed et al. and Demb et al. and tested under pharmacological conditions by Zaghloul et al. (Demb *et al.*, 2001; Freed, Smith and Sterling, 2003; Zaghloul, Boahen and Demb, 2003).

7.7.2 ON and OFF pathway ratio for contrast processing

One can see the difference in RSC values of the ON pathway between Table 7.1 and Table 7.2. As mentioned above, the OFF pathway receives more information from OFF cone bipolar cells in low-contrast conditions, and vice-versa for the ON pathway. A weight function in cone and rod pathways was utilized to construct these pathways. The optimal weights for the integration of information from ON and OFF bipolar cells in experiment 2 at ON ganglion cell dendrites (i.e. 1.0 and -0.1) can be explained as the signals in the OFF cone pathway being dominated by the ON pathway for the high-contrast case, as described in the previous section. On the other hand, future studies needed to focus and explore these ratio although this study presents optimum weights for contrast processing pathway. One reason is that the training dataset for heuristic optimization as mentioned above is limited to 8 sets and the contrast level is categorized to 4 levels. Besides increasing contrast level and number of datasets, future studies also can focuses on the switching mechanism between contrast processing pathway cone-rod and rod-AII to explore the transition inside the retina for contrast processing.

The edge detection results of processing at ganglion cell dendrites are based on preliminary contrast-related integration in the third simulation. With the contrast enhancement, in the third experiment, the edge detection result of ganglion cell dendritic processing was based on preliminary contrast-related integration. The intensity of edges in ganglion cell outputs was stronger in ON ganglion cells for high-contrast conditions, whereas it was stronger in OFF ganglion cells for low-contrast conditions. This edge intensification is a direct result of the aforementioned contrast modulation.

7.7.3 Different temporal responses in ganglion cells for contrast processing

The final experiment presented the spiking signals from ON and OFF ganglion cells. For the low-contrast cases (i.e. contrast levels 1 and 2 in Figure 7.7 and Figure 7.8), the responses of OFF ganglion cells were shorter than those of ON ganglion cells, indicating that OFF ganglion cells achieved a faster response for low-contrast cases. By contrast, ON ganglion cells achieved faster response times in the case of high-contrast signals (i.e. contrast levels 3 and 4 in Figure 7.7 and Figure 7.8). This result reinforces the finding of the first experiment that low- and high-contrast signals are processed in separate pathways and reflect the temporal responses from ganglion cells, as reported by other researchers (Tsukada, Terasawa and Hauske, 1983; Chander and Chichilnisky, 2001; Kim and Rieke, 2001; Field *et al.*, 2010). From the retinal prosthesis stimulation point of view, this finding implies that the stimulation at ganglion

cells for contrast processing may be different for low and high contrast. The OFF ganglion cells may need stimulation with higher frequency while ON cells may need a lower stimulation frequency. This would allow future prostheses to stimulate ganglion cells more precisely and efficiently by using differing amounts of energy to stimulate ON or OFF cells, respectively, in contrast processing.

7.7.4 Analysis summary

In summary, the proposed model exhibits the capability to adjust contrast from low to high levels through the involvement of the rod pathway in mesopic vision. It is important for cones and rods to work together in mesopic vision for the proper adjustment and integration of signals from both ON and OFF pathways. Moreover, the model also hints at the complexity of the dendritic computations taking place in ganglion cell contrast modulation and highlights the need for models to simulate retinal processing under high mesopic light as well as models to replicate the adaptation of the retina, especially in temporal and spatial domain processing under changing light conditions (Cao and Lu, 2012; Zele *et al.*, 2014).

Although this model specifically targets mesopic conditions, it contains aspects that are relevant to photopic and scotopic conditions as well. In the case of photopic vision, most rods are ‘disabled’, and most cones are active in the photoreceptor layer. A small number of rods remain functional, but the signals are not as strong as in the mesopic or scotopic conditions (Stabell, 1967; Sugita

and Tasaki, 1988). As discussed with regard to equation 7.3 in the previous section, the ON pathway signals address contrast adjustment in this case, which is consistent with the fact that in photopic vision, contrast tends to be higher (Bühren *et al.*, 2006). In the case of scotopic vision, in which mean light levels are low and contrast tends to be low, the signals from the OFF pathway, which contains rod information, would be utilized to adjust contrast, since primarily rods are active in this condition.

7.8 Summary

This chapter presents a model of the retina for enhancing contrast automatically with the involvement of the rod pathway. The results from the model suggest that ON and OFF pathways in the retina have different mechanisms for processing signals from the photoreceptor layer. The ON pathway appears to be responsible for high contrast, while the OFF pathway appears to be the primary agent for low-contrast signals. In mesopic vision, this mechanism includes the rod pathway, in which AII amacrine cells play a role as transmitters of the rod bipolar signal to cone bipolar cells. Additionally, the scaling of the signals from the ON and OFF pathways is also an important factor underlying retinal contrast enhancement.

Through this model, this study hopes to have clarified one important aspect of contrast adjustment, with regard to the relative effectiveness of the ON and OFF pathways and their integration. Furthermore, this study is expected to provide some insight into how the contrast control mechanism can be

reconstructed in the damaged retina via retinal prostheses. New epiretinal prosthetic designs should take into account the different natures and roles of ON and OFF pathways when stimulating ganglion cells in the hope of emulating accurate dendritic integration.

CHAPTER 8

A RETINAL MODEL OF COLOUR ADJUSTMENT

8.1 Introduction

In previous chapters, the roles of receptive field heterogeneity and contrast enhancement were highlighted and examined through different simulations. The aim of these simulations is to inform the development of retinal prostheses in the near future, when high-resolution vision will be possible and contrast adjustment will help the blind to recognize and differentiate objects under conditions of low light. In this chapter, the aim is redirected to colour enhancement, in order to improve colour perception in future retinal prostheses whereby the blind will be able to perceive colour vision. In order to achieve this goal, the connectivity and mechanism of colour correction must be addressed by simulating the colour processing circuit in the retina. This section will give a brief review on colour correction, and the later sections will describe the colour pathway in the retina, the proposed model used, model simulation, and the simulation results. Finally, the results will be discussed from the perspective of how colour correction can be realized in future retinal prostheses.

In the last decades, colour correction has received considerable attention from vision researchers for the purpose of restoring images (distorted due to different light conditions) back to their original colour (Young and Kelland, 1845;

Helmholtz, 1867; von Frey, 1903; von Kries and In, 1905; Helson and Jeffers, 1940; Judd, 1940; Hering *et al.*, 1964; Land and McCann, 1971; Kuehni, 1997). To achieve this goal, many different approaches have been developed, both from the image processing perspective with algorithms such as Grey World (Buchsbaum, 1980; Barnard, Ciurea and Funt, 2002), max-RGB (Maloney, 1986; Maloney and Wandell, 1986), Shades of Grey (Horn, 1974; Finlayson, 1996), Grey-Edge (West and Brill, 1982; Lebedev and Marshak, 2007), and weighted Grey-Edge (Finlayson, Drew and Funt, 1994; Gijsenij, Gevers and van de Weijer, 2012) and from the biologically inspired perspective with algorithms such as Retinex and extended-Retinex (Land and McCann, 1971; Hurlbert, 1989; Barnard and Funt, 1999; Funt and Ciurea, 2001; Spitzer and Semo, 2002; Funt and Xiong, 2004; Meylan and Süsstrunk, 2004; Gao *et al.*, 2013; Ureña, Morillas and Pelayo, 2013). In this chapter, a model for colour correction in the retina was developed following the biological approach to explore the connectivity of the colour pathway involving cone; red, green, and blue bipolar; amacrine; and ganglion cells. This model focuses on the spatial and temporal responses of ganglion cells in order to establish the relationship between the colour correction mechanism and the spiking behaviours of ganglion cells. As described in the previous chapters, the model was implemented with receptive field and contrast processing pathways to examine the Hermann grid (Kien *et al.*, 2012) and adjust contrast in mesopic conditions, respectively. From this ‘foundational’ model, the colour pathway was added to

restore colour in different lighting conditions in the spatial domain and to encode that signal in the temporal domain.

Apart from the model's colour correcting capabilities, its response in the temporal domain also emphasizes the origin of the blue-OFF signal in colour coding. Initially, the blue-OFF signal was believed to be absent from the colour pathway, but later studies have shown that it may exist as a simple inversion of the blue-ON signal (Roska, Molnar and Werblin, 2013). An overview of the retinal colour pathway will be summarized in the next section, followed by a description of the model, experiments, results, and discussion in subsequent sections.

8.2 Colour pathway and colour correction in the retina

A high-level understanding of the colour pathway in the primate retina is illustrated in Figure 8.1. As described in CHAPTER 5, the retina encodes colour information and then transfers this information to the brain at the lateral geniculate nucleus through the optic nerve. These signals are then decoded by an area called V4 in human cortex, which is believed to restore the original colour of objects under various light conditions such as outdoor, indoor, moonlight, or light bulb. Midget amacrine cells that receive signals from bipolar cells and send inhibitory signals to midget ganglion cells are also involved in correcting colour information in the retina. The signal integration at ganglion cells was based on the receptive field concept, in which the centre receptive field cells receive signals from midget

bipolar cells and midget amacrine cells and convey them to cells in the surround receptive field. Note that receptive fields vary across species, both in terms of type and shape. For instance, goldfish have double-opponent receptive fields, while humans have concentric double-opponent receptive fields.

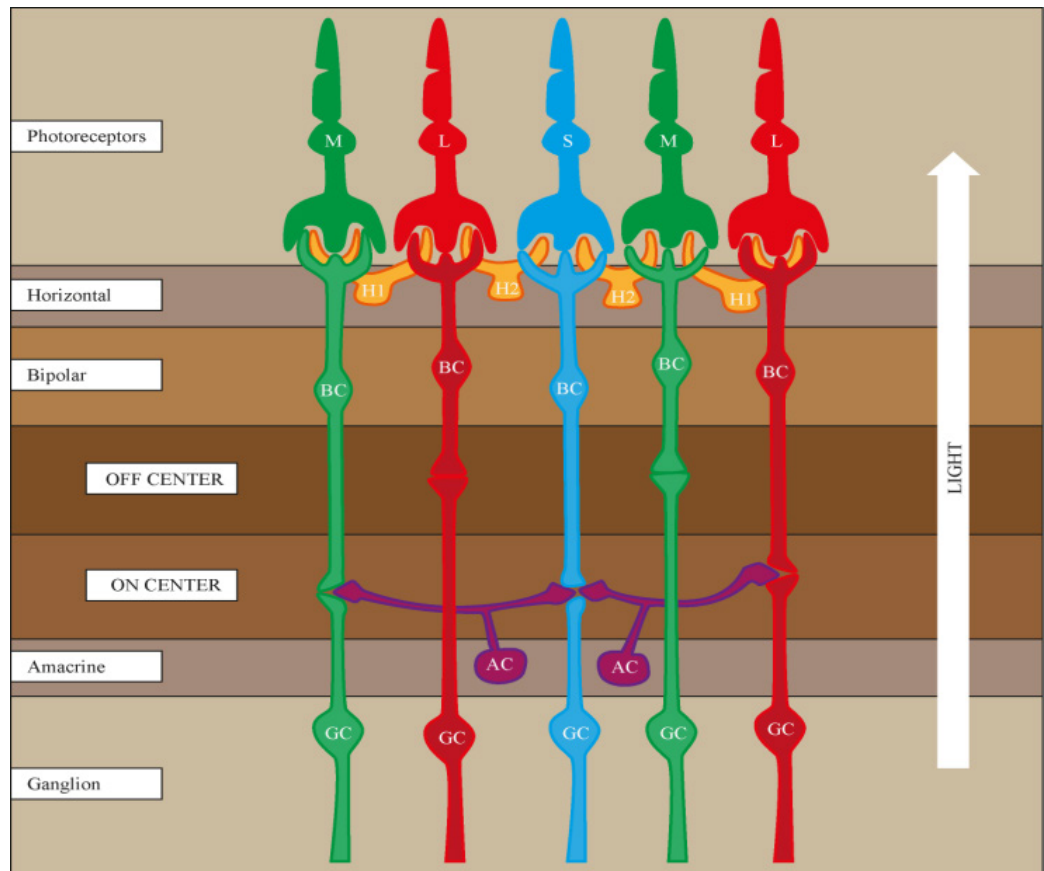


Figure 8.1: The retinal colour pathway.

Some evidence suggests that the colour correction process also occurs in the retina, although V4 has been strongly believed to play a major role participate in this function. Van Leeuwen et al. discussed colour correction at the horizontal cell

layer (van Leeuwen M T, Numan R, 2004; Vanleeuwen *et al.*, 2007), while Spitzer and Rosenbluth and Maksimova discussed this mechanism at the ganglion cell layer (Maksimova, 1977; Spitzer and Rosenbluth, 2002). In this study, a hypothesis for colour correction is proposed based on a non-linear circuit at the ganglion cell level, with midget amacrine cells as critical factors for known spatial and temporal responses.

8.3 Colour correction hypothesis

As mentioned above, midget amacrine cells are the focus of this chapter due to the contribution of their non-linear synapses to the colour correction process. Lebedev and Marshak stated that ON and OFF amacrine cells are involved in establishing colour constancy in the retina. The theory presented in this thesis extends this claim and hypothesizes that midget amacrine cells may adjust the signal from long (L), medium (M), and short (S) pathways to adjust the colour information via their circuitry to ganglion cells. Based on the fact that ON and OFF midget amacrine cells synapse on both ON and OFF ganglion cells and bipolar cells, the present thesis proposes that the non-linear connection originating from these amacrine cells is critical to the modulation of the proposed colour correction mechanism. This non-linearity is applied to all synapses between bipolar, amacrine, and ganglion cells, where ganglion cell receptive field centres result from bipolar cell signals and receptive field surrounds from amacrine cells, and where each receptive field-

contributing cell is affected by adjacent cells via gap junctions. According to Schwartz and Rieke, such non-linearity is important for producing inhibitory signals from amacrine cells to ganglion cells compared to linear spatial integration (Schwartz and Rieke, 2011). The next section will describe this non-linear synapse between midget amacrine and midget ganglion cells.

8.4 The model of colour processing in the retina

In previous chapters, the ‘foundation’ of this model is presented, consisting of photoreceptor, horizontal, bipolar, amacrine, and ganglion cell layers and with each cell in each layer connected to other cells in the same layer as well as to cells in other layers. In CHAPTER 7, a rod pathway was also developed to demonstrate retinal processing under mesopic conditions, and the results demonstrated that the model was capable of contrast enhancement in both low- and high-contrast conditions. In particular, AII amacrine cells were connected to the OFF cone pathway via chemical synapses and the ON cone bipolar cells via gap junctions. In this chapter, the model has been extended by adding a colour pathway involving midget bipolar, midget amacrine, and ganglion cells. Furthermore, the rod pathway has been disabled, as rods are deactivated in colour vision according to Sugita et al. (Sugita and Tasaki, 1988). Figure 5.8 illustrates the details of the implemented colour pathway in the retinal model. As shown in Figure 5.8, the model contains spatial (SF) and temporal filters (TF) to generate spatial responses at each layer.

The spatial filters are applied to generate outputs at photoreceptors, horizontal cells, and bipolar cells, and the temporal filters are applied to simulate the suppression of the output at each layer (Decuypere and Capron, 2011). The spatial and temporal filters are described in sections 5.2.

Photoreceptor, bipolar, amacrine and ganglion layers were implemented in this model to process different connectivity patterns for colour vision. The input signal was split into three different signals for corresponding channels such as L, M, and S, which were then fed to bipolar cells after going through SF and TF, as in equation 5.2. At the bipolar cell layer, these cone signals were used as excitatory inputs in bipolar receptor fields for different types of bipolar cell. The inhibitory signals were taken from horizontal cells, which in turn were generated from photoreceptor inputs using different sets of parameters. For colour vision, H1 and H2 horizontal cells were implemented to receive input from L and M cones and from M and S cones, respectively. The excitatory and inhibitory signals were used to compute the output from bipolar cells according to equation 5.3, as also described in sections 5.2. Applying this equation to different cone pathways in colour vision as in Figure 5.8, L and M bipolar cells received excitatory signals from L and M cones, respectively, and inhibitory signals from H1 horizontal cells, while S bipolar cells integrated signals from S cones and H2 cells. This arrangement resulted in six types of bipolar cells, as described in section 5.5 was also used to generate signals from ganglion cells, with excitatory signals taken from bipolar cells and inhibitory signals from

amacrine cells. As can be seen in Figure 5.8, the signals from amacrine cells were generated from bipolar cells and used in the IPL layer primarily as surround signals for ganglion cell receptor fields.

As mentioned in previous sections, the synapses between bipolar, ganglion, and amacrine cells were hypothesized to be a crucial factors behind the retinal colour correction mechanism. Maloney and Wandell and other authors (Maloney, 1986; Maloney and Wandell, 1986; Gomila Salas and Lisani, 2011) stated the equation for recovering surface reflection as

$$\text{Output} = (\text{Input})^{2^{\left(\frac{128-M}{128}\right)}} \quad 8.1$$

In equation 8.1, the input refers to an image, and M refers to a mask generated by applying a Gaussian filter to the inverted input image. The mask is defined by equation 8.2:

$$M(x, y) = \text{Gaussian}(x, y) * (255 - I(x, y)) \quad 8.2$$

The Gaussian filter was applied to the inverted version of the input image in order to adjust the light and dark regions of the image: dark regions were lightened while light regions were darkened.

In equation 8.1 the range of colour values can range from 0 to 255, but in the proposed model the range is from 0 to 1. Hence equation 8.1 becomes:

$$\Leftrightarrow \begin{aligned} \text{Output} &= (\text{Input})^{2^{\left(\frac{\frac{1}{2}-M}{\frac{1}{2}}\right)}} \\ \text{Output} &= (\text{Input})^{2^{(1-2M)}} \end{aligned}$$

$$\Leftrightarrow \text{Output} = (\text{Input})^{2^{(1-2(\text{Gaussian}*(1-\text{Input}))}}$$

$$\Leftrightarrow \text{Output} = (\text{Input})^{2^{(1-2(1-\text{Gaussian}*\text{Input}))}} \quad 8.3$$

$$\Leftrightarrow \text{Output} = (\text{Input})^{2^{(2*\text{Gaussian}*\text{Input}-1)}}$$

$$\Leftrightarrow \text{Output} = (\text{Input})^{2^{(2M'-1)}}$$

where M' is the mask image generated from convolving the Gaussian filter with the input image. Finally, the equation for adjusting surface reflection can be written in the form of equation 8.4:

$$\text{Output} = \text{Input}^{2^{2M'-1}} \quad 8.4$$

As above, M' is defined as a masked image resulting from convolving a Gaussian filter with the input image. In the proposed model, M' corresponds to the signal originating from midget bipolar cells that synapse onto ganglion cells. As explained by Gomila Salas and Lisani (Gomila Salas and Lisani, 2011), the M' mask image is a blurred version of the input image using a Gaussian filter. The purpose of this filter is to ignore redundant features in the image, which is consistent with the report of Bloomfield and Völgyi (Bloomfield and Völgyi, 2009) stating that the lateral inhibition provided by midget amacrine cells leads to a reduction of unnecessary details. After mapping the equation to the underlying retinal circuitry, equation 8.4 becomes equation 8.5:

$$\text{Ganglion} = \text{Bipolar}^{2^{2\text{Amacrine} - 1}} \quad 8.5$$

where the input signals are mapped to inputs from bipolar and amacrine cells and output signals are mapped to ganglion cells.

In this chapter, a spiking network at the ganglion cell layer was also implemented to study the temporal responses of different types of ganglion cells in colour vision, as can be seen in Figure 5.8. The network was constructed based on a neuron model by Izhikevich (Izhikevich, 2003), which was chosen for its computational efficiency and sufficient realism based on the objectives of this thesis. The spiking model was based on equation 5.4. For the spatial domain, all ganglion cells were connected with centre-surround antagonism for red-green, green-red, and blue-yellow ganglion cells, as depicted in Figure 5.8 . These cells were used to analyse the temporal responses of ganglion cells in colour correction as mentioned above.

8.5 Experimental setups

Four different experiments were conducted to simulate the colour correction capabilities of the model. In the first simulation, the spatial outputs of the model were compared to colour-deficient images. In this test, the colour channel in the model was deactivated successively from red, green, and blue in order to simulate different forms of colour blindness. This experiment acted somewhat as a ‘reality check’ to verify that the model was correctly implemented and validate that the model did indeed possess the necessary rudiments for colour representation and

therefore colour processing. The input was taken from Ishihara colour-blindness test patterns (Ishihara, 1943), and the dichromatic outputs were produced using an image-processing tool called Fiji (Schindelin *et al.*, 2012). In general there are three main types of colour blindness, protanopia, deuteranopia, and tritanopia. Protanopia results from missing red cones, and people with this disease only see green and blue. People with deuteranopia, in turn, see only red and blue, and in tritanopia, the perception of blue is lacking (Ishihara, 1943). In this experiment, deuteranopia was examined because it is easier to observe the effects of this condition using Ishihara plates. In the second experiment the colour correction capability of the model was verified by visually observing and comparing the outputs from the model to the reference outputs generated from other algorithms including Grey-World, Shades of Grey, Grey-Edge, Weighted Grey-Edge, and Retinex. To make the comparison clearer, root mean square error (RMSE) was used to measure the difference between model outputs and ideal images as well as reference images and ideal images. The ideal images were generated using histogram equalization for each colour channel. The final experiment focused on the response properties of ganglion cells in the temporal domain, which included an examination of the spiking synchronization of ON and OFF blue ganglion cells.

8.6 Results

In the first experiment, the pattern plates from Ishihara's book (Ishihara, 1943) were inputted into the model to simulate colour-blind vision, and the simulated outputs were visually compared to outputs from Fiji software. Figure 8.2 depicts the inputs, the proposed model simulated outputs, outputs from Fiji, and visual outputs by the human naked eye from top to bottom for comparison.

In Figure 8.2, only number 2, number 4, and the upper half of the line pattern are visible with sufficient intensity and contrast in the outputs from the simulated model, which is consistent with the output from Fiji. This result provides some preliminary verification and validation that the colour circuitry inside the model is correctly implemented and adequate for modelling colour processing.

Figure 8.3 depicts the resulting outputs that were generated by simulating the model with input images under different lighting conditions. Input images resulting from scenes under different lighting conditions (top row) were transformed into model outputs (middle row), which were verified by visual inspection. The results show that the simulated outputs were more similar to the ground truth images (bottom row), meaning that colour correction did indeed occur in the model.

For instance, the colour of leaves (first column) and the surface of papers (second column) were adjusted to their original colour under 'white' light. The same observation applies to the third and fourth columns, where the reddish and

yellowish walls were adjusted to white, as would be expected from colour constancy in human perception.

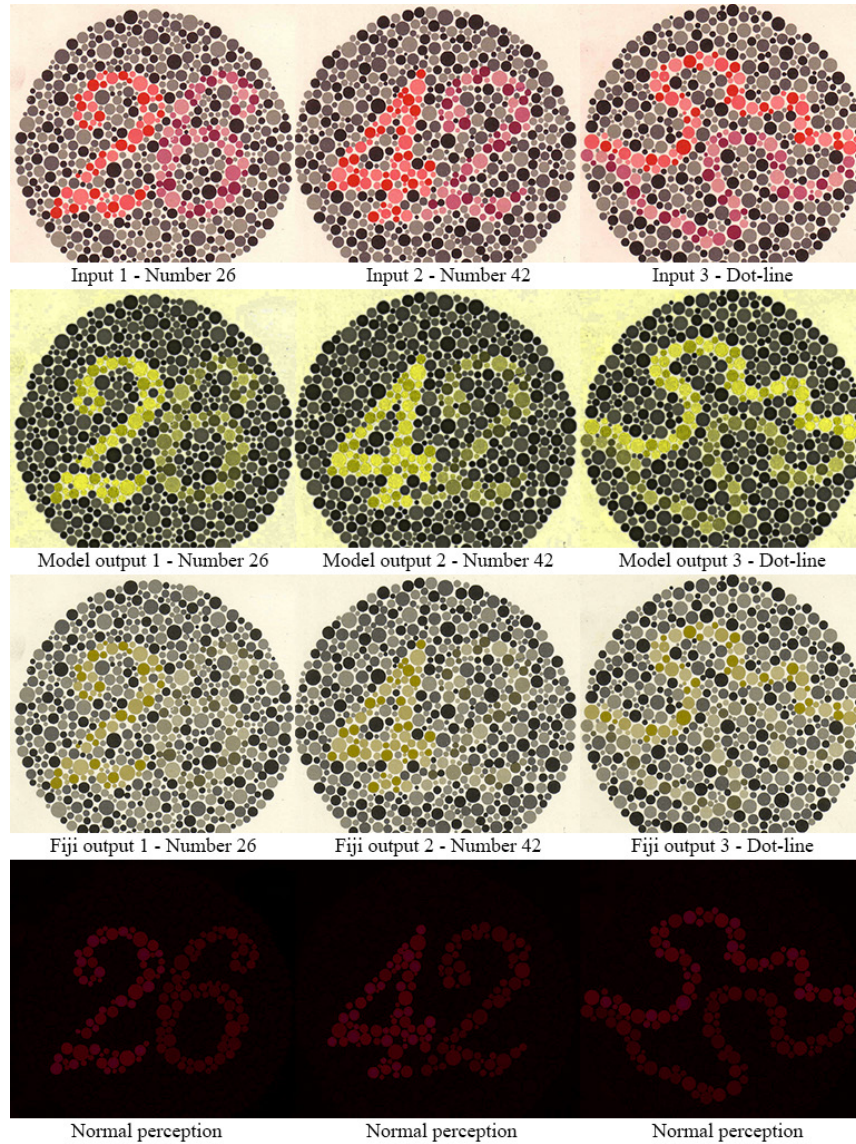


Figure 8.2: Results for simulated deuteranopia. The top row corresponds to the input images, consisting of three Ishihara plates (26, 42, and a line pattern from left to right). The second row depicts the model outputs, whereas the third row depicts outputs from Fiji. The last row depicts what should be perceived with normal vision. In this experiment, subjects with normal vision can see the complete pattern

on each plate (26, 42, and line pattern from left to right), whereas subjects with deuteranopia can see only limited content in the plates.



Figure 8.3: Colour correction output from the model. Four different input images are shown in the first row. The second row depicts the output from the model, and the third row depicts the original image without colour distortion.

Figure 8.4 compares output images from the model and other standard algorithms in the field of colour correction. In this figure, two images were selected from the dataset: the garden and Mondrian-style scenes. This experiment tested the capacity of the model to adjust colour under outdoor and indoor lighting conditions (i.e., the garden and Mondrian scenes, respectively) and generate colour perception similar to other approaches. This capacity was confirmed using a dataset of 100

images acquired from Gehler et al. (Gehler *et al.*, 2008), as shown in Figure 8.5 and Figure 8.6, which illustrate the RMSE between the output and ideal images for the proposed retinal model and seven other algorithms Bayesian Estimation, Gamut Mapping, Grey World, Shades of Grey, Grey-Edge, weighted Grey-Edge, and Retinex).

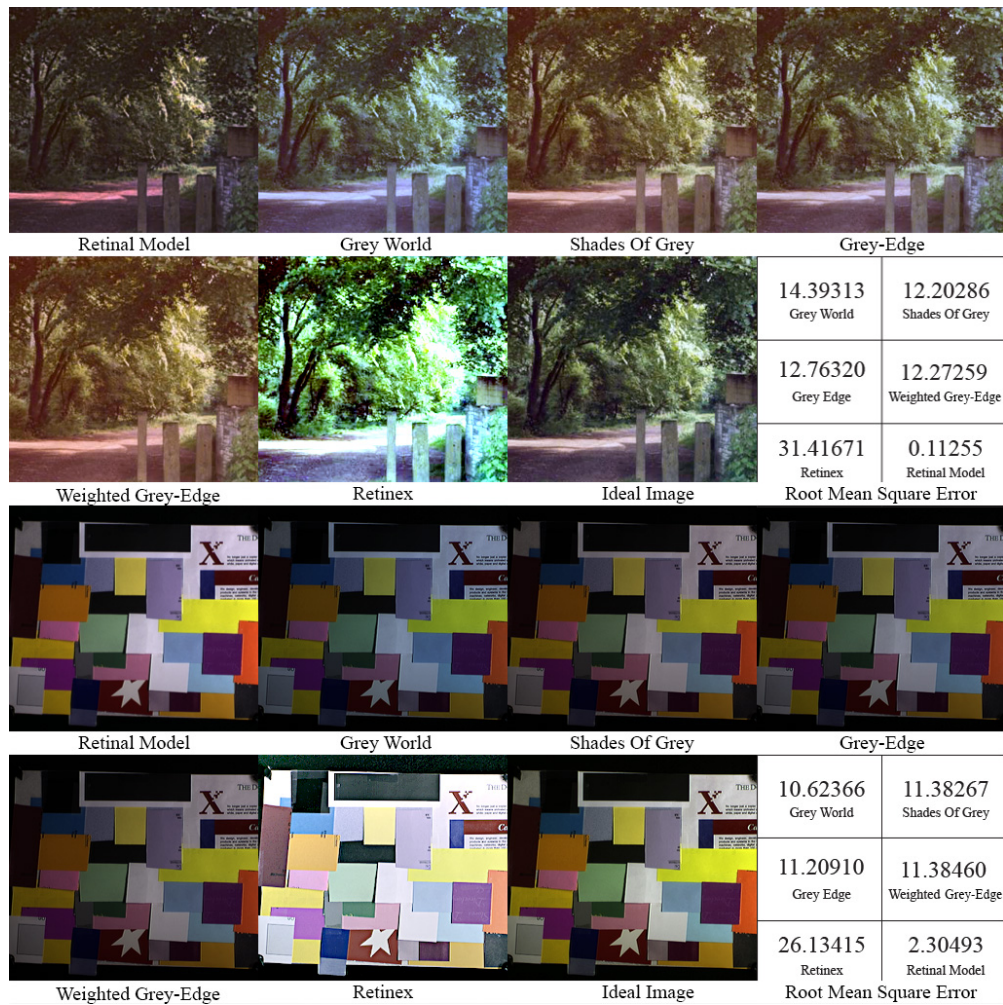


Figure 8.4: Comparison of the proposed model outcomes with output images from other approaches. The first two rows display the outputs generated using the garden scene as input. From left to right, the outputs of the proposed model, Grey World,

Shades of Grey, and Grey-Edge approaches are shown in the first row, and those of the weighted Grey-Edge and Retinex approaches and the ideal image are shown in the second row. The next two rows display the outputs generated using the Mondrian-style scene as input. The relative positions of various approaches are the same as in the first two rows. For each input image, the root mean square error distances from each output image to the ideal images are also included.

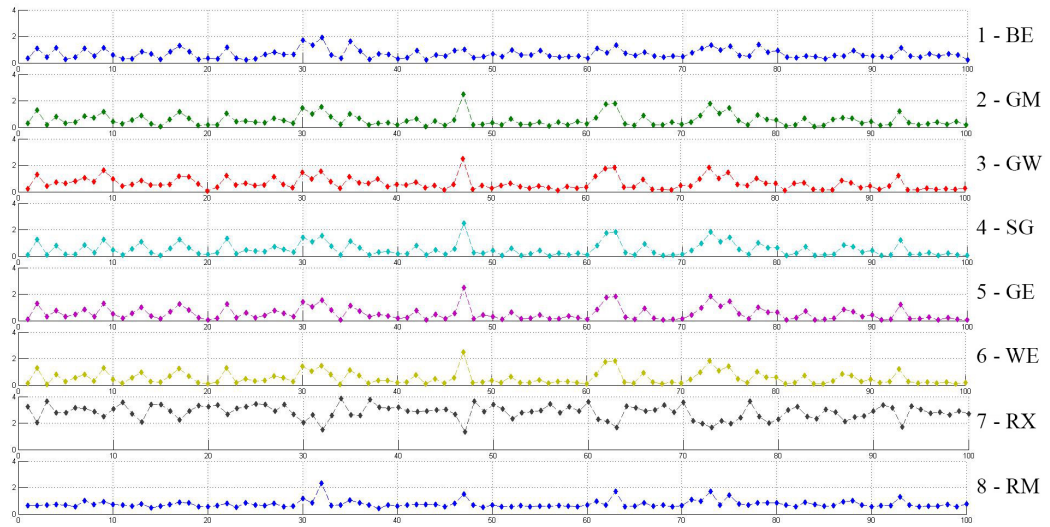


Figure 8.5: The root mean square error (RMSE) from several standard algorithms compared to that of the proposed model. The dataset consists of a set of 100 images acquired from Gehler et al. (Gehler *et al.*, 2008). Apart from the proposed model, seven algorithms were utilized to generate the RMSE curves (from top to bottom): Bayesian Estimation, Gamut Mapping, Grey World, Shades of Grey, Grey-Edge, weighted Grey-Edge, and Retinex. The last row corresponds to the RMSE of the proposed retinal model. The x-axis indicates image index. Note that the first 50 images are indoor images, and the remaining 50 are outdoor images. The y-axis indicates the error of the output images compared to the corresponding ground truths, which is scaled for visualization purposes.

Figure 8.6 illustrates the number of outputs for which each algorithm had the lowest RMSE. The outputs of the proposed retinal model had the lowest RMSE from ideal images in 56% of indoor scenes (28/50) and 36% of outdoor scenes (18/50) compared to the outputs of the other seven algorithms.

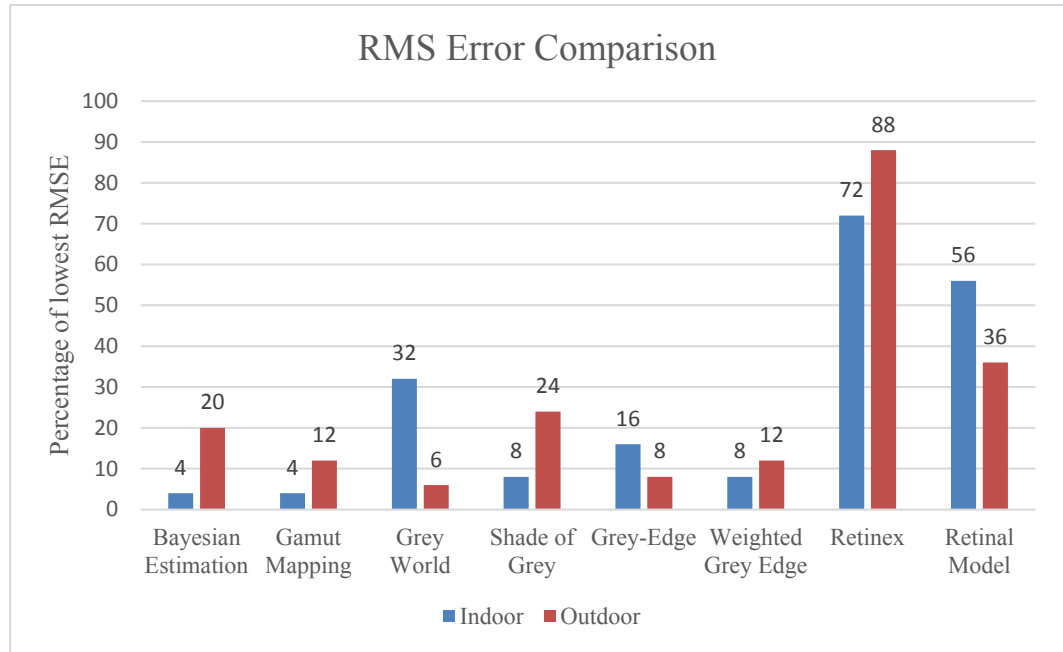


Figure 8.6: Comparison of RMSE across eight different algorithms, derived from Figure 8.5. The chart shows the percentage of lowest RMSE across all datasets (i.e. a bar at 10% indicates that 10% of output images (5/50) have the lowest RMSE using that approach). According to these results, Retinex was the overall best colour correction algorithm, followed closely by the proposed model.

In the final experiment, the model was set up to generate temporal responses from 29 ganglion cells within a 7×7 centre-surround receptive field configuration, which is illustrated in Figure 8.7. The temporal outputs from ganglion cells in the final experiment are shown in Figure 8.8 and Figure Figure 8.9. Figure 8.8 illustrates the ON and OFF responses of blue ganglion cells in general, while Figure 8.9 provides more detail pertaining to the temporal response patterns of these cells. In Figure 8.8, the surround cells are highlighted in red rectangles while the centre

cells are green, and these ganglion cells were used to analyse spiking synchronization in Figure 8.9.

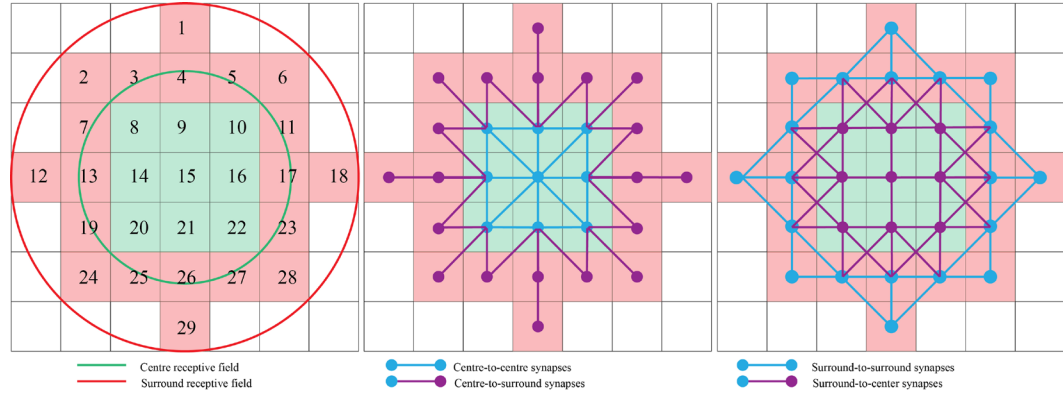


Figure 8.7: Connective topology of ganglion cell receptive fields. On the left, 29 ganglion cells are arranged in a 7×7 grid according to a centre-surround receptive field configuration. The middle diagram illustrates centre-to-centre synapses (blue line) and centre-to-surround synapses (purple line), while the diagram on the right depicts connections in the opposite direction.

In Figure 8.7, the middle map describes connections from centre cells to surround cells, while the map on the right displays connections from surround cells to centre cells. The blue lines in both diagrams indicate connections from one cell to its neighbouring cells within the central region of a receptive field, while purple lines represent connections with cells in the surround regions of the receptive field. Note that these connections are bi-directional for both centre-centre and centre-surround cases. Receptive field surround cells consist of amacrine cells, and therefore the connections between centre and surround cells consist of synapses and gap junctions between ganglion cells and amacrine cells. Centre-centre connections involve synapses and gap junctions involving either bipolar or ganglion cells.

Figure 8.8 illustrates responses from 29 ganglion cells in the receptive field as depicted in Figure 8.7. In this figure, the red rectangles indicate blue ganglion cells in the surround regions of a central ganglion cell, as illustrated by the cells in red squares in Figure 8.7. Green lines indicate ganglion cell responses with inhibition from amacrine cells, whereas blue lines indicate responses without amacrine cell involvement. The x-axis depicts the timeline in milliseconds, and the y-axis indicates the index of different spiking neurons. From top to bottom, there are 29 lines and each line presents the spiking frequency of one ganglion cell. The ganglion cells illustrated in this experiment are Blue-ON/Yellow-OFF and Blue-OFF/Yellow-ON. These cells are the major output pathways from the retina for colour processing. All spikes are aligned in order to compare the responses of ganglion cells when there are amacrine cells and no amacrine cells involved in processing colour information. In particular, green spike trains indicate the responses of ganglion cells with amacrine cells involved, while blue spikes represent responses with amacrine cells connected to the surround receptive field. Conversely, Figure 8.9 illustrates the analysis of 16 ganglion cells in the surround receptive field. The spiking neurons are taken from Figure 8.8 and aligned for comparison purposes. The ON and OFF ganglion cells are depicted in blue and red rectangles, respectively. Green lines indicate responses with inhibition from amacrine cells, whereas blue lines depict responses without amacrine cell involvement. The green and red shaded columns indicate the firing periods of ON

and OFF ganglion cell respectively. The x-axis depicts the timeline in milliseconds, and the y-axis indicates the index of different spiking neurons. Here only 16 cells from surround regions are depicted. Here this study just depicts only 16 cells from surround regions for analysis. This figure implies that the delay between with and without amacrine cells involved in ON and OFF pathways are highlighted by red and blue shading, respectively.

8.7 Discussion

In the first simulation, the model made plausible predictions regarding normal and abnormal perception and was verified using Ishihara patterns as inputs. Thus, the model faithfully reflected the perceptual symptoms experienced by people with colour blindness, providing a critical verification and preliminary validation step for subsequent experiments. According to Solomon and Lennie, amacrine cells are involved in signal inhibition of ganglion cells as a ‘mixed surround’ (Solomon and Lennie, 2007), and Lebedev and Marshak confirmed that amacrine cells are also involved in forming colour opponency in ganglion cells (Lebedev and Marshak, 2007), especially in the red and green opponency pathway. In addition, colour opponency is the core function of early colour correction in the retina (Gao *et al.*, 2013). Together, all these findings suggest that amacrine cells have a critical role in colour correction at ganglion cells via surround inhibition. The role of the retina

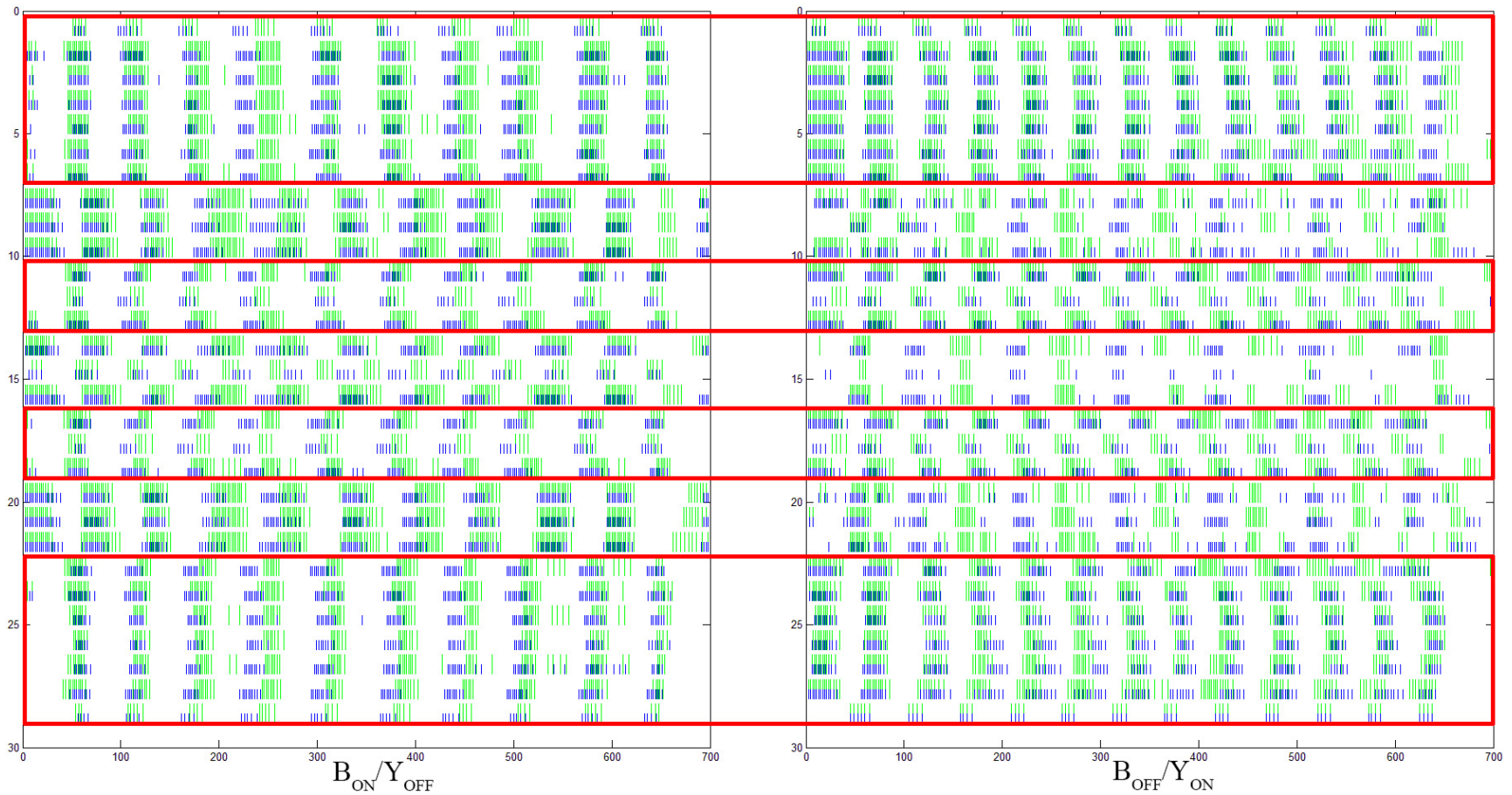


Figure 8.8: Temporal responses of blue ganglion cells from the proposed retinal model with ON and OFF responses on the left and right sides, respectively.

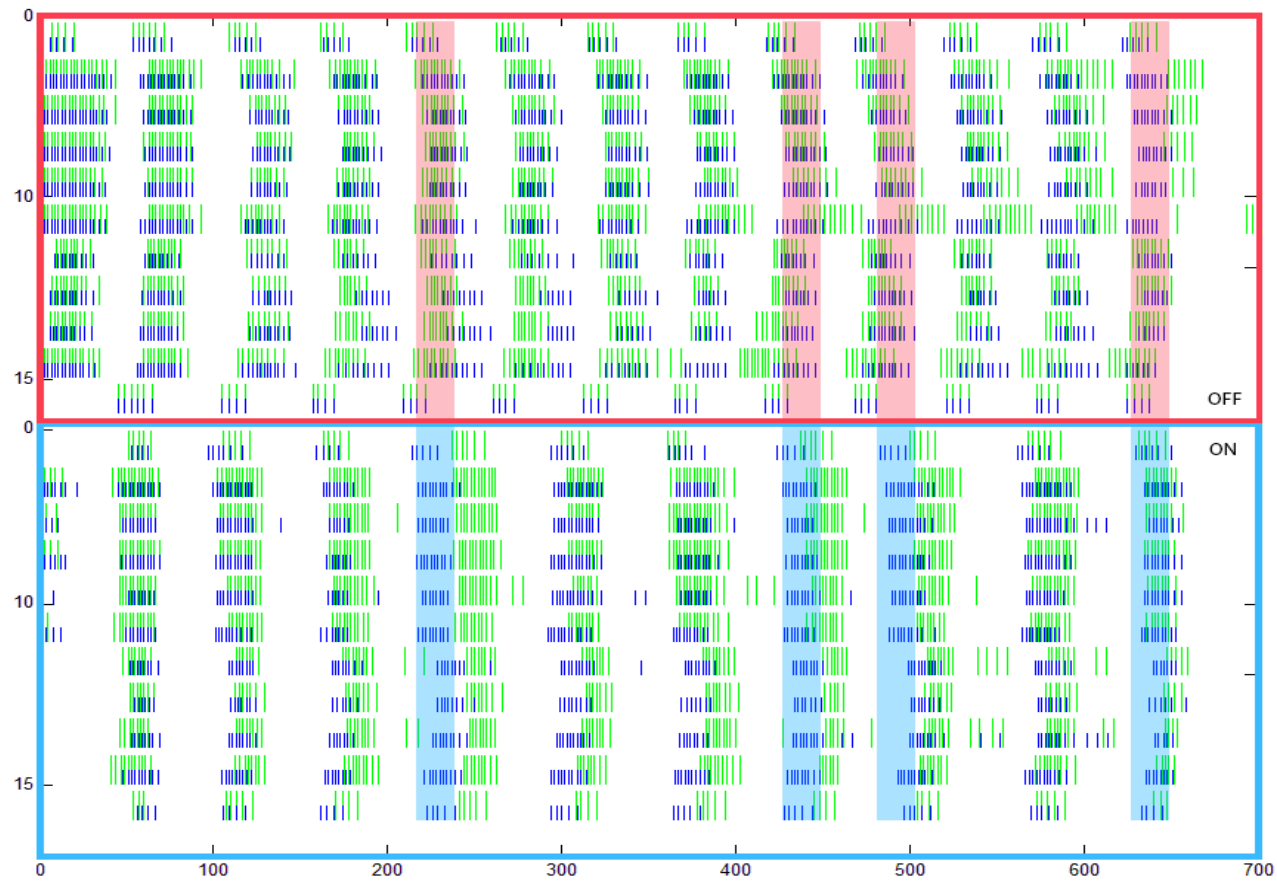


Figure 8.9: Spike synchronization analysis of ganglion cells with and without amacrine cell involvement.

in general and the inner retina in particular are emphasized, thus strengthening the evidence supporting a crucial role of amacrine cells in colour correction.

This result is consistent with the results of Roska et al. (Roska, Molnar and Werblin, 2013), who described a ‘push–pull’ mechanism in ON and OFF ganglion cells whereby the ganglion cells simultaneously excite ON cells and inhibit OFF cells via an amacrine cell-dependent mechanism. In addition, Masland et al. reported an interneuron that is responsible for converting ON signals to OFF signals to generate the retinal blue-OFF signal. The results in this chapter indicate that amacrine cells control this mechanism by creating a delay in spike timing for the synchronization of signals between ON and OFF ganglion cells, and this finding may further support the hypothesis of Masland et al. to resolve the mystery behind the creation of blue-OFF signals in the retina (Masland, 2012).

The results generated by different simulations in this chapter present the connectivity of colour correction, with amacrine cells playing a crucial role in mediating the signals from bipolar and ganglion cells in a ‘push–pull’ fashion. This finding is helpful in terms of understanding information processing in the retina, because if the behaviours of ganglion cells are understood properly, the simulations of ganglion cells can be more precise and efficient. Specifically, blue-OFF signals can be generated by stimulating only ON signals, thus necessitating the use of fewer stimulating electrodes and saving more energy. Although more exploration in the area of colour correction in the retina is needed, this result gives futuristic vision to

research in the development of retinal prostheses that can make colour vision possible for the blind.

Although the model is successful in simulating and also highlights the role of amacrine cells in processing colour in the retina, future works are needed to improve the complement of the model. In particular, the ratio between L, M, and S cones as well as the ratio between rods and cones in this study was set to uniform; thus the outputs will be affected while set to a different ratio. More research is needed to address the relationship between this distribution and the asymmetrical connectivity pattern in the receptive field.

8.8 Summary

In summary, the proposed model provides supporting evidence for the hypothesis that colour correction mechanisms do indeed take place in the retina, particularly in the IPL and with the crucial involvement of amacrine cells. The effect of amacrine cells can be seen mainly in ON ganglion cells, where specific connectivity patterns cause ganglion cells to respond in a ‘push–pull’ fashion. Together with previous retinal modelling studies, this chapter provides a deeper understanding of information processing up to the level of retinal ganglion cells. Based on the knowledge gained from this and all previous simulations, design concepts for next-generation retinal prostheses are introduced in the next chapter.

CHAPTER 9

CONCLUSIONS AND FUTURE WORK

9.1 Discussion

In the previous sections, the functionalities of the proposed model were validated for aspects of information processing by using alternative receptive field formations and computing contrast and colour under different conditions. These experiments demonstrate that the model is able to operate as a retina in a biological context by encoding visual inputs to spike trains and adjusting the contrast and colour of input signals through image processing. Notably, the model was able to replicate the Hermann grid illusion and produced visual outputs similar to those perceived by the naked eye when a non-circular processing distribution was applied to the receptive field. With this asymmetrical processing formation, the illusion created by the Hermann grid can be fully explained in the case of various geometrical transformations such as scaling, rotating, and distorting the grid.

In addition, the model is also able to process contrast and colour information to generate spatial and temporal outputs by simulating information processing circuits that involve different types of amacrine cells. The results from these simulations show that in order to process contrast and colour information under specific light conditions such as mesopic and photopic, the

retina must process information in different ON and OFF pathways, and this process occurs in parallel with the inhibition of amacrine cells. These visual and temporal results imply that asymmetrical and parallel processing approaches are necessary for the retina to elicit visual perception properly and precisely. Furthermore, these results are helpful for the design of the next-generation prostheses, because devices in the future may be able to assist the blind to perceive and interact with objects in colour. This chapter will introduce a conceptual design for next-generation retinal prostheses in three sections: the device concept in general, and the hardware and software implementation in detail.

9.1.1 Device concept

The major function of a retinal prosthesis is to restore vision to the blind, and this device should operate comfortably over a long term without causing any damage to the user. In order to achieve this goal, the conceptual device must fulfil some compulsory requirements:

- First, the prosthesis device, especially the external part, should have a compact size to be easily wearable or comfortably carried throughout all daily activities.
- Second, the power to supply the device must be long lasting for continuous usage.
- Third, the implanted component inside the eye must be comfortable and should not cause any side effects after implantation.

The retinal prosthesis consists of intraocular and extra-ocular parts, which are placed inside and outside the eye, respectively. The intraocular part is responsible for stimulation, while the extra-ocular part is for processing, powering the device, and transferring data to the intraocular part. Due to this arrangement, users need to carry both parts while using the device, making its size and weight important factors. Since users will carry the external component throughout their daily activities, a lighter-weight device will be more comfortable and easier to carry. Thus, the first criterion is a lightweight and wearable device that can be attached or placed inside users' clothing and that operates using a wireless power supply, so that it can be worn without interfering with daily activities.

This leads to the second requirement, that the power capacity of the device be sufficiently large, and the charging time sufficiently short, to allow the device to operate for a long time and be easy to use whenever desired. For the purpose of portability, the power source of the prosthesis should be a rechargeable battery with a large capacity but small in size. This battery will be attached to the external device and supply power to both the internal and external parts of the prosthesis. Such a lightweight design combined with a high-capacity battery should be sufficient for the prosthesis to operate continuously over a long period without recharging and for users to have no difficulty carrying the device in daily activities. On the other hand, the intra-ocular part of the device must be improved not only in the design level but also in the manufacture level in order

to provide comfort to the user and not damage the retina over the long-term use. The next section will describe the concept of the intraocular part and discuss possibilities to implement these concepts in the near future.

9.1.2 Intraocular part

In the retinal prosthesis review in CHAPTER 3, different prosthesis approaches were reviewed with respect to the design and the implantation positions in the blind. Currently, only epiretinal and subretinal prostheses are approved for human trials and commercial purposes; hence this chapter focuses on these devices for the possible development of the proposed concept prosthesis in the future. In epiretinal prostheses, the intraocular part consists of an electrode array that is implanted to contact the ganglion cell layer, while in subretinal prostheses it contacts the bipolar cell layer. This section will discuss the intraocular part, consisting of an electrode array to stimulate the retinal cells, and the placement of this part inside the retina as well as the arrangement of electrodes in the array.

As discussed in the previous section, nanotechnology could be a key to solving the problems in the design and manufacturing of a prosthesis electrode array. Using nanotechnology, the size of one electrode can be minimized, and thus more electrodes can be placed in the array to increase the resolution of the image perceived by the user. In the current prostheses, the resolution is 60 pixels in the Argus II epiretinal prosthesis and 1500 pixels in the Alpha-IMS subretinal prosthesis. In addition to improving the resolution of the future devices, smaller electrodes have many other advantages. The reduced size of electrodes will help

them penetrate further to make better contact with the ganglion cells, thus reducing the cross-talk effect in the stimulation. Smaller electrodes will also help to stimulate ganglion cells more precisely and also to reduce the stimulation current, thus improving the overall usage time of the device. Moreover, precise stimulation will help to reduce damage to retinal cells because only the necessary cells are stimulated. Based on these advantages, nanotechnology is a compulsory technology in the concept design.

In the current retinal prostheses, the electrodes are designed symmetrically in an array as a grid with fixed gaps between electrodes. In our proposed device, the electrodes will be placed dynamically on an array, and each electrode will be movable to change the grid topology. Thus, depending on the patient's retinal cell population, the position of each electrode can be configured to match the distribution of stimulated cells. This concept arises from the fact that the retinal cells are distributed differently among people and from the modelling results in the previous chapters. In particular, the results of the experiment assessing the receptive field of the proposed model with the Hermann grid (CHAPTER 6) demonstrated that it was possible for the receptive field to be a shape other than circular, and this issue has been emphasized by other authors as well (Gijzenij, Gevers and van de Weijer, 2012). With a position-configurable mechanism, the electrodes could more easily penetrate the ganglion cell or bipolar cell layer with a custom shape and thus stimulate only the necessary cells. For example, at the initial stage, the electrodes of the prosthesis may be immobile and form a

standard shape, but upon contact with the retinal cells each electrode can be moved to a position corresponding to the cell population. Thus the electrode grid will match the receptive field shape formed by the retinal cells. The rearrangement of electrodes can be processed as a precise speed in order to reduce the cell damage and migration in the ganglion cell layer. This concept is illustrated in Figure 9.1 and Figure 9.2.

In Figure 9.1, the prosthesis consists of two major parts: internal and external. The external part is a small pocket-sized device that can be worn on the arm or carried in the pocket (number 1). The internal part is a contact lens that can be placed on the eyeball and consists of: a circular antenna for wireless transmission of energy and data between internal and external parts (number 2); three different sensors, an RGB colour sensor, depth sensor, and retinal health sensor (number 3); and an electrical stimulation array at the back that attaches to the retina (number 4). Number 5 depicts a close look at one electrode placed on the electrode array.

In Figure 9.2, one can see that the electrodes are allowed to move not only on the electrode plane but also in the depth direction. This functionality helps the electrodes to penetrate deeper into the retinal cells and thus provides better contact with the retinal cells. In this manner, the electrode piles remain stable in the retina, and the retinal cell movement or migration is reduced after electrodes are implanted. On the left is the array of electrodes at an initial position, and on the right are the same electrodes but with the position of each one re-arranged

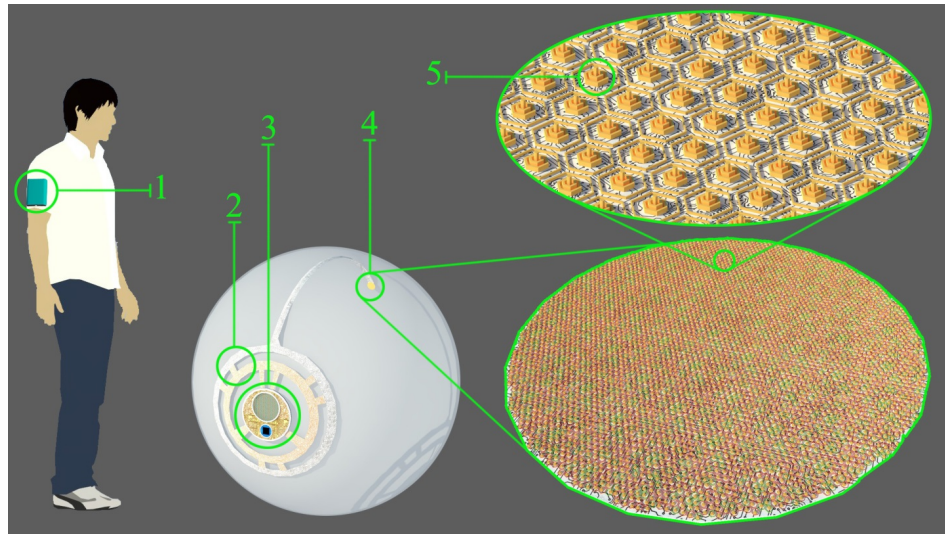


Figure 9.1: The conceptual prosthesis.

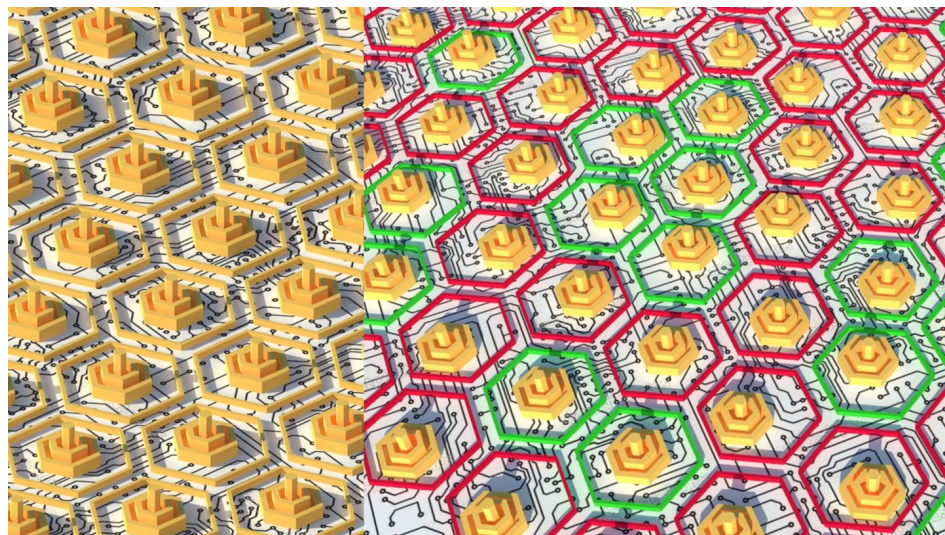


Figure 9.2: The electrode array in operation.

to match the population of ganglion cells in an epiretinal prosthesis or bipolar cells in a subretinal prosthesis. Consequently, the device will operate for a longer period of time without causing damage to the retina. Furthermore, with the small and mobilized electrodes, the energy required for stimulation is reduced, as the electrodes contact and stimulate retinal cells precisely, and less

power is required to the intraocular part, thus improving battery life for the whole device.

The green and red hexagons on the right side indicate electrodes that stimulate centre and surround cells to form the receptive field, respectively. The advancement of this concept in the near future is predicated on the development of nanotechnologies, especially research in nano-mechanical systems (NEMS) and the discovery of the carbon nanotube (CNT), along with nano-wires, nano-coils, nano-walls, and other nano-materials (Iijima, 1991; Morales and Lieber, 1998; Pan, Dai and Wang, 2001). Currently, with the help of these technologies, some approaches have been introduced in the last decade for developing nanoscale mechanical systems. In 1999, Baughman et al. introduced a NEMS actuator assembled from billions of individual nanoscale actuators with muscle-like material strength, low operating voltages, and longer usage life (Baughman *et al.*, 1999). Fennimore et al. in 2003 and Dong et al. in 2006 presented a rotational actuator and linear servomotor, respectively, assembled from multi-walled CNTs that were able to perform motions like rotating and protruding (Dong, Nelson and Fukuda, 2006; Nelson *et al.*, 2007). The same avenue was explored by Bailey et al. in 2008 when they proposed a driving mechanism called a CNT electron windmill that rotates a nanotube using the torque generated from a flux of electrons, a mechanism that could be applied to make a nanoscale motor (Bailey, Amanatidis and Lambert, 2008). In 2012, Hao et al. applied single-walled CNTs to make more efficient and robust solar cells with

a lower cost compared to traditional silicon-based solar cells (Hao *et al.*, 2012). Most directly relevant to retinal prosthesis development, Andrew and his team in 2006 developed a nano-electrode array assembled from multiwall CNTs in order to provide deep brain stimulation as well as more precise electrical signals (Andrews *et al.*, 2006).

From this brief review on the recent advances and applications of nanotechnology, the reality of a reconfigurable electrode array in the future is possible with CNTs and variant materials. Specifically, a nano-electrode will be placed on a three-axis servo made from CNTs, with the servo direction controlled by a nanoscale motor using electron flux. With the aid of this servomotor, the electrode will be able to penetrate deeper to the retinal cells to provide more precise stimulation and minimize damage.

In terms of visual quality, the current prostheses provide resolution of 60 pixels in total, and users are able to perceive only 2D vision in black and white dots (Ahuja and Behrend, 2013). In the next generation of devices, different visual information such as depth and colour will be acquired, processed, and then sent to the brain to improve users' visual perception. Recently, different approaches have been proposed by Stiles *et al.* and McCarthy *et al.* to solve the problem of depth perception (McCarthy and Barnes, 2011; McCarthy, Barnes and Lieby, 2011; Stiles *et al.*, 2014). Stiles and colleagues used ground surface segmentation and visualized depth information based on the intensity of elicited phosphenes (i.e. closer objects elicit larger phosphenes) to visualize depth and

obstacles in low resolution, while McCarthy and his team applied image processing algorithms such as pixelation and filtering to visualize depth information. In the next-generation device, a depth sensor will be integrated as a visual acquisition component to transfer depth information to the processing component and ultimately to the brain by stimulating both Parvo and Magno ganglion cells (i.e. midget and parasol ganglion cells). In terms of colour information, colour correction results from experiments using the proposed model suggest that ON and OFF channels play an important role in altering colour information through inhibition of the OFF channel and excitation of the ON channel via amacrine cells. In current prostheses, only the ON or OFF channel is stimulated due to limited hardware, but in the conceptual prosthesis, with help from nanotechnology, this obstacle can be overcome by stimulating ON and OFF channels concurrently. As discussed earlier, an increased number of stimulating electrodes, and thus increased coverage area of the electrode array, will help to achieve concurrent stimulation.

9.1.3 Extra-ocular part

In current epiretinal and subretinal prostheses, a camera is used to acquire visual scenes and mounted on a glass for users to wear. In this conceptual design, the camera size is reduced and mounted on a contact lens instead of a glass. This lens consists of three sensors: an RGB sensor for image, a depth sensor for stereo information, and a retinal health care sensor to check the condition of the retina. With the depth information from the depth sensor, users will be able to

receive a stereo signal about the surrounding environment and use this information to dodge obstacles while navigating. The last type of sensor which is used to observe and inform the user about the health status of the retina so that users can stop using the prosthesis when the retina is diagnosed as needing a rest. It can also provide information about the status of the retina to doctors to detect any possible issues. This concept is based on the current state of research in embedding technology into the optic lens in order to monitor glucose levels and pressure in the eye, according to Google (Suzanne, 2014). With the visual acquisition component on the lens, users will be able to control the gaze of the eye and thus increase their comfort and convenience while using the device. Data and energy transfer between this lens and external components will occur through wireless communication.

9.1.4 Informational configuration components

As mentioned in the previous sections, the results of simulating different types of information processing inside the retina imply that asymmetrical and parallel processing approaches are required in the future retinal devices to improve the quality of perceived vision. To achieve this goal without changing the hardware in the prostheses, the mapping process of electrical signals to the electrode array will be taken into account. Specifically, in the retinal prostheses that are built with current technologies, the electrodes are placed statically with a constant gap between electrodes; thus, the electrode array will provide a constant map of stimulation to the retinal cells. Although the electrodes are immobile, the

intensity of current applied to each electrode can be controlled through a software or hardware interface. Based on this technique, this thesis proposes a next-generation retinal prosthesis capable of information reconfiguration to match the electrical stimulation map to the target cells. The adjustment of electrical signals will be processed by the external hardware, and the user feedback will be used to improve the adjusted parameters.

This approach was first introduced by Rolf Eckmiller and his team using a tunable retinal encoder and stimulator, as described in CHAPTER 3 (Eckmiller, 1997; Eckmiller, Hünemann and Becker, 1999). The difference between this concept and the work of Eckmiller and colleagues is the electrode array used, together with the information configuration component. In the Eckmiller device and current prostheses, the electrode array consists of fixed electrodes, and thus the customization of stimulation is actually completed before reaching the electrode. The concept proposed in this thesis changes this system by introducing a reconfigurable electrode array that is able to provide different stimulation maps to the retinal cells. By using positioning reconfigurable electrodes, the conceptual device is expected to provide more precise stimulation to retinal cells and thus elicit the perception of useful visual information such as colour and depth for the blind.

9.2 Conclusions

In this thesis, a model of the retina is proposed with respect to receptive field processing and contrast and colour adjustment based on the knowledge gained

from existing retina prostheses and modelling results. In CHAPTER 3, different types of prostheses such as epiretinal, subretinal, optic nerve, and visual cortex prostheses are introduced, and their advantages and disadvantages are compared. CHAPTER 4 introduces various retinal modelling approaches from different authors that replicate visual processing pathways inside the retina. In this chapter, methods used to model retinal processing pathways are reviewed, along with their applications to both image processing and biological simulation. The next four chapters present the proposed model and theories about receptive field processing, contrast, and colour processing in the retina as well as experiments to evaluate the model responses and verify the theories proposed. The results from model simulations are then used to propose a design for next-generation prostheses.

The key of this design is inspired by results from simulating receptive field responses of the model in the Hermann grid illusion showing that a non-circular receptive field is possible for retinal processing and affects the spatial responses of ganglion cells. In the simulations of contrast and colour adjustment using the model, the role of ON and OFF channels in retinal processing was highlighted as a factor in enhancing contrast under mesopic conditions and adjusting colour under photopic conditions. Especially in colour adjustment experiments, the ON and OFF signals were generated simultaneously, with the ON signal excited and the OFF signal inhibited during the colour-adjusting process.

These results indicate that parallel and asymmetric stimulation affect the responses of ganglion cells, and these findings are major factors in the proposed concept for next-generation retinal prostheses. Thus, the retinal prosthesis design proposed in CHAPTER 9 is focused on the asymmetric and parallel stimulation characteristics of the device and how it can be implemented in the near future. The proposed concepts for retinal prostheses highlight the roles of asymmetrical and parallel stimulation as factors in designing the devices of the future. Although it will be a long time before the concept retinal prosthesis described in this thesis becomes a realistic device for human testing, this concept is expected to provide new avenues for other researchers in this field to explore more deeply in terms of device software, hardware, and bioengineering aspects. Using the proposed design, future retinal prostheses will be able to provide better visual perception through precise stimulation as well as restore colour and depth information to help the blind operate more flexibly but still feel comfortable when using the device over a long term.

9.3 Future work

This thesis presents a conceptual design of next generation retinal prostheses from various discoveries in processing pathways inside the retina. These explorations were based on the different experiments in connectivity, contrast, and colour processing in the retina through a retinal model. Although the results from the experiments using this model show the potential concept for next generation prostheses, there are limitations that need to be addressed, which are

the focus of future work. In the Hermann grid experiment, the response of the model to colour needs further exploration to examine the relationship between asymmetrical connectivity and the colour processing pathway. In the contrast processing experiment, the parameters can be optimized by increasing the number of contrast levels. In the colour processing experiment, the distribution of rods and cones in the photoreceptor layer can be adjusted to the ratio in humans to achieve results that are more accurate. By making these improvements, the future model may provide more evidence toward the concept of creating next-generation retinal prostheses that are more realistic and applicable.

9.4 Summary

In summary, this chapter presents a conceptual design for next-generation prostheses based on the knowledge gained through various experiments on the proposed model. Nanotechnology will play a key role in overcoming hardware limitations for manufacturing the device including both intraocular components and power supply. A small, compact, and powerful battery is required to provide sufficient energy to operate the device and aid users throughout their daily activities without recharging. Furthermore, nanotechnology will permit the construction of a shape-customizable stimulating electrode array used in the intraocular part to maximize stimulation efficiency. This concept originated from experimentation with the proposed model using the Hermann grid, with results indicating the feasibility of a retinal receptive field of non-circular shape.

A shape-customizable electrode array will provide better contact between electrodes and retinal cells, thus reducing adverse effects on retinal cells. Furthermore, this reconfigurable electrode array is combined with a reconfigurable electrical mapping tool to map the stimulating currents to target cells depending on the information provided to users such as depth, contrast, or colour. Moreover, peripheral components such as the image processing component are intended to be wearable and easily carried by users in order not to disturb them while using the device continuously in daily life. When device resolution is sufficiently increased, depth information, contrast, and colour can be provided to prosthesis users, to allow the blind to better experience their surrounding environment.

CHAPTER 10

REFERENCES

- Abbott, L. . (1999) ‘Lapicque’s introduction of the integrate-and-fire model neuron (1907)’, *Brain Research Bulletin*, 50(5-6), pp. 303–304. doi: 10.1016/S0361-9230(99)00161-6.
- Adelson, E. H. (1982) ‘Saturation and adaptation in the rod system.’, *Vision research*, 22(10), pp. 1299–1312.
- Agmon-Snir, H., Carr, C. and Rinzel, J. (1998) ‘The role of dendrites in auditory coincidence detection’, *Nature*, 393(May), pp. 268–272.
- Aguilar, M. and Stiles, W. S. (1954) ‘Saturation of the rod mechanism of the retina at high levels of stimulation.’, *Opt Acta Lond*, 1, pp. 59–65.
- Ahuja, A. K. and Behrend, M. R. (2013) ‘The Argus™ II retinal prosthesis: factors affecting patient selection for implantation.’, *Progress in retinal and eye research*. Elsevier Ltd, 36, pp. 1–23. doi: 10.1016/j.preteyeres.2013.01.002.
- Ahuja, A. K., Behrend, M. R., Kuroda, M., Humayun, M. S. and Weiland, J. D. (2008) ‘An in vitro model of a retinal prosthesis.’, *IEEE transactions on bio-medical engineering*, 55(6), pp. 1744–53.
- Almeida, R. and Ledberg, A. (2010) ‘A biologically plausible model of time-scale invariant interval timing.’, *Journal of computational neuroscience*, 28(1), pp. 155–75. doi: 10.1007/s10827-009-0197-8.
- Andrews, R., Li, J., Cassell, A., Koehne, J., Meyyappan, M., Nguyen-Vu, B., Huang, N. and Chen, L. (2006) ‘The NASA Nanoelectrode Array for Deep Brain Stimulation: Monitoring Neurotransmitters and Electrical Activity Plus Precise Stimulation’, in Kanno, T. and Kato, Y. (eds) *Minimally Invasive Neurosurgery and Multidisciplinary Neurotraumatology SE - 33*. Springer Japan, pp. 212–215. doi: 10.1007/4-431-28576-8_33.
- Ash, J., Comerford, J., Thorn, F. and Science, E. (2003) ‘The effect of head tilt on orientation tuning of the Hermann Grid Illusion’. *Investigative Ophthalmology & Visual Abstract* 4090, .’, 44 SRC - .
- Asher, A., Segal, W. a, Baccus, S. a, Yaroslavsky, L. P. and Palanker, D. V (2007) ‘Image processing for a high-resolution optoelectronic retinal prosthesis.’, *IEEE transactions on bio-medical engineering*, 54(6 Pt 1), pp. 993–1004. doi: 10.1109/TBME.2007.894828.
- Baccus, S. a, Olveczky, B. P., Manu, M. and Meister, M. (2008) ‘A retinal circuit that computes object motion.’, *The Journal of neuroscience : the official journal of the Society for Neuroscience*, 28(27), pp. 6807–17. doi: 10.1523/JNEUROSCI.4206-07.2008.

-
- Baccus, S. A. and Meister, M. (2002) 'Fast and slow contrast adaptation in retinal circuitry.', *Neuron*. Elsevier, 36(5), pp. 909–919.
- Baden, T., Berens, P., Bethge, M. and Euler, T. (2013) 'Spikes in mammalian bipolar cells support temporal layering of the inner retina.', *Current biology : CB*. Elsevier Ltd, 23(1), pp. 48–52. doi: 10.1016/j.cub.2012.11.006.
- Baden, T., Esposti, F., Nikolaev, A. and Lagnado, L. (2011) 'Spikes in retinal bipolar cells phase-lock to visual stimuli with millisecond precision.', *Current biology : CB*. Elsevier Ltd, 21(22), pp. 1859–69. doi: 10.1016/j.cub.2011.09.042.
- Bailey, S., Amanatidis, I. and Lambert, C. (2008) 'Carbon Nanotube Electron Windmills: A Novel Design for Nanomotors', *Physical Review Letters*, 100(25), p. 256802. doi: 10.1103/PhysRevLett.100.256802.
- Banarji, B. A., Gurunadh, C. V. S., Patyal, C. S., Ahluwalia, C. T. S., Gen, M. and Vats, D. P. (2009) 'Visual Prosthesis : Artificial Vision', pp. 348–352.
- Barlow, H. B. (1981) 'The Ferrier Lecture, 1980. Critical limiting factors in the design of the eye and visual cortex.', *Proceedings of the Royal Society of London. Series B, Containing papers of a Biological character. Royal Society (Great Britain)*, 212(1186), pp. 1–34.
- Barlow, H. B. and Levick, W. R. (1965) 'The mechanism of directionally selective units in rabbit's retina.', *The Journal of physiology*, 178(3), pp. 477–504.
- Barnard, K., Ciurea, F. and Funt, B. (2002) 'Sensor sharpening for computational color constancy.', *Journal of the Optical Society of America. A, Optics, image science, and vision*. Computer Division, University of California, Berkeley, 94720-1776, USA. SRC - Pubmed ID2 - 11688863 FG - 0, 18(11), pp. 2728–2743.
- Barnard, K. and Funt, B. (1999) 'Investigations into Multi-Scale Retinex', in *Color Imaging in Multimedia. Technology*, (Wiley), pp. 9–17.
- Barnes, S. and Hille, B. (1989) 'Ionic channels of the inner segment of tiger salamander cone photoreceptors.', *The Journal of general physiology*, 94(4), pp. 719–43.
- Bartlett, N. R. and Graham, C. H. (1965) *Dark and light adaptation*.
- Baughman, R., Cui, C., Zakhidov, A. and Iqbal, Z. (1999) 'Carbon nanotube actuators', *Science*, 284, pp. 1340–1344.
- Baumgartner, G. and Levine, J. (1971) *Micheal Bach, online document, retrieved at <http://www.michaelbach.de/ot/>. 'Indirekte grossenbestimmung der rezeptiven Felder der retina beim Menschen mittels der Hermannschen Gittertauschung'. Pflugers Archiv fur die gesamte, Physiologie, vol. 272, pp.*
- Baylor, D. A., Lamb, T. D. and Yau, K. W. (1979) 'Responses of retinal rods to single photons.', *The Journal of physiology*, 288, pp. 613–634.

REFERENCES

- Beaudoin, D. L., Manookin, M. B. and Demb, J. B. (2008) 'Distinct expressions of contrast gain control in parallel synaptic pathways converging on a retinal ganglion cell.', *The Journal of physiology*, 586(Pt 22), pp. 5487–502. doi: 10.1113/jphysiol.2008.156224.
- Behn, C. G. D., Brown, E. N., Scammell, T. E. and Kopell, N. J. (2007) 'Mathematical model of network dynamics governing mouse sleep-wake behavior.', *Journal of neurophysiology*. Department of Mathematics and Center for BioDynamics, Boston University, MA, USA. cbehn@bidmc.harvard.edu DOI - 10.1152/jn.01184.2006 SRC - Pubmed ID2 - 17409167 FG - 0, 97(6), pp. 3828–3840.
- Benav, H., Bartz-Schmidt, K. U., Besch, D., Bruckmann, A., Gekeler, F., Greppmaier, U., Harscher, A., Kibbel, S., Kusnyerik, A., Peters, T., Sachs, H., Stett, A., Stingl, K., Wilhelm, B., Wilke, R., Wrobel, W. and Zrenner, E. (2010) 'Restoration of useful vision up to letter recognition capabilities using subretinal microphotodiodes.', *Conference proceedings : ... Annual International Conference of the IEEE Engineering in Medicine and Biology Society. IEEE Engineering in Medicine and Biology Society. Conference*, 2010, pp. 5919–22. doi: 10.1109/IEMBS.2010.5627549.
- Benison, G., Keizer, J., Chalupa, L. M. and Robinson, D. W. (2001) 'Modeling temporal behavior of postnatal cat retinal ganglion cells.', *Journal of theoretical biology*. Institute of Theoretical Dynamics, University of California, Davis, CA 95616, USA. DOI - 10.1006/jtbi.2000.2289 SRC - Pubmed ID2 - 11371174 FG - 0, 210(2), pp. 187–199.
- Bennett, M. V. . and Zukin, R. S. (2004) 'Electrical Coupling and Neuronal Synchronization in the Mammalian Brain', *Neuron*, 41(4), pp. 495–511. doi: 10.1016/S0896-6273(04)00043-1.
- Berry, M. J., Proceedings, M. E. A., Stett, A., Burkhardt, D. A. and Fahey, P. K. (2013) *Studying the population code of the retina*". In: *meeting (ed), pp . Stuttgart, Germany: GmbH. Contrast Enhancement and Distributed Encoding by Bipolar Cells in the Retina*", 1070-1081.
- Berson, E. L. (1993) 'Retinitis pigmentosa. The Friedenwald Lecture.', *Investigative ophthalmology & visual science*, 34(5), pp. 1659–1676.
- Bichler, O., Querlioz, D., Thorpe, S. J., Bourgoin, J.-P. and Gamrat, C. (2012) 'Extraction of temporally correlated features from dynamic vision sensors with spike-timing-dependent plasticity.', *Neural networks : the official journal of the International Neural Network Society*, 32, pp. 339–48. doi: 10.1016/j.neunet.2012.02.022.
- Bloomfield, S. a and Völgyi, B. (2009) 'The diverse functional roles and regulation of neuronal gap junctions in the retina.', *Nature reviews. Neuroscience*. Nature Publishing Group, 10(7), pp. 495–506. doi: 10.1038/nrn2636.
- Bodkin, D. B. (2008) 'COLOR , TILT , AND THE HERMANN GRID ILLUSION A thesis presented to the graduate faculty of The New England College of Optometry in partial fulfillment of the requirements for the degree of Master of Science.'
- Bradski, D. G. R. and Kaehler, A. (2008) *Learning Opencv, 1st Edition*. First. O'Reilly Media, Inc.
- Bradski, G. (2000) 'The OpenCV Library', *Dr. Dobb's Journal of Software Tools*.

REFERENCES

- Breakspear, M. and Stam, C. J. (2005) 'Dynamics of a neural system with a multiscale architecture.', *Philosophical transactions of the Royal Society of London. Series B, Biological sciences*, 360(1457), pp. 1051–74. doi: 10.1098/rstb.2005.1643.
- Brindley, G. (1965) 'The number of information channels needed for efficient reading', *44*, 177.
- Buchsbaum, G. (1980) 'A spatial processor model for object colour perception', *Journal of the Franklin Institute*, 310(1), pp. 1–26. doi: 10.1016/0016-0032(80)90058-7.
- Bugmann, G. (2012) 'Modeling fast stimulus-response association learning along the occipito-parieto-frontal pathway following rule instructions.', *Brain research*, 1434, pp. 73–89. doi: 10.1016/j.brainres.2011.09.028.
- Bühren, J., Terzi, E., Bach, M., Wesemann, W. and Kohnen, T. (2006) 'Measuring contrast sensitivity under different lighting conditions: comparison of three tests.', *Optometry and vision science : official publication of the American Academy of Optometry*. Department of Ophthalmology, Johann Wolfgang Goethe-University, Frankfurt am Main, Germany. DOI - 10.1097/01.opx.0000216100.93302.2d SRC - Pubmed ID2 - 16699441 FG - 0, 83(5), pp. 290–298.
- Burkhardt, D. a (2011) 'Contrast processing by ON and OFF bipolar cells.', *Visual neuroscience*, 28(1), pp. 69–75. doi: 10.1017/S0952523810000313.
- Bychkovsky, V., Paris, S., Chan, E. and Durand, F. (2011) 'Learning Photographic Global Tonal Adjustment with a Database of Input / Output Image Pairs'. The Twenty-Fourth on Computer Vision and Pattern Recognition.'
- Cao, D. and Lu, Y. H. (2012) 'Lateral suppression of mesopic rod and cone flicker detection.', *Journal of the Optical Society of America. A, Optics, image science, and vision*. Department of Ophthalmology and Visual Sciences, University of Illinois at Chicago, 1905 W. Taylor Street, Room 149, Chicago, Illinois 60612, USA. dcdo98@uic.edu SRC - Pubmed ID2 - 22330377 FG - 0, 29(2), pp. A188–93.
- Capela, S., Tomás, P. and Sousa, L. (2007) 'Stochastic integrate-and-fire model for the retina', *Proc. of the 15th European Signal ...*, (Eusipco), pp. 2514–2518.
- Carandini, M., Horton, J. and Sincich, L. (2007) 'Thalamic filtering of retinal spike trains by postsynaptic summation', *Journal of Vision*, 7, pp. 1–11. doi: 10.1167/7.14.20.Introduction.
- Caspi, A., Dorn, J. D., Mcclure, K. H., Humayun, M. S., Greenberg, R. J. and McMahon, M. J. (2009) 'Feasibility Study of a Retinal Prosthesis', 127(4), pp. 398–401.
- Cassidy, A. S., Georgiou, J. and Andreou, A. G. (2013) 'Design of silicon brains in the nano-CMOS era: spiking neurons, learning synapses and neural architecture optimization.', *Neural networks : the official journal of the International Neural Network Society*. Elsevier Ltd, 45, pp. 4–26. doi: 10.1016/j.neunet.2013.05.011.
- Cembrowski, M. S., Logan, S. M., Tian, M., Jia, L., Li, W., Kath, W. L., Riecke, H. and Singer, J. H. (2012) 'The mechanisms of repetitive spike generation in an axonless retinal interneuron.', *Cell reports*. The Authors, 1(2), pp. 155–66. doi: 10.1016/j.celrep.2011.12.006.

REFERENCES

- Cevikbas, I. and Yildirim, T. (2013) 'Digit recognition in a simplified visual cortex model', *Innovations in Intelligent Systems and ...*, pp. 3–5.
- Chader, G. J., Weiland, J. and Humayun, M. S. (2009) *Artificial vision: needs, functioning, and testing of a retinal electronic prosthesis.*, *Progress in brain research*. Elsevier. doi: 10.1016/S0079-6123(09)17522-2.
- Chander, D. and Chichilnisky, E. J. (2001) 'Adaptation to temporal contrast in primate and salamander retina.', *The Journal of neuroscience : the official journal of the Society for Neuroscience*. Systems Neurobiology, The Salk Institute, La Jolla, California 92037-1099, USA. SRC - Pubmed ID2 - 11739598 FG - 0, 21(24), pp. 9904–9916.
- Chang, L. and He, S. (2014) 'Light adaptation increases response latency of alpha ganglion cells via a threshold-like nonlinearity.', *Neuroscience*, 256, pp. 101–16. doi: 10.1016/j.neuroscience.2013.10.006.
- Cho, M. W. and Choi, M. Y. (2014) 'A model for the receptive field of retinal ganglion cells.', *Neural networks : the official journal of the International Neural Network Society*. Elsevier Ltd, 49, pp. 51–8. doi: 10.1016/j.neunet.2013.09.005.
- Chow, a Y. and Chow, V. Y. (1997) 'Subretinal electrical stimulation of the rabbit retina.', *Neuroscience letters*, 225(1), pp. 13–6.
- Chow, A. Y., Chow, V. Y., Packo, K. H., Pollack, J. S., Peyman, G. a and Schuchard, R. (2004) 'The artificial silicon retina microchip for the treatment of vision loss from retinitis pigmentosa.', *Archives of ophthalmology*, 122(4), pp. 460–9. doi: 10.1001/archophth.122.4.460.
- Chow, A. Y., Pardue, M. T., Perlman, J. I., Ball, S. L., Chow, V. Y., Hetling, J. R., Peyman, G. A., Liang, C., Stubbs, E. B. and Peachey, N. S. (2002) 'Subretinal implantation of semiconductor-based photodiodes: durability of novel implant designs.', *Journal of rehabilitation research and development*, 39(3), pp. 313–321.
- Chow, A. Y. and Peachey, N. S. (1998) 'The subretinal microphotodiode array retinal prosthesis.', *Ophthalmic research*, 30(3), pp. 195–198.
- Chuang, A. T., Margo, C. E. and Greenberg, P. B. (2014) 'Retinal implants: a systematic review.', *The British journal of ophthalmology*. doi: 10.1136/bjophthalmol-2013-303708.
- Coelho, R. and Gerai, M. (2005) 'A Review of Spiking Neuron Models', (November).
- Conway, B. R., Chatterjee, S., Field, G. D., Horwitz, G. D., Johnson, E. N., Koida, K. and Mancuso, K. (2010) 'Advances in color science: from retina to behavior.', *The Journal of neuroscience : the official journal of the Society for Neuroscience*, 30(45), pp. 14955–63. doi: 10.1523/JNEUROSCI.4348-10.2010.
- Corney, D. and Lotto, R. B. (2007) 'What are lightness illusions and why do we see them?', *PLoS computational biology*, 3(9), pp. 1790–800. doi: 10.1371/journal.pcbi.0030180.
- Curlander, J. C. and Marmarelis, V. Z. (1983) 'Processing of visual information in the distal neurons of the vertebrate retina,' *Systems, Man and Cybernetics*, on , vol.SMC- no.', 5 pp934943 SeptOct doi 101109TSMC6313089, 13 SRC - .

REFERENCES

- Dacey, D., Packer, O. S., Diller, L., Brainard, D., Peterson, B. and Lee, B. (2000) *Center surround receptive field structure of cone bipolar cells in primate retina*. *Vision research*, vol. , pp. . Retrieved from <http://www.ncbi.nlm.nih.gov/pubmed/10837827>.
- Decuypere, J. and Capron, J. (2011) 'Implementation Of Model Extended To Mesopic Vision', *27th Session of the ...*, pp. 1–9.
- Demb, J. B. (2007) 'Cellular mechanisms for direction selectivity in the retina.', *Neuron*, 55(2), pp. 179–86. doi: 10.1016/j.neuron.2007.07.001.
- Demb, J. B., Zaghloul, K., Haarsma, L. and Sterling, P. (2001) 'Bipolar cells contribute to nonlinear spatial summation in the brisk-transient (Y) ganglion cell in mammalian retina.', *The Journal of neuroscience : the official journal of the Society for Neuroscience*. Department of Neuroscience, University of Pennsylvania School of Medicine, Philadelphia, Pennsylvania 19104-6058, USA. demb@retina.anatomy.upenn.edu SRC - Pubmed ID2 - 11567034 FG - 0, 21(19), pp. 7447–7454.
- Destexhe, a (1997) 'Conductance-based integrate-and-fire models.', *Neural computation*, 9(3), pp. 503–14.
- Dhruv, N. T. and Carandini, M. (2014) 'Cascaded effects of spatial adaptation in the early visual system.', *Neuron*. The Authors, 81(3), pp. 529–35. doi: 10.1016/j.neuron.2013.11.025.
- Dobelle, W. H. (2000) 'Artificial vision for the blind by connecting a television camera to the visual cortex.', *ASAIO journal (American Society for Artificial Internal Organs : 1992)*, 46(1), pp. 3–9.
- Dong, L., Nelson, B. J. and Fukuda, T. (2006) 'Towards Nanotube Linear Servomotors', 3(3), pp. 228–235.
- Dowling, J. E. and Ripps, H. (1973) 'Effect of magnesium on horizontal cell activity in the skate retina.', *Nature*, 242(5393), pp. 101–103.
- Durackova, D. and Grega, P. (2006) 'Image Processing by Using a Novel Neural Network Simulator', *2006 Sixth International Conference on Hybrid Intelligent Systems (HIS'06)*. Ieee, pp. 61–61. doi: 10.1109/HIS.2006.264944.
- Ebrey, T. and Koutalos, Y. (2001) 'Vertebrate Photoreceptors', *Progress in Retinal and Eye Research*, 20(1), pp. 49–94. doi: 10.1016/S1350-9462(00)00014-8.
- Eckhorn, R., Wilms, M., Schanze, T., Eger, M., Hesse, L., Eysel, U. T., Kisvárdy, Z. F., Zrenner, E., Gekeler, F., Schwahn, H., Shinoda, K., Sachs, H. and Walter, P. (2006) 'Visual resolution with retinal implants estimated from recordings in cat visual cortex.', *Vision research*, 46(17), pp. 2675–90. doi: 10.1016/j.visres.2006.01.034.
- Eckmiller, R. (1997) 'Learning retina implants with epiretinal contacts.', *Ophthalmic research*, 29(5), pp. 281–289.
- Eckmiller, R., Hünemann, R. and Becker, M. (1999) 'Exploration of a dialog-based tunable retina encoder for retina implants', *Neurocomputing*, 27, pp. 1005–1011.
- Egelhaaf, M. and Warzechat, A. (1999) 'Encoding of motion in real time by the fly visual system', *Current opinion in neurobiology*, pp. 454–460.

REFERENCES

- Enroth-Cugell, C. and Robson, J. G. (1966) 'The contrast sensitivity of retinal ganglion cells of the cat.', *The Journal of physiology*. Biomedical Engineering Center, Technological Institute, Northwestern University, Evanston, Illinois, USA. SRC - Pubmed ID2 - 16783910 FG - 0, 187(3), pp. 517–552.
- Famiglietti, E. V and Kolb, H. (1975) 'A bistratified amacrine cell and synaptic circuitry in the inner plexiform layer of the retina.', *Brain research*, 84(2), pp. 293–300.
- Federici, D. (2005) 'A regenerating spiking neural network.', *Neural networks : the official journal of the International Neural Network Society*, 18(5-6), pp. 746–54. doi: 10.1016/j.neunet.2005.06.006.
- Feller, M. B., Butts, D. a, Aaron, H. L., Rokhsar, D. S. and Shatz, C. J. (1997) 'Dynamic processes shape spatiotemporal properties of retinal waves.', *Neuron*, 19(2), pp. 293–306.
- Fernandes, R. a B., Diniz, B., Ribeiro, R. and Humayun, M. (2012) 'Artificial vision through neuronal stimulation.', *Neuroscience letters*. Elsevier Ireland Ltd, 519(2), pp. 122–8. doi: 10.1016/j.neulet.2012.01.063.
- Field, G. D., Gauthier, J. L., Sher, A., Greschner, M., Machado, T. A., Jepson, L. H., Shlens, J., Gunning, D. E., Mathieson, K., Dabrowski, W., Paninski, L., Litke, A. M. and Chichilnisky, E. J. (2010) 'Functional connectivity in the retina at the resolution of photoreceptors', *Nature*. Nature Publishing Group, 467(7316), pp. 673–677. doi: 10.1038/nature09424.
- Field, G. D. and Rieke, F. (2002) 'Nonlinear signal transfer from mouse rods to bipolar cells and implications for visual sensitivity.', *Neuron*, 34(5), pp. 773–85.
- Finlayson, G. D. (1996) 'Color in perspective', *Pattern Analysis and Machine Intelligence, IEEE Transactions on*. IEEE, 18(10), pp. 1034–1038.
- Finlayson, G. D., Drew, M. S. and Funt, B. V (1994) 'Spectral sharpening: sensor transformations for improved color constancy.', *Journal of the Optical Society of America. A, Optics, image science, and vision*. School of Computing Science, Simon Fraser University, Vancouver, B.C., Canada. SRC - Pubmed ID2 - 8006721 FG - 0, 11(5), pp. 1553–1563.
- Foerster, O., J., , and Javaheri, M. (2006) 'Beitrage zur pathophysiologie der sehbahn und der spehsphare.', *Neurol 39 In Retinal prostheses for the blind Annals of the Academy of Medicine Singapore pp13744*, 35(3), pp. 435–463.
- Fohlmeister, J. F., Coleman, P. A. and Miller, R. F. (1990) 'Modeling the repetitive firing of retinal ganglion cells', *Brain Research*, 510(2), pp. 343–345. doi: 10.1016/0006-8993(90)91388-W.
- Freed, M., Smith, R. G. and Sterling, P. (2003) 'Timing of quantal release from the retinal bipolar terminal is regulated by a feedback circuit', *Neuron*, 38(1), pp. 89–101.
- Freeman, D. K., Rizzo, J. F. and Fried, S. I. (2011) 'Encoding visual information in retinal ganglion cells with prosthetic stimulation.', *Journal of neural engineering*, 8(3), p. 035005. doi: 10.1088/1741-2560/8/3/035005.
- Von Frey, M. (1903) 'Theoretische Studien ber Umstimmung des Sehorgans', *Zeitschrift Psychologie und Physiologie der Sinnesorgane*, 32, pp. 146–148.

REFERENCES

- Fromherz, P. (2008) 'Joining microelectronics and microionics: Nerve cells and brain tissue on semiconductor chips', *Solid-State Electronics*, 52(9), pp. 1364–1373. doi: 10.1016/j.sse.2008.04.024.
- Funt, B. and Ciurea, F. (2001) 'Control parameters for Retinex', in *Proc. 9th Cong. Intl. Color Assoc.*, pp. 287–290.
- Funt, B. V and Xiong, W. (2004) 'Estimating Illumination Chromaticity via Support Vector Regression', in *Color Imaging Conference. IS&T - The Society for Imaging Science and Technology*, pp. 47–52.
- Gao, S., Yang, K., Li, C. and Li, Y. (2013) 'A Color Constancy Model with Double-Opponency Mechanisms', in *Proceedings of the 2013 IEEE International Conference on Computer Vision*. Washington, DC, USA: IEEE Computer Society (ICCV '13), pp. 929–936. doi: 10.1109/ICCV.2013.119.
- Garvert, M. M. and Gollisch, T. (2013) 'Local and global contrast adaptation in retinal ganglion cells.', *Neuron*. Elsevier Inc., 77(5), pp. 915–28. doi: 10.1016/j.neuron.2012.12.030.
- Gehler, P. V, Rother, C., Blake, A., Minka, T. and Sharp, T. (2008) 'Bayesian colour constancy revisited.', *on Computer Vision and Pattern Recognition*, pp. 0–1.
- Geier, J., Bernáth, L., Hudák, M. and Séra, L. (2008) 'Straightness as the main factor of the Hermann grid illusion', *Perception*, 37(5), pp. 651–665. doi: 10.1068/p5622.
- Geisler, W. S. (1981) 'Effects of bleaching and backgrounds on the flash response of the cone system.', *The Journal of physiology*, 312, pp. 413–434.
- Gerstner, W. and van Hemmen, J. L. (1992) 'Associative memory in a network of "spiking" neurons. Network', 3 SRC - G, pp. 139–164.
- Gerstner, W., Ritz, R. and van Hemmen, J. L. (1993) 'Why spikes? Hebbian learning and retrieval of time-resolved excitation patterns.', *Biological cybernetics*. Physik-Department der TU München, Garching bei München, Germany. SRC - Pubmed ID2 - 7903867 FG - 0, 69(5-6), pp. 503–515.
- Ghani, a., McDaid, L., Belatreche, a., Hall, S., Huang, S., Marsland, J., Dowrick, T. and Smith, a. (2012) 'Evaluating the generalisation capability of a CMOS based synapse', *Neurocomputing*. Elsevier, 83, pp. 188–197. doi: 10.1016/j.neucom.2011.12.010.
- Gibson, J. R., Beierlein, M. and Connors, B. W. (2005) 'Functional properties of electrical synapses between inhibitory interneurons of neocortical layer 4.', *Journal of neurophysiology*, 93(1), pp. 467–80. doi: 10.1152/jn.00520.2004.
- Gijsenij, A., Gevers, T. and van de Weijer, J. (2012) 'Improving color constancy by photometric edge weighting.', *IEEE transactions on pattern analysis and machine intelligence*, 34(5), pp. 918–29. doi: 10.1109/TPAMI.2011.197.
- Gjorgjieva, J., Toyozumi, T. and Eglén, S. J. (2009) 'Burst-time-dependent plasticity robustly guides ON/OFF segregation in the lateral geniculate nucleus.', *PLoS computational biology*, 5(12), p. e1000618. doi: 10.1371/journal.pcbi.1000618.

-
- Glackin, C., Maguire, L., McDaid, L. and Sayers, H. (2011) 'Receptive field optimisation and supervision of a fuzzy spiking neural network.', *Neural networks : the official journal of the International Neural Network Society*. Elsevier Ltd, 24(3), pp. 247–56. doi: 10.1016/j.neunet.2010.11.008.
- Gomila Salas, J. G. and Lisani, J. L. (2011) 'Local Color Correction', *Image Processing On Line*, 1. doi: 10.5201/ipol.2011.gl_lcc.
- Graham, N., Hood, D. C. and Finkelstein, M. A. (1979) *Visual pattern analyzers*, New York: Oxford University Press". *Comparison of changes in sensitivity and sensation: implications for the response-intensity function of the human photopic system". Journal of Experimental Psychology: Human Perceptual Perform.*
- Grumet, a E., Wyatt, J. L. and Rizzo, J. F. (2000) 'Multi-electrode stimulation and recording in the isolated retina.', *Journal of neuroscience methods*, 101(1), pp. 31–42.
- Gutierrez, G. J. and Marder, E. (2013) 'Rectifying Electrical Synapses Can Affect the Influence of Synaptic Modulation on Output Pattern Robustness', 33(32), pp. 13238–13248. doi: 10.1523/JNEUROSCI.0937-13.2013.
- Haefner, R. M. and Cumming, B. G. (2008) 'Adaptation to natural binocular disparities in primate V1 explained by a generalized energy model.', *Neuron*, 57(1), pp. 147–58. doi: 10.1016/j.neuron.2007.10.042.
- Halupka, B. M. C. (2014) 'A linear-nonlinear model accurately predicts cortical responses to simultaneous electrical stimulation with a retinal implant.', *15Suppl 1P95*.
- Hao, F., Dong, P., Zhang, J. and Zhang, Y. (2012) 'High electrocatalytic activity of vertically aligned single-walled carbon nanotubes towards sulfide redox shuttles', *Scientific reports*, 2, p. 368. doi: 10.1038/srep00368.
- Hateren, H. Van (2005) 'A cellular and molecular model of response kinetics and adaptation in primate cones and horizontal cells', *Journal of Vision*, 5, pp. 331–347. doi: 10.1167/5.4.5.
- Hateren, J. Van (2007) 'A model of spatiotemporal signal processing by primate cones and horizontal cells', *Journal of Vision*, 7, pp. 1–19. doi: 10.1167/7.3.3.Introduction.
- Heckenlively, J. R., Boughman, J., Friedman, L., Philadelphia, P. A. and JR, , (1988) *Diagnosis and classification of retinitis pigmentosa*.
- Heflin, S. J. and Cook, P. B. (2007) 'Narrow and wide field amacrine cells fire action potentials in response to depolarization and light stimulation', *Visual Neuroscience*, pp. 197–206.
- Helmholtz, H. (1867) *Handbuch der physiologischen Optik*, Karsten, G. (ed.). Allgemeine Encyclopädie der Physik.
- Helson, H. and Jeffers, V. B. (1940) 'Fundamental Problems in Color Vision. II. Hue, Lightness, and Saturation of Selective Samples in Chromatic Illumination', *Journal of Experimental Psychology*, 26(1), p. 1.
- Hennig, M. H., Adams, C., Willshaw, D. and Sernagor, E. (2009) 'Early-stage waves in the retinal network emerge close to a critical state transition between local and global functional connectivity.', *The Journal of*

REFERENCES

- neuroscience : the official journal of the Society for Neuroscience*, 29(4), pp. 1077–86. doi: 10.1523/JNEUROSCI.4880-08.2009.
- Hering, E., Hurvich, L. M., Jameson, D., Cambridge, M. A. and Hering, E. (1964) *Outlines of a theory of the light sense*.
- Heywood, C. a, Gadotti, a and Cowey, a (1992) ‘Cortical area V4 and its role in the perception of color.’, *The Journal of neuroscience : the official journal of the Society for Neuroscience*, 12(10), pp. 4056–65.
- Holliday, I. E., Ruddock, K. H. and Skinner, P. (1984) ‘Spatial Filtering Of Retinal Images By the Human Visual System And Its Consequences For Visual Thresholds’, in Williams, T. L. (ed.) *Image Assessment Infrared and Visible*. International Society for Optics and Photonics, pp. 2–6. doi: 10.1117/12.941575.
- Hood, D. C., Finkelstein, M. A. and Boff, L. (1986) ‘Sensitivity to light.’, *Handbook of Perception and Human Processes and Perception KR Kaufman JP Thomas Eds John Wiley Sons Toronto*, 1 SRC - G.
- Hormuzdi, S. G., Filippov, M. A., Mitropoulou, G., Monyer, H. and Bruzzone, R. (2004) ‘Electrical synapses: a dynamic signaling system that shapes the activity of neuronal networks.’, *Biochimica et biophysica acta*, 1662(1-2), pp. 113–37. doi: 10.1016/j.bbamem.2003.10.023.
- Horn, B. K. P. (1974) ‘Determining lightness from an image’, *Computer Graphics and Image Processing*, 3(4), pp. 277–299. doi: 10.1016/0146-664X(74)90022-7.
- Hornig, R. and Eckmiller, R. (2001) ‘Optimizing stimulus parameters by modeling multi-electrode electrical stimulation for retina implants’, *Neural Networks, 2001. Proceedings.*, pp. 860–865.
- Hornstein, E. P., Verweij, J., Li, P. H. and Schnapf, J. L. (2005) ‘Gap-junctional coupling and absolute sensitivity of photoreceptors in macaque retina.’, *The Journal of neuroscience : the official journal of the Society for Neuroscience*. Department of Ophthalmology, University of California, San Francisco, California 94143-0730, USA. DOI - 10.1523/JNEUROSCI.3416-05.2005 SRC - Pubmed ID2 - 16319320 FG - 0, 25(48), pp. 11201–11209.
- Hornstein, E. P., Verweij, J. and Schnapf, J. L. (2004) ‘Electrical coupling between red and green cones in primate retina.’, *Nature neuroscience*. Department of Ophthalmology, University of California, 10 Kirkham Street, San Francisco, California 94143-0730, USA. ehorn@phy.ucsf.edu DOI - 10.1038/nn1274 SRC - Pubmed ID2 - 15208634 FG - 0, 7(7), pp. 745–750.
- Huang, S. J. and Robinson, D. W. (1998) ‘Activation and inactivation properties of voltage-gated calcium currents in developing cat retinal ganglion cells.’, *Neuroscience*. Department of Biochemistry, University of California, Davis 95616, USA. SRC - Pubmed ID2 - 9607715 FG - 0, 85(1), pp. 239–247.
- Hubbard, R. and Kropf, A. (1958) ‘The Action of Light on Rhodopsin.’, *Proceedings of the National Academy of Sciences of the United States of America*, 44(2), pp. 130–139.
- Hubbard, R., Wald, G. and J., (1952) ‘Cis-trans isomers of vitamin A and retinene in the rhodopsin system.’, *Physiol*, 36(2), pp. 269–315.
- Hubel, D. H. and Wiesel, T. N. (1968) ‘Receptive fields and functional architecture of monkey striate cortex.’, *The Journal of physiology*, 195(1), pp. 215–243.

-
- Huk, A. (2014) *Visual Pathways*. Available at: <http://www-psych.stanford.edu/~lera/psych115s/notes/lecture3/figures1.html>.
- Humayun, M. S., Dorn, J. D., da Cruz, L., Dagnelie, G., Sahel, J.-A., Stanga, P. E., Cideciyan, A. V., Duncan, J. L., Elliott, D., Filley, E., Ho, A. C., Santos, A., Safran, A. B., Ardit, A., Del Priore, L. V and Greenberg, R. J. (2012) 'Interim results from the international trial of Second Sight's visual prosthesis.', *Ophthalmology*, 119(4), pp. 779–88. doi: 10.1016/j.ophtha.2011.09.028.
- Humayun, M. S., de Juan, E., Dagnelie, G., Greenberg, R. J., Propst, R. H. and Phillips, D. H. (1996) 'Visual perception elicited by electrical stimulation of retina in blind humans.', *Archives of ophthalmology*, 114(1), pp. 40–46.
- Humayun, M. S., de Juan, E., Weiland, J. D., Dagnelie, G., Katona, S., Greenberg, R. and Suzuki, S. (1999) 'Pattern electrical stimulation of the human retina.', *Vision research*, 39(15), pp. 2569–2576.
- Hunter, I. W. and Korenberg, M. J. (1986) 'The identification of nonlinear biological systems: Wiener and Hammerstein cascade models.', *Biological cybernetics*, 55(2-3), pp. 135–144.
- Hurlbert, A. C. (1989) *The Computation of Color*.
- Iezzi, R. and Finlayson, P. (2009) 'Microfluidic neurotransmitter-based neural interfaces for retinal prosthesis', *Engineering in Medicine ...*, 2009, pp. 4563–5. doi: 10.1109/IEMBS.2009.5332694.
- Iijima, S. (1991) 'Helical microtubules of graphitic carbon', *Nature*, 354(6348), pp. 56–58. doi: 10.1038/354056a0.
- Ishihara, S. (1943) *Ishihara Tests for Colour Blindness*. Sydney: Shephard & Newman.
- Izhikevich, E. M. (2003) 'Simple model of spiking neurons.', *IEEE transactions on neural networks / a publication of the IEEE Neural Networks Council*, 14(6), pp. 1569–72. doi: 10.1109/TNN.2003.820440.
- Izhikevich, E. M. (2004) 'Which model to use for cortical spiking neurons?', *IEEE transactions on neural networks / a publication of the IEEE Neural Networks Council*, 15(5), pp. 1063–70. doi: 10.1109/TNN.2004.832719.
- Jacobs, A., Roska, T. and Werblin, F. (1996) 'Methods for constructing physiologically motivated neuromorphic models in CNNs', *International Journal of Circuit Theory and Applications*, 24(3), pp. 315–339.
- Javaheri, M., Hahn, D. S., Lakhnopal, R. R., Weiland, J. D. and Humayun, M. S. (2006) 'Retinal prostheses for the blind.', *Annals of the Academy of Medicine, Singapore*, 35(3), pp. 137–44.
- Jolivet, R., Kobayashi, R., Rauch, A., Naud, R., Shinomoto, S. and Gerstner, W. (2008) 'A benchmark test for a quantitative assessment of simple neuron models.', *Journal of neuroscience methods*, 169(2), pp. 417–24. doi: 10.1016/j.jneumeth.2007.11.006.
- Jolivet, R., Lewis, T. J. and Gerstner, W. (2004) 'Generalized integrate-and-fire models of neuronal activity approximate spike trains of a detailed model to a high degree of accuracy.', *Journal of neurophysiology*, 92(2), pp. 959–76. doi: 10.1152/jn.00190.2004.

REFERENCES

- Jolivet, R., Rauch, A., Lüscher, H.-R. and Gerstner, W. (2006) 'Predicting spike timing of neocortical pyramidal neurons by simple threshold models.', *Journal of computational neuroscience*, 21(1), pp. 35–49. doi: 10.1007/s10827-006-7074-5.
- Judd, D. B. (1940) 'Hue saturation and lightness of surface colours with chromatic illumination'. *Journal of the Optical Society of America*, . . ., 30 SRC - , pp. 2–32.
- Kamermans, M., Kraaij, D. a and Spekrijse, H. (1998) 'The cone/horizontal cell network: a possible site for color constancy.', *Visual neuroscience*, 15(5), pp. 787–97.
- Kamiyama, Y., Ogura, T. and Usui, S. (1996) 'Ionic current model of the vertebrate rod photoreceptor.', *Vision research*, 36(24), pp. 4059–68.
- Kampeter, B. a, Cej, A. and Jonas, J. B. (2008) 'Intraocular concentration of triamcinolone acetone after intravitreal injection in the rabbit eye.', *Ophthalmology*, 115(8), pp. 1372–5. doi: 10.1016/j.ophtha.2008.01.019.
- Kandel, E. R., Schwartz, J. H. and Jessell, T. M. (2000) *Principles of Neural Science*. 4th edn. McGraw-Hill Medical.
- Kaneko, A. (1970) 'Physiological and morphological identification of horizontal, bipolar and amacrine cells in goldfish retina.', *The Journal of physiology*, 207(3), pp. 623–633.
- Karagoz, I. and Ozden, M. (2011) 'Adaptive artificial retina model to improve perception quality of retina implant recipients', *2011 4th International Conference on Biomedical Engineering and Informatics (BMEI)*. Ieee, pp. 91–95. doi: 10.1109/BMEI.2011.6098353.
- Keat, J., Reinagel, P., Reid, R. C. and Meister, M. (2001) 'Predicting every spike: a model for the responses of visual neurons.', *Neuron*, 30(3), pp. 803–17.
- Kelly, D. H. (1984) 'Retinal inhomogeneity. I. Spatiotemporal contrast sensitivity.', *Journal of the Optical Society of America. A, Optics and image science*, 1(1), pp. 107–113.
- Kelly, S. K., Shire, D. B., Doyle, P., Gingerich, M. D., Drohan, W. a., Rizzo, J. F., Chen, J., Cogan, S. F. and Wyatt, J. L. (2009) 'The boston retinal prosthesis: A 15-channel hermetic wireless neural stimulator', *2009 2nd International Symposium on Applied Sciences in Biomedical and Communication Technologies*. Ieee, pp. 1–6. doi: 10.1109/ISABEL.2009.5373638.
- Kenyon, G. T., George, J., Travis, B. and Blagoev, K. (2005) 'Models of the Retina with Application to the Design of a Visual Prosthesis', *Los Alamos Science*, (29), pp. 110–123.
- Kien, T. T., Maul, T. and Bargiela, A. (2012) 'A review of retinal prosthesis approaches', *International Journal of Modern Physics: Conference Series*, 9, pp. 209–231.
- Kien, T. T., Ren, L. J., Maul, T. and Bargiela, A. (2012) 'Outer plexiform layer receptive fields as underlying factors of the Hermann grid illusion', in *Biomedical Engineering and Sciences (IECBES), 2012 IEEE EMBS Conference on*, pp. 34–39. doi: 10.1109/IECBES.2012.6498072.

-
- Kim, K. J. and Rieke, F. (2001) 'Temporal Contrast Adaptation in the Input and Output Signals of Salamander Retinal Ganglion Cells', 21(1), pp. 287–299.
- Kim, S. Y., Saddy, S., Pearlman, J., Humayun, M. S., de Juan, E., Melia, B. M. and Green, W. R. (2002) 'Morphometric analysis of the macula in eyes with disciform age-related macular degeneration.', *Retina (Philadelphia, Pa.)*, 22(4), pp. 471–7.
- Klauke, S., Goertz, M., Rein, S., Hoehl, D., Thomas, U., Eckhorn, R., Bremmer, F. and Wachtler, T. (2011) 'Stimulation with a wireless intraocular epiretinal implant elicits visual percepts in blind humans.', *Investigative ophthalmology & visual science*, 52(1), pp. 449–55. doi: 10.1167/iovs.09-4410.
- Kolb, H., Nelson, R. and Mariani, a (1981) 'Amacrine cells, bipolar cells and ganglion cells of the cat retina: a Golgi study.', *Vision research*, 21(7), pp. 1081–1114.
- Kourennyi, D. E., Liu, X., Hart, J., Mahmud, F., Baldrige, W. H. and Barnes, S. (2004) 'Reciprocal modulation of calcium dynamics at rod and cone photoreceptor synapses by nitric oxide.', *Journal of neurophysiology*. Department of Biomedical Engineering, Case Western Reserve University, Cleveland, Ohio 44106, USA. DOI - 10.1152/jn.00606.2003 SRC - Pubmed ID2 - 14985410 FG - 0, 92(1), pp. 477–483.
- Von Kries, J. and In, W. (1905) *Gesichtsempfindungen*. Nagel (Ed.), *Handbuch der Physiologie des Menschen* (pp.). .
- Kuehni, R. G. (1997) 'Memoir concerning certain phenomena of vision by M. Monge "Memoire sur quelques phénomènes de la vision" Annales de Chimie 3 131–147 (1789)', *Color Research & Application*. Wiley Subscription Services, Inc., A Wiley Company, 22(3), pp. 199–203. doi: 10.1002/(SICI)1520-6378(199706)22:3<199::AID-COL8>3.0.CO;2-M.
- Kuffler, S. W. (1953) 'Discharge patterns and functional organization of mammalian retina', *Neurophysiol*, 16 SRC - G, pp. 37–68.
- Kusnyerik, A., Greppmaier, U., Wilke, R., Gekeler, F., Wilhelm, B., Sachs, H. G., Bartz-Schmidt, K. U., Klose, U., Stingl, K., Resch, M. D., Hekmat, A., Bruckmann, A., Karacs, K., Nemeth, J., Suveges, I. and Zrenner, E. (2012) 'Positioning of electronic subretinal implants in blind retinitis pigmentosa patients through multimodal assessment of retinal structures.', *Investigative ophthalmology & visual science*, 53(7), pp. 3748–55. doi: 10.1167/iovs.11-9409.
- De Lafuente, V. and Ruiz, O. (2004) 'The orientation dependence of the Hermann grid illusion.', *Experimental brain research. Experimentelle Hirnforschung. Expérimentation cérébrale*, 154(2), pp. 255–60. doi: 10.1007/s00221-003-1700-5.
- Land, E. H. and McCann, J. J. (1971) 'Lightness and retinex theory.', *Journal of the Optical Society of America*, 61(1), pp. 1–11.
- Lankheet, M. J., Molenaar, J. and van de Grind, W. a (1989) 'The spike generating mechanism of cat retinal ganglion cells.', *Vision research*, 29(5), pp. 505–17.
- Lazar, A. a, Pnevmatikakis, E. a and Zhou, Y. (2010) 'Encoding natural scenes with neural circuits with random thresholds.', *Vision research*. Elsevier Ltd, 50(22), pp. 2200–12. doi: 10.1016/j.visres.2010.03.015.

REFERENCES

- Lebedev, D. S. and Marshak, D. W. (2007) 'Amacrine cell contributions to red-green color opponency in central primate retina: a model study.', *Visual neuroscience*, 24(4), pp. 535–47. doi: 10.1017/S0952523807070502.
- Van Leeuwen M T, Numan R, K. M. (2004) 'Colour-constancy is coded in the retina', *Perception ECVF*. Pion Ltd., 33. doi: 10.1068/v040155.
- Leskov, I. B., Klenchin, V. A., Handy, J. W., Whitlock, G. G., Govardovskii, V. I., Bownds, M. D., Lamb, T. D., Pugh, E. N. and Arshavsky, V. Y. (2000) 'The gain of rod phototransduction: reconciliation of biochemical and electrophysiological measurements.', *Neuron*, 27(3), pp. 525–537.
- Levine, J., Spillmann, L. and Wolf, E. (1980) 'Saturation enhancement in colored Hermann grids varying only in chroma.', *Vision research*, 20(4), pp. 307–313.
- Levine, W. (1992) 'Modeling the Variability of Firing Rate of Retinal Ganglion Cells here are concerned with this variability , with an emphasis on how the noise may be introduced . The thesis of this paper is that neural impulses are generated by a mechanism that can be ap', 242.
- Lindsay, T. and Andrew, S. (1999) 'Rod pathways: the importance of seeing nothing', *Trends in Neurosciences*, 22(11, 1 November), pp. 0166–2236.
- Liu, X.-D. and Kourennyi, D. E. (2004) 'Effects of tetraethylammonium on Kx channels and simulated light response in rod photoreceptors.', *Annals of biomedical engineering*. Department of Biomedical Engineering, Case Western Reserve University, Cleveland, OH 44106, USA. SRC - Pubmed ID2 - 15535060 FG - 0, 32(10), pp. 1428–1442.
- Llinás, R., Steinberg, I. Z. and Walton, K. (1981) 'Relationship between presynaptic calcium current and postsynaptic potential in squid giant synapse.', *Biophysical journal*, 33(3), pp. 323–351. doi: 10.1016/S0006-3495(81)84899-0.
- Lorach, H., Benosman, R., Marre, O., Ieng, S.-H., Sahel, J. a and Picaud, S. (2012) 'Artificial retina: the multichannel processing of the mammalian retina achieved with a neuromorphic asynchronous light acquisition device.', *Journal of neural engineering*, 9(6), p. 066004. doi: 10.1088/1741-2560/9/6/066004.
- Lorach, H., Marre, O., Sahel, J.-A., Benosman, R. and Picaud, S. (2013) 'Neural stimulation for visual rehabilitation: advances and challenges.', *Journal of physiology, Paris*. Elsevier Ltd, 107(5), pp. 421–31. doi: 10.1016/j.jphysparis.2012.10.003.
- Lu, S. and Madhukar, A. (2013) 'Inducing repetitive action potential firing in neurons via synthesized photoresponsive nanoscale cellular prostheses.', *Nanomedicine : nanotechnology, biology, and medicine*. Elsevier Inc., 9(2), pp. 293–301. doi: 10.1016/j.nano.2012.07.001.
- Luo, Y. H.-L. and da Cruz, L. (2014) 'A review and update on the current status of retinal prostheses (bionic eye).', *British medical bulletin*, 109(February), pp. 31–44. doi: 10.1093/bmb/ldu002.
- Lytton and William, W. (2002) 'From Computer to Brain: Foundations of Computational Neuroscience.', *Springer p 28 ISBN 387955261*, pp. 970–978.

-
- Maidenbaum, S., Abboud, S. and Amedi, A. (2013) 'Sensory substitution: Closing the gap between basic research and widespread practical visual rehabilitation.', *Neuroscience and biobehavioral reviews*. Elsevier Ltd, pp. 1–13. doi: 10.1016/j.neubiorev.2013.11.007.
- Maksimova, E. M. (1977) 'Cellular mechanisms of colour constancy [proceedings].', *Activitas nervosa superior*, 19(3), pp. 199–201.
- Maloney, L. T. (1986) 'Evaluation of linear models of surface spectral reflectance with small numbers of parameters.', *Journal of the Optical Society of America. A, Optics and image science*, 3(10), pp. 1673–1683.
- Maloney, L. T. and Wandell, B. A. (1986) 'Color constancy: a method for recovering surface spectral reflectance.', *Journal of the Optical Society of America. A, Optics and image science*, 3(1), pp. 29–33.
- Maravall, M., Alenda, A., Bale, M. R. and Petersen, R. S. (2013) 'Transformation of Adaptation and Gain Rescaling along the Whisker Sensory Pathway.', *PloS one*, 8(12), p. e82418. doi: 10.1371/journal.pone.0082418.
- Margalit, E., Maia, M., Weiland, J. D., Greenberg, R. J., Fujii, G. Y., Torres, G., Piyathaisere, D. V., O'Hearn, T. M., Liu, W., Lazzi, G., Dagnelie, G., Scribner, D. A., de Juan, E. and Humayun, M. S. (2002) 'Retinal prosthesis for the blind.', *Survey of ophthalmology*, 47(4), pp. 335–356.
- Marian, I. D. and Reilly, R. G. (2002) 'A computational biologically inspired model of motor control of direction.'
- Masland, R. H. (2012) 'Another blue neuron in the retina.', *Nature neuroscience*, 15(7), pp. 930–931.
- Maul, T. H., Bargiela, A. and Ren, L. J. (2011) 'Cybernetics of Vision Systems: Toward an Understanding of Putative Functions of the Outer Retina', *IEEE Transactions on Systems Man and Cybernetics - Part A Systems and Humans*, pp. 398–409. doi: <http://dx.doi.org/10.1109/TSMCA.2010.2085432>.
- Maynard, E. M. (2001) 'Visual prostheses.'
- Maynard, E. M., Nordhausen, C. T. and Normann, R. A. (1997) 'The Utah intracortical Electrode Array: a recording structure for potential brain-computer interfaces.', *Electroencephalography and clinical neurophysiology*, 102(3), pp. 228–239.
- McCarter, A. (1979) 'Chromatic induction effects in the Hermann grid illusion.', *Perception*, 8(1), pp. 105–114.
- McCarthy, C. and Barnes, N. (2011) 'Surface extraction from iso-disparity contours', *Computer Vision–ACCV 2010*, pp. 1–12.
- McCarthy, C., Barnes, N. and Lieby, P. (2011) 'Ground surface segmentation for navigation with a low resolution visual prosthesis.', *Conference proceedings : ... Annual International Conference of the IEEE Engineering in Medicine and Biology Society. IEEE Engineering in Medicine and Biology Society. Annual Conference*, 2011, pp. 4457–60. doi: 10.1109/IEMBS.2011.6091105.

REFERENCES

- Meylan, L., Alleysson, D. and Süsstrunk, S. (2007) 'Model of retinal local adaptation for the tone mapping of color filter array images.', *Journal of the Optical Society of America. A, Optics, image science, and vision*, 24(9), pp. 2807–16.
- Meylan, L. and Süsstrunk, S. (2004) 'Bio-Inspired Color Image Enhancement', in *IN PROCEEDINGS OF SPIE: HUMAN VISION AND ELECTRONIC IMAGING*, pp. 46–56.
- Morales and Lieber (1998) 'A laser ablation method for the synthesis of crystalline semiconductor nanowires', *Science (New York, N.Y.)*. A. M. Morales, Department of Chemistry and Chemical Biology, Harvard University, Cambridge, MA 02138, USA. C. M. Lieber, Department of Chemistry and Chemical Biology, and Division of Engineering and Applied Sciences, Harvard University, Cambridge. SRC - Pu, 279(5348), pp. 208–211.
- Morgan, M. and Watt, R. (1997) 'The combination of filters in early spatial vision: a retrospective analysis of the MIRAGE model', *PERCEPTION-LONDON*.
- Muller, F., Wassle, H. and Voight, T. (1988) 'Pharmacological modulation of rod pathway in the cat retina'.', 59 SRC -, pp. 1657–1672.
- Murakoshi, K. and Nakamura, K. (2001) 'Firing patterns depending on model neurons', *IEICE TRANSACTIONS on Information ...*, (3), pp. 394–402.
- Naka, K. I. and Rushton, W. (2012) 'S-Potentials from luminosity units in the retina of fish', *Cyprinidae JPhysiol London*, 185 SRC -, pp. 587–599.
- Nanduri, D., Humayun, M. S., Greenberg, R. J., McMahon, M. J. and Weiland, J. D. (2008) 'Retinal prosthesis phosphene shape analysis.', *Conference proceedings : ... Annual International Conference of the IEEE Engineering in Medicine and Biology Society. IEEE Engineering in Medicine and Biology Society. Conference*, 2008, pp. 1785–8. doi: 10.1109/IEMBS.2008.4649524.
- Nelson, B., Dong, L., Subramanian, A. and Bell, D. (2007) 'Hybrid nanorobotic approaches to NEMS', *Robotics Research*.
- Neumann, H., Yazdanbakhsh, A. and Mingolla, E. (2007) 'Seeing surfaces: The brain's vision of the world.', *Physics of Life Reviews* doi101016/jplrev09001, 4(3 SRC - GoogleScholar FG - 0), pp. 189–222.
- Nickolls, J., Buck, I., Garland, M. and Skadron, K. (2008) 'Scalable Parallel Programming with CUDA', *Queue*. New York, NY, USA: ACM, 6(2), pp. 40–53. doi: 10.1145/1365490.1365500.
- Noolandi, J., Peterman, M. and Huie, P. (2003) 'Towards a neurotransmitter-based retinal prosthesis using an inkjet print-head', *Biomedical ...*, pp. 195–199.
- Northmore, D. P. M. (2004) 'A network of spiking neurons develops sensorimotor mechanisms while guiding behavior', *Neurocomputing*, 58-60, pp. 1057–1063. doi: 10.1016/j.neucom.2004.01.166.
- Oehler, R. and Spillmann, L. (1981) 'Illusory colour changes in Hermann grids varying only in hue.', *Vision research*, 21(4), pp. 527–541.

REFERENCES

- Ohshima, S., Yagi, T. and Funahashi, Y. (1995) 'Computational studies on the interaction between red cone and H1 horizontal cell.', *Vision research*, 35(1), pp. 149–60.
- Oozeer, M., Veraart, C., Legat, V. and Delbeke, J. (2006) 'A model of the mammalian optic nerve fibre based on experimental data.', *Vision research*, pp. 2513–24. doi: 10.1016/j.visres.2006.01.021.
- Ostojic, S. and Brunel, N. (2011) 'From spiking neuron models to linear-nonlinear models.', *PLoS computational biology*, 7(1), p. e1001056. doi: 10.1371/journal.pcbi.1001056.
- Palacios-Prado, N., Hoge, G., Marandykina, A., Rimkute, L., Chapuis, S., Paulauskas, N., Skeberdis, V. a, O'Brien, J., Pereda, A. E., Bennett, M. V. L. and Bukauskas, F. F. (2013) 'Intracellular magnesium-dependent modulation of gap junction channels formed by neuronal connexin36.', *The Journal of neuroscience : the official journal of the Society for Neuroscience*, 33(11), pp. 4741–53. doi: 10.1523/JNEUROSCI.2825-12.2013.
- Pan, Z. W., Dai, Z. R. and Wang, Z. L. (2001) 'Nanobelts of semiconducting oxides.', *Science (New York, N.Y.)*. School of Materials Science and Engineering, School of Chemistry and Biochemistry, Georgia Institute of Technology, Atlanta, GA 30332-0245, USA. DOI - 10.1126/science.1058120 SRC - Pubmed ID2 - 11239151 FG - 0, 291(5510), pp. 1947–1949.
- Paninski, L., Pillow, J. and Lewi, J. (2007) 'Statistical models for neural encoding, decoding, and optimal stimulus design.', *Progress in brain research*, 165, pp. 493–507. doi: 10.1016/S0079-6123(06)65031-0.
- Peyman, G., Chow, A. Y., Liang, C., Chow, V. Y., Perlman, J. I. and Peachey, N. S. (1998) 'Subretinal semiconductor microphotodiode array.', *Ophthalmic surgery and lasers*, 29(3), pp. 234–241.
- Pillow, J., Shlens, J., Paninski, L. and Sher, A. (2008) 'Spatio-temporal correlations and visual signalling in a complete neuronal population', *Nature*.
- Piyathaisere, D. V., Margalit, E., Chen, S.-J., Shyu, J.-S., D'Anna, S. A., Weiland, J. D., Grebe, R. R., Grebe, L., Fujii, G., Kim, S. Y., Greenberg, R. J., De Juan, E. and Humayun, M. S. (2003) 'Heat effects on the retina.', *Ophthalmic surgery, lasers & imaging : the official journal of the International Society for Imaging in the Eye*, 34(2), pp. 114–120.
- Pourcho, R. G. and Goebel, D. J. (1985) 'A combined Golgi and autoradiographic study of (3H)glycine-accumulating amacrine cells in the cat retina.', *The Journal of comparative neurology*, 233(4), pp. 473–480.
- Prescott, S. a, Ratté, S., De Koninck, Y. and Sejnowski, T. J. (2006) 'Nonlinear interaction between shunting and adaptation controls a switch between integration and coincidence detection in pyramidal neurons.', *The Journal of neuroscience : the official journal of the Society for Neuroscience*, 26(36), pp. 9084–97. doi: 10.1523/JNEUROSCI.1388-06.2006.
- Protti, D. a, Flores-Herr, N. and von Gersdorff, H. (2000) 'Light evokes Ca²⁺ spikes in the axon terminal of a retinal bipolar cell.', *Neuron*, 25(1), pp. 215–27.
- Publio, R., Oliveira, R. F. and Roque, A. C. (2006) 'A realistic model of rod photoreceptor for use in a retina network model.'

-
- Publio, R., Oliveira, R. F. and Roque, A. C. (2009) 'A computational study on the role of gap junctions and rod Ih conductance in the enhancement of the dynamic range of the retina.', *PloS one*, 4(9), p. e6970. doi: 10.1371/journal.pone.0006970.
- Publio, R., Oliveira, R. and Roque, a (2006) 'A realistic model of rod photoreceptor for use in a retina network model', *Neurocomputing*, 69(10-12), pp. 1020–1024. doi: 10.1016/j.neucom.2005.12.037.
- Rasch, M. J., Schuch, K., Logothetis, N. K. and Maass, W. (2011) 'Statistical comparison of spike responses to natural stimuli in monkey area V1 with simulated responses of a detailed laminar network model for a patch of V1.', *Journal of neurophysiology*, 105(2), pp. 757–78. doi: 10.1152/jn.00845.2009.
- Ratnasingam, S. and Robles-Kelly, A. (2013) 'A spiking neural network for illuminant-invariant colour discrimination', *The 2013 International Joint Conference on Neural Networks (IJCNN)*. Ieee, pp. 1–8. doi: 10.1109/IJCNN.2013.6706929.
- Rattay, F., Paredes, L. P. and Leao, R. N. (2012) 'Strength-duration relationship for intra- versus extracellular stimulation with microelectrodes.', *Neuroscience*. IBRO, 214, pp. 1–13. doi: 10.1016/j.neuroscience.2012.04.004.
- Raudies, F. and Neumann, H. (2010) 'A neural model of the temporal dynamics of figure-ground segregation in motion perception.', *Neural networks : the official journal of the International Neural Network Society*. Elsevier Ltd, 23(2), pp. 160–76. doi: 10.1016/j.neunet.2009.10.005.
- Rizzi, A., Simone, G. and Cordone, R. (2008) 'A Modified Algorithm for Perceived Contrast Measure in', (1), pp. 249–252.
- Rizzo, J. F. (2003) 'Methods and Perceptual Thresholds for Short-Term Electrical Stimulation of Human Retina with Microelectrode Arrays', *Investigative Ophthalmology & Visual Science*, 44(12), pp. 5355–5361. doi: 10.1167/iovs.02-0819.
- Rizzo, J. F. (2011) 'Update on retinal prosthetic research: the Boston Retinal Implant Project.', *Journal of neuro-ophthalmology : the official journal of the North American Neuro-Ophthalmology Society*, 31(2), pp. 160–8. doi: 10.1097/WNO.0b013e31821eb79e.
- Rizzo, J. F., Wyatt, J., Loewenstein, J., Kelly, S. and Shire, D. (2003) 'Perceptual efficacy of electrical stimulation of human retina with a microelectrode array during short-term surgical trials.', *Investigative ophthalmology & visual science*, 44(12), pp. 5362–5369.
- Rodieck, R. W. (1965) 'Quantitative analysis of cat retinal ganglion cell response to visual stimuli.', *Vision research*, 5(11), pp. 583–601.
- Rodieck, R. W. and Watanabe, M. (1993) 'Survey of the morphology of macaque retinal ganglion cells that project to the pretectum, superior colliculus, and parvicellular laminae of the lateral geniculate nucleus.', *The Journal of comparative neurology*. Department of Ophthalmology, University of Washington, Seattle 98195. DOI - 10.1002/cne.903380211 SRC - Pubmed ID2 - 8308173 FG - 0, 338(2), pp. 289–303.
- Roska, B., Molnar, A. and Werblin, F. S. (2013) 'Parallel Processing in Retinal Ganglion Cells : How Integration of Space-Time Patterns of Excitation and Inhibition Form the Spiking Output Parallel Processing in Retinal Ganglion Cells : How Integration of Space-Time Patterns of Excitation and Inhibition', (March 2006), pp. 3810–3822. doi: 10.1152/jn.00113.2006.

REFERENCES

- Rountree, C. M., Inayat, S., Troy, J. B. and Saggere, L. (2013) 'Development of a chemical retinal prosthesis: Stimulation of rat retina with glutamate.', *Conference proceedings : ... Annual International Conference of the IEEE Engineering in Medicine and Biology Society. IEEE Engineering in Medicine and Biology Society. Conference*, 2013, pp. 3134–7. doi: 10.1109/EMBC.2013.6610205.
- Rudd, M. E. and Brown, L. G. (1997) 'A model of weber and noise gain control in the retina of the toad *Bufo marinus*', *Vision Research*, 37(17), pp. 2433–2453. doi: 10.1016/S0042-6989(96)00321-5.
- Saszik, S. and DeVries, S. H. (2012) 'A mammalian retinal bipolar cell uses both graded changes in membrane voltage and all-or-nothing Na⁺ spikes to encode light.', *The Journal of neuroscience : the official journal of the Society for Neuroscience*, 32(1), pp. 297–307. doi: 10.1523/JNEUROSCI.2739-08.2012.
- Schiller, P. H. and Carvey, C. E. (2005) 'The Hermann grid illusion revisited', 34. doi: 10.1068/p5447.
- Schindelin, I., Frise, V., Longair, T., Preibisch, C., Saalfeld, B., Tinevez, D., White, V., Eliceiri, P., Johannes, E., Mark, S., Stephan, J.-Y. and Kevin and Albert Cardona (2012) 'Fiji: an open-source platform for biological-image analysis, *Nature Methods*', *Nature Methods* 9(7), 9, pp. 676–682.
- Schmolesky, M. (2014) *The Primary Visual Cortex*. Available at: <http://webvision.med.utah.edu/book/part-ix-psychophysics-of-vision/the-primary-visual-cortex/> (Accessed: 4 December 2014).
- Schrauf, M., Lingelbach, B. and Wist, E. R. (1997) 'The scintillating grid illusion.', *Vision research*, 37(8), pp. 1033–8.
- Schwartz, G. and Rieke, F. (2011) 'Nonlinear spatial encoding by retinal ganglion cells: when $1 + 1 \neq 2$ ', *The Journal of general physiology*, pp. 283–290. doi: 10.1085/jgp.201110629.
- Schwartz, O., Pillow, J. W., Rust, N. C. and Simoncelli, E. P. (2006) 'Spike-triggered neural characterization.', *Journal of vision*, 6(4), pp. 484–507. doi: 10.1167/6.4.13.
- Sekerli, M. and Butera, R. J. (2004) 'An implementation of a simple neuron model in field programmable analog arrays.', *Conference proceedings : ... Annual International Conference of the IEEE Engineering in Medicine and Biology Society. IEEE Engineering in Medicine and Biology Society. Conference*, 6, pp. 4564–7. doi: 10.1109/IEMBS.2004.1404266.
- Shah, S. and Levine, M. (1993) 'Information processing in primate retinal cone pathways: A model.'
- Shapley, R. and Lennie, P. (1985) 'Spatial frequency analysis in the visual system.', *Annual review of neuroscience*, 8, pp. 547–583.
- Sharma, R. K. and Ehinger, B. (1999) 'Management of hereditary retinal degenerations: present status and future directions.', *Survey of ophthalmology*, 43(5), pp. 427–444.
- Sharpe, L. T. and Stockman, A. (1999) 'Rod pathways: the importance of seeing nothing.', *Trends in neurosciences*, 22(11), pp. 497–504.
- Sheasby, B. W. and Fohlmeister, J. F. (2013) 'Impulse Encoding Across the Dendritic Morphologies of Retinal Ganglion Cells Impulse Encoding Across the Dendritic Morphologies of Retinal Ganglion Cells', pp. 1685–1698.

-
- Shinomoto, S. (2010) 'Fitting a stochastic spiking model to neuronal current injection data.', *Neural networks : the official journal of the International Neural Network Society*. Elsevier Ltd, 23(6), pp. 764–9. doi: 10.1016/j.neunet.2010.04.004.
- Shlens, J., Rieke, F. and Chichilnisky, E. (2008) 'Synchronized firing in the retina.', *Current opinion in neurobiology*, 18(4), pp. 396–402. doi: 10.1016/j.conb.2008.09.010.
- Siegel, M., Marder, E. and Abbott, L. F. (1994) 'Activity-dependent current distributions in model neurons.', *Proceedings of the National Academy of Sciences of the United States of America*, 91(24), pp. 11308–12.
- Siminoff, R. (1980) 'Modeling of the vertebrate visual system. I. Wiring diagram of the cone retina.', *Journal of theoretical biology*, 86(4), pp. 673–708.
- Simone, G., Pedersen, M. and Hardeberg, J. Y. (2012) 'Measuring perceptual contrast in digital images', *Journal of Visual Communication and Image Representation*. Elsevier Inc., 23(3), pp. 491–506. doi: 10.1016/j.jvcir.2012.01.008.
- Sisak, S., Banin, E. and Blumenthal, E. Z. (2004) 'A two-compartment model of the human retina.', *Medical hypotheses*, 62(5), pp. 808–16. doi: 10.1016/j.mehy.2003.11.035.
- Skaliora, I., Robinson, D. W., Scobey, R. P. and Chalupa, L. M. (1995) 'Properties of K⁺ conductances in cat retinal ganglion cells during the period of activity-mediated refinements in retinofugal pathways.', *The European journal of neuroscience*. Section of Neurobiology, Physiology and Behavior, University of California, Davis 95616, USA. SRC - Pubmed ID2 - 7551182 FG - 0, 7(7), pp. 1558–1568.
- Smith, R. G. and Vardi, N. (1995) 'Simulation of the AII amacrine cell of mammalian retina: functional consequences of electrical coupling and regenerative membrane properties.', *Visual neuroscience*, 12(5), pp. 851–60.
- Solomon, S. G. and Lennie, P. (2007) 'The machinery of colour vision.', *Nature reviews. Neuroscience*. Disciplines of Physiology, Anatomy and Histology, School of Medical Sciences and Bosch Institute, Anderson-Stuart Building F13, The University of Sydney, New South Wales 2006, Australia. DOI - 10.1038/nrn2094 SRC - Pubmed ID2 - 17375040 FG - 0, 8(4), pp. 276–286.
- Spillmann, L. and Levine, J. (1971) 'Contrast enhancement in a Hermann grid with variable figure-ground ratio.', *Experimental brain research*, 13(5), pp. 547–59.
- Spitzer, H. and Rosenbluth, A. (2002) 'Colour constancy: The role of low-level mechanisms', *Spatial vision*. Department of Biomedical Engineering, Faculty of Engineering, Tel Aviv University, Israel. hedva@eng.tau.ac.il SRC - Pubmed ID2 - 12116991 FG - 0, 15(3), pp. 277–302.
- Spitzer, H. and Semo, S. (2002) 'Color constancy: a biological model and its application for still and video images', *Pattern Recognition*, 35(8), pp. 1645–1659. doi: 10.1016/S0031-3203(01)00160-1.
- Stabell, U. (1967) 'Rods as color receptors in photopic vision.', *Scandinavian journal of psychology*, 8(2), pp. 139–144.
- Stett, a, Barth, W., Weiss, S., Haemmerle, H. and Zrenner, E. (2000) 'Electrical multisite stimulation of the isolated chicken retina.', *Vision research*, 40(13), pp. 1785–95.

-
- Stiles, N. R., McIntosh, B., Tanguay, A. R. and Humayun, M. S. (2014) 'Intraocular Retinal Prostheses: Monocular Depth Perception in the Low Resolution Limit', in *Frontiers in Optics 2014*. Washington, D.C.: OSA, p. JW3A.38. doi: 10.1364/FIO.2014.JW3A.38.
- Stingl, K., Bartz-Schmidt, K. U., Besch, D., Braun, A., Bruckmann, A., Gekeler, F., Greppmaier, U., Hipp, S., Hörtdörfer, G., Kernstock, C., Koitschev, A., Kusnyerik, A., Sachs, H., Schatz, A., Stingl, K. T., Peters, T., Wilhelm, B. and Zrenner, E. (2013) 'Artificial vision with wirelessly powered subretinal electronic implant alpha-IMS.', *Proceedings. Biological sciences / The Royal Society*, 280(1757), p. 20130077. doi: 10.1098/rspb.2013.0077.
- Stodilka, R. Z., Modolo, J., Prato, F. S., Robertson, J. a., Cook, C., Patrick, J., Beuter, A., Thomas, A. W. and Legros, A. (2011) 'Pulsed magnetic field exposure induces lasting changes in neural network dynamics', *Neurocomputing*. Elsevier, 74(12-13), pp. 2164–2175. doi: 10.1016/j.neucom.2011.01.025.
- Sugita, Y. and Tasaki, K. (1988) 'The activation of cones in scotopic and rods in photopic vision.', *The Tohoku journal of experimental medicine*. Department of Physiology, Tohoku University School of Medicine, Sendai, Japan. SRC - Pubmed ID2 - 3245038 FG - 0, 156(4), pp. 311–317.
- Suh, B. (2012) *ON and OFF Pathways of Ganglion Cells in the Salamander Retina*, *cs229.stanford.edu*.
- Sun, H., Rüttiger, L. and Lee, B. B. (2004) 'The spatiotemporal precision of ganglion cell signals: a comparison of physiological and psychophysical performance with moving gratings', *Vision Research*, 44(1), pp. 19–33. doi: 10.1016/j.visres.2003.08.017.
- Suzanne, J. (2014) *What Else Could Smart Contact Lenses Do?*, *MIT Technology Review*. Available at: <http://www.technologyreview.com/news/529196/what-else-could-smart-contact-lenses-do/>.
- Tannazzo, T., Kurylo, D. D. and Bukhari, F. (2014) 'Perceptual grouping across eccentricity.', *Vision research*, 103, pp. 101–108. doi: 10.1016/j.visres.2014.08.011.
- Tranchina, D., Gordon, J., Shapley, R. and Toyoda, J. (1981) 'Linear information processing in the retina: a study of horizontal cell responses.', *Proceedings of the National Academy of Sciences of the United States of America*, 78(10), pp. 6540–2.
- Troyk, P., Bak, M., Berg, J., Bradley, D., Cogan, S., Erickson, R., Kufta, C., McCreery, D., Schmidt, E. and Towle, V. (2003) 'A model for intracortical visual prosthesis research.', *Artificial organs*, 27(11), pp. 1005–15.
- Tsaneva-Atanasova, K., Zimlik, C. L., Bertram, R. and Sherman, A. (2006) 'Diffusion of calcium and metabolites in pancreatic islets: killing oscillations with a pitchfork.', *Biophysical journal*, 90(10), pp. 3434–46. doi: 10.1529/biophysj.105.078360.
- Tsukada, M., Terasawa, M. and Hauske, G. (1983) 'Temporal pattern discrimination in the cat's retinal cells and Markov system models', *Systems, Man and Cybernetics, IEEE Transactions on*, SMC-13(5), pp. 953–964. doi: 10.1109/TSMC.1983.6313091.
- Uematsu, S., Chapanis, N., Gucer, G., Konigsmark, B. and Walker, A. E. (1974) 'Electrical stimulation of the cerebral visual system in man.', *Confinia neurologica*, 36(2), pp. 113–124.

- Uhlig, C. E., Taneri, S., Benner, F. P. and Gerding, H. (2001) '[Electrical stimulation of the visual system. From empirical approach to visual prostheses].', *Der Ophthalmologe : Zeitschrift der Deutschen Ophthalmologischen Gesellschaft*, 98(11), pp. 1089–1096.
- Ureña, R., Morillas, C. and Pelayo, F. J. (2013) 'Real-time bio-inspired contrast enhancement on GPU', *Neurocomputing*. Elsevier, 121, pp. 40–52. doi: 10.1016/j.neucom.2012.09.035.
- Valeton, J. M., van Norren, D. and van Wyk, M. (2006) *Light adaptation of primate cones: An analysis based on extracellular data*". *Vision Research*, . *Local edge detectors in the rabbit retina*". Ph The University of Queensland.
- Vanleeuwen, M. T., Joselevitch, C., Fahrenfort, I. and Kamermans, M. (2007) 'The contribution of the outer retina to color constancy: a general model for color constancy synthesized from primate and fish data.', *Visual neuroscience*, 24(3), pp. 277–90. doi: 10.1017/S0952523807070058.
- Vasserman, G., Schneidman, E. and Segev, R. (2013) 'Adaptive colour contrast coding in the salamander retina efficiently matches natural scene statistics.', *PloS one*, 8(10), p. e79163. doi: 10.1371/journal.pone.0079163.
- Veraart, C., Raftopoulos, C., Mortimer, J. T., Delbeke, J., Pins, D., Michaux, G., Vanlierde, a, Parrini, S. and Wanet-Defalque, M. C. (1998) 'Visual sensations produced by optic nerve stimulation using an implanted self-sizing spiral cuff electrode.', *Brain research*, 813(1), pp. 181–6.
- Veraart, C., Wanet-Defalque, M.-C., Gérard, B., Vanlierde, A. and Delbeke, J. (2003) 'Pattern recognition with the optic nerve visual prosthesis.', *Artificial organs*, 27(11), pp. 996–1004.
- Veredas, F. J., Vico, F. J. and Alonso, J.-M. (2005) 'Factors determining the precision of the correlated firing generated by a monosynaptic connection in the cat visual pathway.', *The Journal of physiology*, 567(Pt 3), pp. 1057–78. doi: 10.1113/jphysiol.2005.092882.
- Verweij, J., Hornstein, E. P. and Schnapf, J. L. (2003) 'Surround antagonism in macaque cone photoreceptors.', *The Journal of neuroscience : the official journal of the Society for Neuroscience*. Department of Ophthalmology, University of California, San Francisco, California 94143-0730, USA. SRC - Pubmed ID2 - 14614083 FG - 0, 23(32), pp. 10249–10257.
- Wacongne, C., Changeux, J.-P. and Dehaene, S. (2012) 'A neuronal model of predictive coding accounting for the mismatch negativity.', *The Journal of neuroscience : the official journal of the Society for Neuroscience*, 32(11), pp. 3665–78. doi: 10.1523/JNEUROSCI.5003-11.2012.
- Walraven, J., Valeton, J. M., van Doorn, A. J., de Grind, W. A. and Koenderink, J. J. (1984) *Visual adaptation and response saturation*". In *van and Ed*.
- Walter, P., Szurman, P., Vobig, M., Berk, H., Lüdtke-Handjery, H. C., Richter, H., Mittermayer, C., Heimann, K. and Sellhaus, B. (1999) 'Successful long-term implantation of electrically inactive epiretinal microelectrode arrays in rabbits.', *Retina (Philadelphia, Pa.)*, 19(6), pp. 546–552.
- Wässle, H., Grünert, U., Chun, M. H. and Boycott, B. B. (1995) 'The rod pathway of the macaque monkey retina: identification of AII-amacrine cells with antibodies against calretinin.', *The Journal of comparative neurology*. Max-Planck-Institut für Hirnforschung, Frankfurt, Federal Republic of Germany. DOI - 10.1002/cne.903610315 SRC - Pubmed ID2 - 8550898 FG - 0, 361(3), pp. 537–551.

REFERENCES

- Webster, M. and Mollon, J. D. (1991) 'Changes in colour appearance following post-receptor adaptation', *Nature*, 349(6306), pp. 235–238.
- Weiland, J. D., Cho, A. K. and Humayun, M. S. (2011) 'Retinal prostheses: current clinical results and future needs.', *Ophthalmology*. Elsevier Inc., 118(11), pp. 2227–37. doi: 10.1016/j.ophtha.2011.08.042.
- Weiland, J. D. and Humayun, M. S. (2003) 'Past, present, and future of artificial vision', *Artificial organs*, 27(11), pp. 961–962.
- Weiland, J. D. and Humayun, M. S. (2005) 'A biomimetic retinal stimulating array.', *IEEE engineering in medicine and biology magazine : the quarterly magazine of the Engineering in Medicine & Biology Society*, 24(5), pp. 14–21.
- Weiland, J. D. and Humayun, M. S. (2006) 'Intraocular retinal prosthesis', *IEEE Engineering in Medicine and Biology Magazine*, 25(5), pp. 60–66. doi: 10.1109/MEMB.2006.1705748.
- Weiland, J. D., Liu, W. and Humayun, M. S. (2005) 'Retinal prosthesis.', *Annual review of biomedical engineering*, 7, pp. 361–401. doi: 10.1146/annurev.bioeng.7.060804.100435.
- Werblin, F. S. (2010) 'Six different roles for crossover inhibition in the retina: correcting the nonlinearities of synaptic transmission.', *Visual neuroscience*. Department of Molecular and Cell Biology, University of California at Berkeley, Berkeley, California 94720, USA. werblin@berkeley.edu DOI - 10.1017/S0952523810000076 SRC - Pubmed ID2 - 20392301 FG - 0, 27(1-2), pp. 1–8.
- Werblin, F. S. and Dowling, J. E. (1969) 'Organization of the retina of the mudpuppy, *Necturus maculosus*. II. Intracellular recording.', *Journal of neurophysiology*, 32(3), pp. 339–355.
- West, G. and Brill, M. H. (1982) 'Necessary and sufficient conditions for Von Kries chromatic adaptation to give color constancy.', *Journal of mathematical biology*, 15(2), pp. 249–258.
- Wijekoon, J. H. B. and Dudek, P. (2012) 'VLSI circuits implementing computational models of neocortical circuits.', *Journal of neuroscience methods*. Elsevier B.V., 210(1), pp. 93–109. doi: 10.1016/j.jneumeth.2012.01.019.
- Wilke, R., Gabel, V. P., Sachs, H., Bartz, S., Gekeler, F., Besch, D., Szurman, P., Stett, A., Wilhelm, B., Peters, T., Harscher, A., Greppmaier, U., Kibbel, S., Benav, H., Bruckmann, A., Stingl, K., Kusnyerik, A. and Zrenner, E. (2011) 'Spatial resolution and perception of patterns mediated by a subretinal 16-electrode array in patients blinded by hereditary retinal dystrophies', *Investigative ophthalmology & visual science*, 52(8), pp. 5995–6003.
- Wilson, H. R., Cambridge, M. A., Tranchina, D., Gordon, J. and Sci, U. S. A. (1981) 'Pattern discrimination, Visual Filters, and Spatial Sampling Irregularity, in M.', *S Landy and JA Movshon Eds Computational Models of Visual Processing pp Linear information processing in the retina a study of horizontal cell responses Proc Natl Acad 65402*, 78 SRC - , pp. 153–168.
- Wilson, H. R. and Kim, J. (1998) 'Dynamics of a divisive gain control in human vision.', *Vision research*. Visual Sciences Center, University of Chicago, IL 60637, USA. hrw6@midway.uchicago.edu SRC - Pubmed ID2 - 9775322 FG - 0, 38(18), pp. 2735–2741.

-
- Wohrer, A. and Kornprobst, P. (2009) 'Virtual Retina: a biological retina model and simulator, with contrast gain control.', *Journal of computational neuroscience*, 26(2), pp. 219–249. doi: 10.1007/s10827-008-0108-4.
- Wu, Q. X., McGinnity, T. M., Maguire, L. P., Belatreche, A. and Glackin, B. (2008) 'Processing visual stimuli using hierarchical spiking neural networks', *Neurocomputing*, 71(10-12), pp. 2055–2068. doi: 10.1016/j.neucom.2007.10.020.
- Van Wyk, M., Taylor, W. R. and Vaney, D. I. (2006) 'Local edge detectors: a substrate for fine spatial vision at low temporal frequencies in rabbit retina.', *The Journal of neuroscience : the official journal of the Society for Neuroscience*, 26(51), pp. 13250–63. doi: 10.1523/JNEUROSCI.1991-06.2006.
- Xu, Y., Dhingra, N. K., Smith, R. G. and Sterling, P. (2005) 'Sluggish and brisk ganglion cells detect contrast with similar sensitivity.', *Journal of neurophysiology*. Department of Neuroscience, University of Pennsylvania School of Medicine, Philadelphia, PA 19104-6058, USA. ying@retina.anatomy.upenn.edu DOI - 10.1152/jn.01088.2004 SRC - Pubmed ID2 - 15601731 FG - 0, 93(5), pp. 2388–2395.
- Yanai, D., Weiland, J. D., Mahadevappa, M., Greenberg, R. J., Fine, I. and Humayun, M. S. (2007) 'Visual performance using a retinal prosthesis in three subjects with retinitis pigmentosa.', *American journal of ophthalmology*, 143(5), pp. 820–827. doi: 10.1016/j.ajo.2007.01.027.
- Young, T. and Kelland, P. (1845) *A course of lectures on natural philosophy and the mechanical arts*. (A course of lectures on natural philosophy and the mechanical arts).
- Zaghloul, K. a, Boahen, K. and Demb, J. B. (2003) 'Different circuits for ON and OFF retinal ganglion cells cause different contrast sensitivities.', *The Journal of neuroscience : the official journal of the Society for Neuroscience*, 23(7), pp. 2645–54.
- Zaghloul, K. a, Boahen, K. and Demb, J. B. (2005) 'Contrast adaptation in subthreshold and spiking responses of mammalian Y-type retinal ganglion cells.', *The Journal of neuroscience : the official journal of the Society for Neuroscience*, 25(4), pp. 860–8. doi: 10.1523/JNEUROSCI.2782-04.2005.
- Zeck, G. M., Xiao, Q. and Masland, R. H. (2005) 'The spatial filtering properties of local edge detectors and brisk-sustained retinal ganglion cells.', *The European journal of neuroscience*, 22(8), pp. 2016–26. doi: 10.1111/j.1460-9568.2005.04390.x.
- Zele, A. J., Maynard, M. L., Joyce, D. S. and Cao, D. (2014) 'Effect of rod-cone interactions on mesopic visual performance mediated by chromatic and luminance pathways.', *Journal of the Optical Society of America. A, Optics, image science, and vision*, 31(4), pp. A7–A14.
- Zhijun Pei and Qingli Qiao (2010) 'An Approximate Retina Model with Cascade Structures', *Biomedical Engineering*, (Icnc), pp. 2009–2012.
- Zhou, D., Li, S., Zhang, X. and Cai, D. (2013) 'Phenomenological incorporation of nonlinear dendritic integration using integrate-and-fire neuronal frameworks.', *PloS one*, 8(1), p. e53508. doi: 10.1371/journal.pone.0053508.
- Zhou, Z. J. and Fain, G. L. (1996) 'Starburst amacrine cells change from spiking to nonspiking neurons during retinal development.', *Proceedings of the National Academy of Sciences of the United States of America*, 93(15), pp. 8057–62.

REFERENCES

Zrenner, E. (2002) 'Will retinal implants restore vision?', *Science (New York, N.Y.)*, 295(5557), pp. 1022–5.
doi: 10.1126/science.1067996.